J. FODEN

The Petrology and Timing of the Anabama Granite and Associated Igneous Activity, Olary Region, S.A.

By

Graeme D Mc Donald B.Sc.

This thesis is submitted as partial fulfillment for the Honours degree of Bachelor of Science

Department of Geology and Geophysics
University of Adelaide

November 1992

National Grid Reference (SI - 54) 6932 -IV 1:50 000

COPY 3

ABSTRACT

Two ideologies of thought exist when models of granite genesis are considered. Do they represent the products of direct fractionation of a basaltic mantle melt, or, do they form in accordance with the restite model of White and Chappell (1977) ?

Assimilation and fractional crystalization (AFC) modelling of Nd - and Sr - isotopic data from the Anabama Granite, of this study, and data from the granites of the southern Adelaide Fold Belt, Antarctica and the Lachlan Fold Belt of New South Wales, all of approximately the same age, appears to reflect mixed sources with components derived both from an average Delamerian basalt composition and an average Archean crust composition. Results indicate that the Anabama Granite mostly represents primitive Delamerian basalt, contaminated by 12 - 14 % Archean crustal material.

Field relationships of the Anabama Granite indicate that it was the site of multiple magmatic intrusions, between approximately 490 - 425 Ma. These intrusions are represented by several episodes of hydrothermal alteration and crosscutting dykes. A long lived thermal source, not represented in the southern Adelaide Fold Belt, may be responsible for this ongoing magmatic activity. Examples of these dykes are the lamprophyre dyke, dated at 457 ± 18 Ma, which is similar in composition and appearance to the lamprophyres near Truro (South Australia) and the dacite porphyry dyke which crosscuts all other lithologies and was dated at 425 ± 13Ma. This age corresponds to the onset of thermal activity in the Lachlan Fold Belt, and therefore, leads to the suggestion that the region where the Anabama Granite outcrops may represent the western margin of the thermal perturbation responsible for the production of granitic melts in the Lachlan Fold Belt at around 400 Ma.

Differences in source regions for the Anabama Granite, the granites of Antarctica and those of the Lachlan Fold Belt are recognized by the different Nd - and Sr - isotopic ratios, although all granites may represent the same process of formation, that being AFC. The dacite porphyry's isotopic signature indicates a more primitive source than that suggested for the Anabama Granite, and therefore, its genesis does not represent a remelting of the Anabama Granite or of its source region.

Geochemically, the Anabama Granite is similar to the Reedy Creek granodiorite of the southern Adelaide Fold Belt and the Wando granodiorite of western Victoria. It can also be classified as an I - type granite using the criteria established by Chappell and White (1974).

Geophysical gravity modelling of the Anabama Granite was carried out and it was found that the granite extends to a depth of approximately 15 km and dips uniformly to the north west. Thus giving an indication that fracture propagation, rather than plutonism, is the mechanism of granitic melt transport through the upper crust for the Anabama Granite and granites of the southern Adelaide Fold Belt.

ACKNOWLEDGEMENTS

This project was supervised by Dr. J.D.Foden. His guidance and enthusiasm throughout have been very encouraging and greatly appreciated.

Many thanks go to Ian and Gloria Tiver, of "Netley Gap" station, for allowing me to stay at their homestead whilst undertaking my field studies.

I am indebted to the technical staff of the Geology Department for their assistance, and, to other staff and students who have helped me during this project. A special thank you to John Stanley for his help with XRF analysis, David Bruce and Jo Mawby for their help with isotopic analysis, Huw Rosser for patience and assistance with the electron microprobe and Sherry Proferes for her guidance with any drafting problems.

Many thanks must go to the honours class of 1992. All of them, in their own special way, have made this year bearable and most of all, very enjoyable.

Finally, I would like to thank my family and friends for all their support throughout the year, especially Rachel, for the support, encouragement, help and understanding she has shown me over the last few years.

CONTENTS

Abstract i

Acknowledgements ii

Chapter 1 Introduction 1
1.1 Introduction 1
1.2 Previous Investigations 2

Chapter 2 Regional Geology 4
2.1 Regional Geology 4
2.2 Anabama Granite 5
2.3 Granophyre 6
2.4 Introduction to Dyke Rocks 6
2.4.1 Acid and Intermediate Dykes 6
2.4.2 Microgranodiorite Dykes 7
2.4.3 Aplite Dykes 7
2.4.4 Quartz Porphyry 7
2.4.5 Dacite Porphyry 8
2.4.6 Lamprophyre 8
2.5 Metamorphism 9
2.6 Hydrothermal Alteration 10
2.7 Metasedimentary Strain Analysis 10

Chapter 3 Petrography 12
3.1 Introduction 12
3.2 Anabama Granite 12
3.3 Granophyre 13
3.4 Acid and Intermediate Dykes 13
3.5 Microgranodiorite Dykes 14
3.6 Aplite Dykes 15
3.7 Quartz Porphyry 15
3.8 Dacite Porphyry 15
3.9 Lamprophyre 16
3.10 Metasediments 17

Chapter 4 Geochemistry 18
4.1 Introduction 18
4.2 Anabama Granite 18
4.2.1 Mineral chemistry 19
4.2.2 Comparative Granite Geochemistry 19
4.3 Granophyre 20
4.4 Acid and Intermediate Dykes 21
4.5 Microgranodiorites 22
4.6 Dacite Porphyry 22
4.7 Lamprophyre 23

Chapter 5 Isotope Geology and Geochronology 25
5.1 Introduction 25
5.2 Anabama Granite 25
5.2.1 Isotopic Comparisons 26
5.3 Dacite Porphyry and Lamprophyre Dyke 26
5.4 Discussion 27

Chapter 6 Petrogenesis and Discussion 28

Chapter 7 Geophysics 33
7.1 Geophysical Modelling 33
7.2 Problems with the Modelling 33
7.3 Conclusions 34

Conclusions 35

References

LIST OF APPENDICES

Appendix 1 Hand specimen and thin section descriptions.
Appendix 2 Electron microprobe analyses of mineral compositions.
Appendix 3 Method of whole rock and mineral separation techniques and major element, trace element and normative compositions: Sample Location Diagrams
Appendix 4 Major and trace element fractional crystalization modelling.
Appendix 5 Simplified lithological logs and core locations and numbers.

LIST OF PLATES

Plate 1 - Typical Anabama Granite.
Plate 2 - Foliation within the Anabama Granite.
Plate 3 - Hornblende bearing xenolith within the Anabama Granite.
Plate 4 - Anabama Granite / Metasediment contact.
Plate 5 - Folding of metasediment and granitic vein.
Plate 6 - Dacite Porphyry crosscutting the Anabama Granite.
Plate 7 - Dacite Porphyry containing greisen xenoliths.
Plate 8 - Euhedral apatite within the Anabama Granite.
Plate 9 - Typical thin section of the Anabama Granite.
Plate 10 - Radiating granophyric texture within the Quartz Porphyry.
Plate 11 - Granophyric texture within the Granophyre.
Plate 12 - Typical thin section of the Dacite Porphyry.
Plate 13 - Typical thin section of the Lamprophyre Dyke.
Plate 14a - Remnant olivine grain in the Lamprophyre Dyke (plain light).
Plate 14b - Remnant olivine grain in the Lamprophyre Dyke (polarized light).
Plate 15 - Recrystalized quartz porphyroblast from wihtin a metasediment.

LIST OF TABLES

Table 1a - Rb and Sr isotopic data for the Anabama Granite from Compston et al. (1966) and Webb (1976).
Table 1b - Nd and Sm isotopic data from this study.
Table 1c - Rb and Sr isotopic data from this study.
Table 2a - Nd and Sm isotopic data from selected authors.
Table 2b - Rb and Sr isotopic data from selected authors.

LIST OF FIGURES

Figure 1a - Location of Study Area.
Figure 1b - Generalized geological map of the southern Adelaide Fold Belt (after Foden et al., 1992).
Figure 2 - Block Diagram of the Anabama Granite Region.
Figure 3 - Rf / Ø diagram for Strain Analysis.
Figure 4 - Q v 100 an / (or + an) classification diagram (after Streckeisen, 1976).
Figure 5 - K / Rb v SiO_2 diagram for the Anabama Granite.
Figure 6 - Q - Ab - Or Ternary plot.
Figure 7 - An - Ab - Or Ternary plot.
Figure 8 - Major element variation diagrams.
Figure 9 - Trace element variation diagrams.
Figure 10 - Mg - Fe - Al Ternary plot for mica's.
Figure 11 - Ca - Na - K Ternary plot for feldspars.
Figure 12 - Nb v Zr comparative plot for Lamprophyres.
Figure 13 - Zr v Rb / Sr diagram for the Anabama Granite.
Figure 14a - Anabama Granite isochron.
Figure 14b - Lamprophyre dyke isochron.
Figure 14c - Dacite Porphyry isochron.
Figure 15 - $^{87}Sr / ^{86}Sr$ v Time
Figure 16a - ε Nd v $^{87}Sr / ^{86}Sr$ (500 Ma) simple mixing curve.
Figure 16b - ε Nd v $^{87}Sr / ^{86}Sr$ (400 Ma) simple mixing curve.
Figure 17a - $^{143}Nd / ^{144}Nd$ (500 Ma) v Nd ppm, AFC curve.
Figure 17b - Zr ppm v $^{143}Nd / ^{144}Nd$ (500 Ma), AFC curve.for 500 Ma granites.
Figure 18a - Sm / Nd v ε Nd for 500 Ma granites.
Figure 18b - Sm / Nd v ε Nd for 400 Ma granites.
Figure 18c - Rb / Sr v $^{87}Sr / ^{86}Sr$ (500 Ma).
Figure 19a - R2 V R1 Tectonic plot.
Figure 19b - Rb v Y + Nb Tectonic plot.
Figure 20 - Bouguer gravity anomaly.
Figure 21 - Gravity modelling of the Anabama Granite.
Figure 22 - Sample location map of the Anabama Region. }
Figure 23 - Sample location map of Anabama Hill. } Appendix 3
Figure 24 - Sample location map of Netley Hill. }
Figure 25 - Geological map of the Anabama Region.)
Figure 26 - Geological map of Anabama Hill.) In back pocket of thesis
Figure 27 - Geological map of Netley Hill.)

CHAPTER 1 - INTRODUCTION

1.1 Introduction

The Adelaide Fold Belt forms part of a Late Proterozoic to Early Palaeozoic continental marginal orogen which extended over 5000 km along the south eastern edge of the Gondwana supercontinent (Sandiford et al., 1992). Rocks of the Adelaide Fold Belt were deformed, metamorphosed and intruded by granites during the Delamerian Orogeny (520 - 480 Ma).

The Anabama Granite is one of the largest and most northern of all the South Australian Cambrian / Ordovician granites. It is situated along the inner Nackara Arc, some 350 km NE of Adelaide and 35 km S of Mannahill (Figure 1a).

Unlike most other Delamerian granites, the Anabama Granite does not intrude Cambrian, Kanmantoo like sediments. It does, however, lie within a thick sequence of Upper Proterozoic sediments - the Burra and Umberatana Groups of the Adelaidean system.

Evidence for the Anabama area as the site of multiple magmatic intrusions and of superimposed hydrothermal events is present in the form of secondary alteration of the granite and several episodes of hydrothermally altered and unaltered crosscutting dykes. It was an aim of this study to investigate the major and trace element geochemistry and petrology of the Anabama Granite and geographically associated dykes and draw comparisons with the granites of the southern Adelaide Fold Belt, western Victoria and the Lachlan Fold Belt of New South Wales. The relationship of the dyke rocks, both to each other and to the Anabama Granite were investigated to clarify and constrain the timing of thermal, igneous and structural events. This study indicates that the ongoing igneous activity in the area spans a range of 50 - 75 Ma, from the initial intrusion of the Anabama Granite at about 500 - 475 Ma to the younger crosscutting dacite porphyry dykes during the Silurian (425 Ma). Lamprophyre dykes were noted in the area and dated at 456 Ma using the Rb / Sr method, with a mica mineral separate and a whole rock sample.

Recently, Sandiford et al. (1992) discussed the origin and sources of the granites of the Southern Adelaide Fold Belt. The processes of assimilation (mixing) and fractional crystalization, (AFC), were shown to be responsible for producing the observed isotopic signatures of these granites. Using end member compositions of a typical Delamerian mafic and an average Archean crust, this study also showed that the Anabama Granite, Victor Harbor granite (data from Cock, 1992) and the Granite Harbour granites of Antarctica are products of the same processes, but with differing amounts of involvement.

The possible mechanisms of granite genesis during the Delamerian Orogeny and sources of heat both at this time and during the Silurian magmatism observed within the Anabama Granite, will be discussed. Differences and similarities between the source regions of the Adelaide Fold Belt granites, the Lachlan Fold Belt granites (both at 500 and 400 Ma), the Antarctica granites (both at 500 and 400 Ma) and the younger dykes associated with the Anabama Granite will also be addressed.

Geophysics, and in particular gravity, will be used to gain an insight into the subsurface nature of the Anabama Granite. It will be shown that the Anabama Granite is more of a sheet like body which dips down to the NW back under the host Adelaidean metasediments. Gravity modelling also indicates that the Anabama Granite extends to a depth of approximately 15 km.

1.2 Previous Investigations

Previous investigations into the Anabama Granite are minimal. The bulk of the work carried out to date has focussed on the possibility of economic copper and molybdenum mineralisation being associated with the Anabama granite. Very little work has been undertaken to investigate the geochemical and isotopic nature of the Anabama Granite and any relationship to the Delamerian granites of the Southern Adelaide Fold Belt.

Regional geochemical sampling by Blissett and Mason, in 1966 at Netley Hill, initiated recognition of possible copper and molybdenum mineralisation associated with the Anabama Granite. In December 1969, Asarco (Aust.) Pty. Ltd. commenced a programme of geological mapping, petrological sampling, grid based rotary percussion drilling, and diamond drilling of three holes at Anabama Hill (DDH 1, 2, and 3). Asarco relinquished the lease in December 1970. Then Blissett and Reed undertook further investigations in the area during 1971 - 1972. An I.P. survey, supported by a rotary drilling programme, petrological and geochemical studies and extended mapping, resulted in recommendations for future investigation. Further exploration at Anabama Hill by the South Australian Department of Mines and Energy was begun with the acquisition of Exploration Licences (E.L.) 16 (1972 - 1974) and E.L. 173 (1975 - 1976). Investigations, inclusive within E.L. 173, comprised of soil sampling, three diamond drill holes (DDH 4, 5, and 6) and a magnetometer survey over the greisen - granite complex at Anabama Hill.

A minor investigation of the gravity and magnetic anomalies created by the Anabama Granite was completed as part of a PhD, by Tucker, at Adelaide University in 1972.

Since 1977 exploration interest has declined abruptly at Anabama Hill due to the lack of success in finding economic mineralisation. However, during 1980 Richards undertook an Honours project titled "Copper and Molybdenum Mineralisation Associated with the Anabama Granite, Olary Region, S.A."

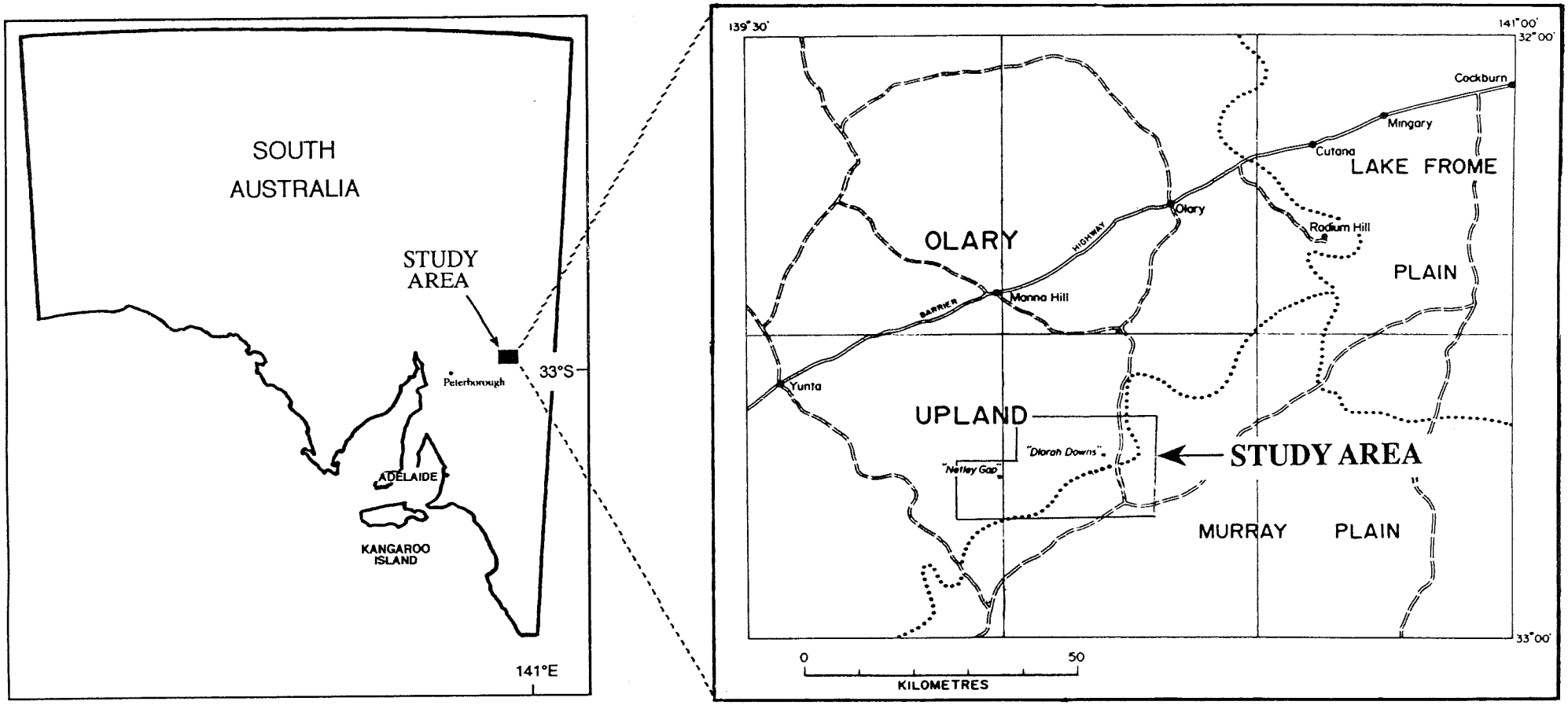

FIGURE 1a - Location of study area within South Australia

CHAPTER 2 - REGIONAL GEOLOGY

2.1 Regional Geology

The study area encompassed the majority of the interpreted Anabama Granite outcrop and areas with suspected outcrop of related dykes. A regional coverage of approximately 400 km^2. In general, the topography grades from undulating low hills, in the north, to salt bush covered plains, in the south. Within the study area only two prominant regions rise up from the plains, namely Anabama Hill and Netley Hill.

The Anabama Granite, together with the Bendigo granite (approximately 100 km SW of the field area) and the Bungadillina suite (Peake and Denison Ranges, northern South Australia), are the only Delamerian granites to intrude Adelaidean metasediments. The metasediments hosting the Anabama Granite trend NE - SW and are predominantly tillites, quartzites, siltstones, dolomites and slates. Regional metamorphism of the sediments has occurred to greenschist facies, with the formation of a 300m wide contact metamorphic aureole to almandine / amphibolite facies, around the granite.

Phases of folding and metamorphism, during the Delamerian Orogeny, produced broad anticlinal and synclinal structures, locally represented by the Wadnaminga Anticlinorium and Yunta Syncline.

The Anabama Granite is a northeasterly trending, elliptical shaped body, approximately 65 km long and up to 13 km wide. The strike of the body is concordant with surrounding metasediments on a regional scale (~ 070°), while being locally crosscutting. At the only observed contact with the host metasediments north of Netley Hill (Figure 27), the Anabama Granite dips at approximately 55° to the NW. The Anabama Granite is primarily exposed as low profile superficial outcrops (Mirams, 1961), dispersed amongst more recent sediments of the Murray Basin, which extend to the south and south east.

Blissett and Reed (1973) suggest that the intrusion of the Anabama Granite may have taken place along a complex fault zone on the southern limb of the Wadnaminga Anticlinorium. Evidence is based upon the interpretation of lineaments from Landsat imagery.

Examination of regional magnetic and Bouguer anomaly maps for the Olary region reveal distinctive signatures associated with the Anabama Granite.

The Anabama Granite is relatively non - magnetic when compared to nearby metasediments. This is rather surprising, since the granite contains magnetite and is generally quite iron rich. Nevertheless, the north eastern half of the anomaly appears

noisier and slightly more magnetic than the south western half, which may be indicative of two separate plutons (Boyd, 1992, pers. com.). There is no further evidence, as yet, which supports this notion. The Anabama Granite is also responsible for producing a very large negative Bouguer gravity anomaly. However, it is possible that the main geophysical signatures are not due to the Anabama Granite but to something underneath.

2.2 Anabama Granite

Sampling of the Anabama Granite was from field outcrops and drill core (Appendix 5). It displays varying degrees of hydrothermal alteration, from fresh material through to highly altered greisen, with quartz and muscovite as the dominant mineralogy. Between these extremes are varying degrees of partially altered granite whose mineralogy is essentially dominated by epidote, potassium feldspar and chlorite alteration of the unaltered granite.

In unaltered outcrop, the Anabama Granite occurs as a massive, homogeneous, coarse - grained, biotite rich granite (Plate 1), whose dominant mineralogy is quartz, plagioclase and biotite with minor hornblende. The granite, on the whole, is unfoliated, but in the vicinity of Anabama and Netley Hills a near vertical, approximately east - west trending foliation has developed (Plate 2), often associated with small, discrete shear zones. This foliation is interpreted to have formed after the emplacement of the granite, during periods of hydrothermal alteration and brecciation, as observed at Anabama and Netley Hills.

Occasionally, xenoliths of hornblende bearing mafic material, are included within the granite (Plate 3). It is most probable that these represent the sampling of a mafic source material of the granite.

The contact of the Anabama Granite with surrounding metasediments is rarely seen due to the cover of more recent sediments. When observed north of Netley Hill (Figure 27), it occurs as a sharp obvious contact with little evidence for large scale perturbations of granitic material into the metasediments (Plate 4). However, in a few locations, small granitic veinlets and occasional pegmatite dykes radiate out from the main granite body (Plate 5).

Deformation, associated with the main granitic intrusion, appears to be minimal. There is, however, evidence of small granite veinlets intruding the metasediments and subsequently folded by the rising pluton (Plate 5), which implies plastic deformation. This deformation is restricted to the margins of a small body north of the main outcrop, north of Boulder Dam (Figure 25).

2.3 Granophyre

A microscopically fine grained pale pink to yellow granophyre occurs at the contact between the Anabama Granite and Adelaidean metasediments, north of Netley Hill. The granophyre varies in width, from 30 - 50 cm, and may be the result of rapid cooling due to large thermal gradients at the granite / sediment interface. This is essentially a contact metamorphic affect, as described by Ramakrishnan and Bhattacharyya (1985). The occurrence of a granophyre at the granite margin is good evidence for the contact being of an intrusive nature rather than a faulted one. It also suggests that the bulk of the granite mass has had little contact and interaction with the present host rocks, as implied by the lack of metasedimentary xenoliths. Consequently, the Anabama Granite would have gained the bulk of its geochemical and isotopic signature early on in its history.

A small outcrop of a finer grained (2 - 4 mm) granophyre was observed approximately 1 km west of Boulder Dam. The presence of an outcrop of granophyric material in the middle of the main granite outcrop may suggest that only the very upper most portion of the Anabama Granite is currently exposed.

2.4 Introduction to Dyke Rocks

Several episodes of dyke rock are associated with the Anabama Granite. The acid and intermediate dykes are directly related to it while the microgranodiorite dykes, aplite dykes, quartz porphyry and dacite porphyry and lamprophyre dykes are generally later and crosscutting. Some of the later dykes are associated with the hydrothermal alteration seen within the Anabama Granite, and often observed to be hydrothermally altered themselves.

2.4.1 Acid and Intermediate Dykes

Both acid and intermediate dykes intrude the Adelaidean Metasediments north of the main granite outcrop (Figure 25). In the field the dykes vary in width, from 0.5 m to 2 - 2.5 m, and in strike length, from 50 m to several hundred metres.

The dykes are brown to grey in colour with a massive homogeneous appearance. Occasional fabrics occur within the dykes parallel to the strike and interpreted as intrusive in nature.

The orientation of the dykes is variable with respect to the regional metasediment fabric. Some dykes crosscut the strike of the metasediment cleavage while others are

aligned parallel to the cleavage. Those dykes parallel to the cleavage may have used it as a weakness and hence intruded along it.

Higher grade metamorphic zones are observed adjacent to some dykes. Within a 1 - 2 m wide contact metamorphic zone, andalusite mineral growth is seen.

2.4.2 Microgranodiorite Dykes

The microgranodiorite dykes are primarily light grey to white in colour and have a dominant mineralogy of quartz, plagioclase, potassium feldspar and variable amounts of biotite.

The majority of these dykes occur in and around Anabama Hill (Figure 26). They trend approximately north - south and outcrop with strike lengths between 5 and 30 m and widths up to 1.5 m. They generally have a massive, fresh appearance and are seen to crosscut the already altered granite.

El - Raghy (1980) suggests that the microgranodiorite dykes seen at the surface are representative of a much larger stock at depth. Diamond drill core taken from the area shows no indication of a large microgranodiorite body at depth, however, they do intersect microgranodiorite dykes which display clear crosscutting relationships (Appendix 5).

2.4.3 Aplite Dykes

Aplite dykes occur only in the vicinity of Anabama Hill (Figure 26). They occur as pale pink, fine grained rocks and have a dominant mineralogy of quartz and potassium feldspar.

The aplite dykes exhibit a crosscutting relationship with respect to greisened granite, however, the timing of the intrusion and relationship to other bodies, such as the microgranodiorite dykes, is unknown.

2.4.4 Quartz Porphyry

The quartz porphyry outcrops as a grey, very fine grained rock with small (2 - 3 mm) quartz phenocrysts. Small (2 - 3 mm), platy biotite grains are seen in some fresh examples. Fresh, unaltered dykes of quartz porphyry are seen at Netley Hill, Anabama Hill and north of Boulder Dam (Figures 25, 26 and 27), with hydrothermally altered quartz porphyry present at Anabama Hill (Figure 26).

In general, the unaltered quartz porphyry appears to post date and crosscut the hydrothermally altered variety. This indicates (as suggested by Blissett and Reed (1973), El - Raghy (1980) and CSR Ltd. (1982)), that Anabama Hill may be a site of on-going igneous and hydrothermal activity.

2.4.5 Dacite Porphyry

Dacite porphyry dykes - or, according to CSR Ltd. (1982), porphyritic microdiorites - are seen outcropping north of Netley Hill (Figure 27), at Anabama Hill (Figure 26) and in drill core (Appendix 5). A clear crosscutting relationship is displayed in all three areas.

The dacite porphyry dykes have a fresh appearance and occur as a black, fine grained matrix with plagioclase and occasional biotite phenocrysts (≤ 4 mm). Dykes vary in width, from 1 - 2 m, and in strike length from 100 - 200 m to over 1 km.

Field relationships of the dacite add another dimension to the already complicated thermal and igneous history. North of Netley Hill the dacite porphyry clearly crosscuts the granite (Plate 6) and the fabric of the surrounding metasediments (Figure 27). The dacite exhibits flow banding and contains xenoliths of greisened granite material (Plate 7). This suggests that the phase of dacite porphyry intrusion post dates the hydrothermal alteration of the Anabama Granite.

On top of Anabama Hill there is an altered dyke rock with a quartz / muscovite mineralogy and relict porphyritic textures. The trend of this dyke corresponds to an unaltered dacite porphyry, crosscutting altered granite, lower down on the slopes of Anabama Hill. It is interpreted that these two exposures represent the same dyke and that hydrothermal alteration to part of it has occurred. An indication that at least two stages of hydrothermal alteration have occurred in the area.

2.4.6 Lamprophyre

A single lamprophyre dyke outcrops north of Palina Dam (Figure 25). The lamprophyre has a dark grey to black appearance with abundant mica phenocrysts. It has a width of approximately 1.5 - 2 m, strikes approximately north - south crosscutting the regional metasediment fabric, for over a length of 1 km. The lamprophyre dyke has not caused any obvious alteration to the host Adelaidean metasediments.

The lamprophyre is generally massive but does show some signs of a fabric parallel to the strike of the dyke. This is most likely the result of the intrusive forces acting on the

dyke. Small faults trending approximately 070°, with displacements between 10 - 30 m, crosscut the lamprophyre dyke.

Xenoliths of metasediment were included within the dyke along with evidence of finer grained chilled margins.

Lamprophyres have previously been documented from elsewhere within the Adelaide Fold Belt. They have been noted in the Peake and Denison Range (Morrison & Foden, 1991), associated with the Reedy Creek granodiorite (Moeller, 1980), elsewhere within the Olary region (Forbes, 1991) and (of greater interest for diamond exploration) are the Truro lamprophyres (Morris, 1991).

The relationship between the lamprophyre dyke of this study and previously discussed lithologies and hydrothermal activity is unknown.

2.5 Metamorphism

Locally, the Anabama Granite is flanked to the south by the Sturtian Paulco Tillite and to the north by the Paulco Tillite and the Mintaro Shale and the siltstone and dolomite rich Saddleworth Formation of the Burra Group.

Regional metamorphism during the Delamerian Orogeny has affected these sediments and metamorphosed them to greenschist facies, creating a prominent slaty cleavage. Intrusion of the Anabama Granite locally metamorphosed the surrounding sediments to almandine / amphibolite facies. Coarse spotting is observed within the sediments in the vicinity of the Anabama Granite and appears to be the result of concentrations of muscovite and / or sericite, which may be remnants of andalusite porphyroblasts, formed by the contact metamorphism. Blissett and Reed (1973) suggest that the limit of spotting in the metasediments marks the limit of contact metamorphism. The situation is a little more complicated, however, as the bulk chemistry of the metasediments plays a critical role. Porphyroblast growth appears to only have occurred in the more alluminous sediments.

Towards the northeastern end of the granite exposure, north and west of Pine Bore (Figure 25), porphyroblast growth is large ($\leq$ 1 cm) and obvious. Here, the metasediments form part of the Saddleworth Formation. Yet, towards the centre and south western end of the granite exposure, the Paulco Tillite and Mintaro shale, respectively, lie closest to the granite contact. The Paulco Tillite shows little evidence of porphyroblast growth while the Mintaro shale exhibits only small ($\leq$ 5 mm) porphyroblasts whenever present.

2.6 Hydrothermal Alteration

Hydrothermal alteration of the Anabama Granite has occurred at some stage after its emplacement. The timing and igneous rocks associated with the alteration event(s) is uncertain but is partly constrained by the intrusive sequence and age of the dyke rocks.

The progressive hydrothermal alteration is reflected in the mineralogy of rock types found in the area. The sequence of fresh through to hydrothermally altered rocks displays a progressive increase in muscovite, sericite, epidote, chlorite and quartz alteration with the final composition being a quartz - muscovite assemblage or greissen. Studies by Blissett and Reed (1973) and Morris (1977) attempted to equate the Anabama Hill prospect with typical porphyry copper deposits. Their studies concluded that there were marked dissimilarities in observed and expected alteration zones. Richards (1980) recognized that rock types, mineralization, hydrothermal alteration and geological characteristics observed were similar to porphyry copper deposits, but stated that the classification as a porhyry copper deposit was invalid.

Interestingly, porphyry style copper deposits are often associated with subduction zone magmatism in other orogenic belts.

2.7 Metasedimentary Strain Analysis

Strain analysis was carried out on deformed retrogressed porphyroblasts from within the Saddleworth Formation, north of Pine Bore (sample A981 - 122, Figure 27). The strain analysis method used was the Rf / Ø technique.

The sample was cut along the X and Z planes, then the porphyroblasts were traced and digitized into the Macintosh computer. The data was manipulated and plotted as a Rf / Ø diagram using INSTRAIN, a strain analysis program. The results are shown in Figure 3.

From the Rf range of Figure 3, Ri (initial axial ratio) and Rs (strain ratio) were calculated via the following equations (the graphical method of calculating Rs and Ri, developed by Dunnet, was not used due to the lack of suitable graphs to fit the INSTRAIN produced Rf / Ø plot).

$Rs > Ri$ $\qquad Ri = (Rf\ max / Rf\ min)^{1/2}$ $\qquad (1)$

$Rs = (Rf\ max \cdot Rf\ min)^{1/2}$ $\qquad (2)$

From Figure 3, the initial ratio Ri = 1.50 and the final ratio Rs = 1.66 were established. Percentage shortening in the XZ plane may also be determined via the following equation:

$$\% \text{ shortening} = ((r-z) / r) * 100 \qquad (3)$$

where $r = (x^2 * z^2)^{1/2}$

$x = 1$

$z = 1.105$ (from Figure 3)

Therefore, from equation 3, the percentage shortening exhibited within these deformed porphyroblasts is 9.50 %, which is considered to be minimal and representative of low grade deformation.

Hence, from this and from the overall shape of the porphyroblasts in 3 dimensions, the deformation of the porphyroblasts is related to simple flattening rather than simple extension. Suggesting that the porphyroblasts were deformed as a result of the forces associated with the intrusion of the Anabama Granite, rather than the regional deformation and extension associated with the Delamerian Orogeny. Consequently, the deformation of the porphyroblasts, and hence the granite intrusion, post dates the deformation associated with the Delamerian Orogeny.

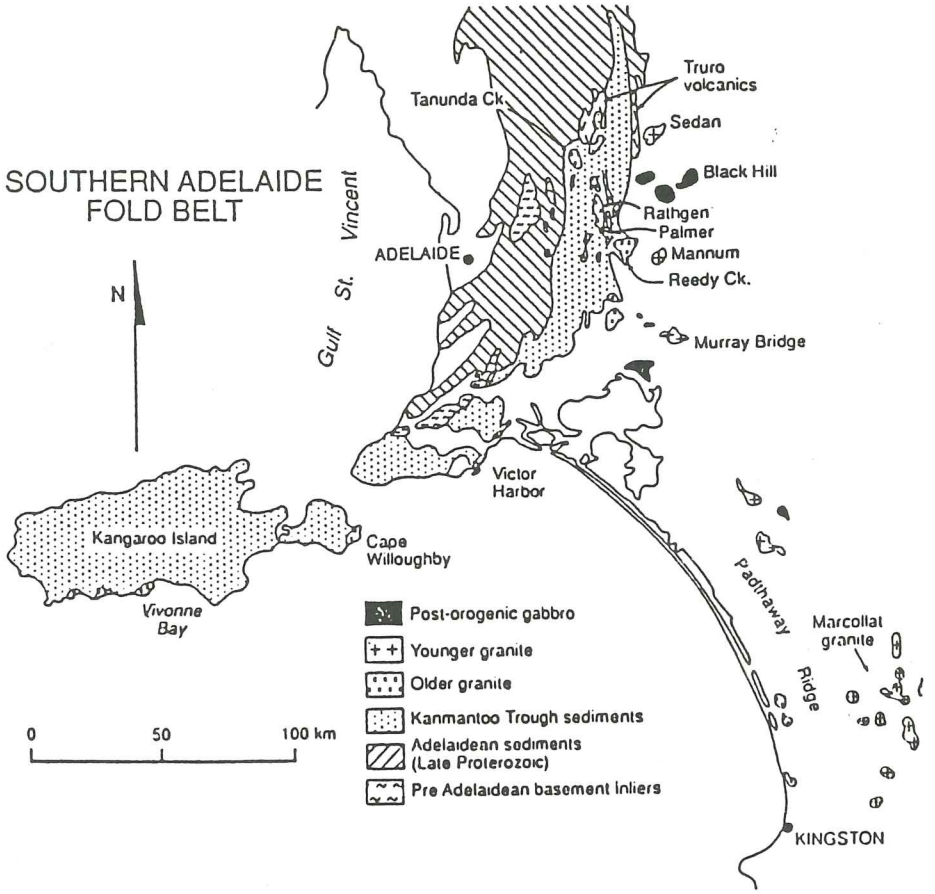

FIGURE 1b - Geological map showing the distribution of magmatic bodies within the southern Adelaide Fold Belt (Foden et al. 1992).

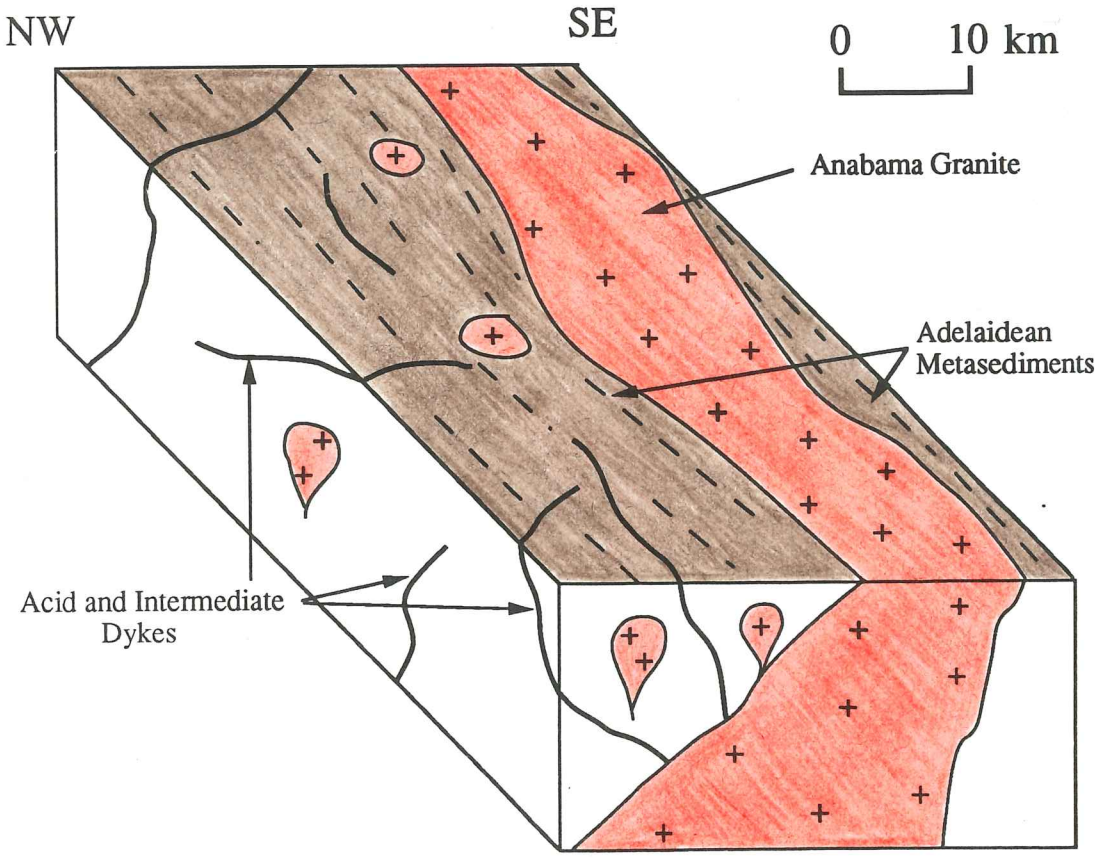

FIGURE 2 - Block diagram showing the characteristic features to the north of the main granite outcrop.

CHAPTER 3 - PETROGRAPHY

3.1 Introduction

The following chapter summarizes the important aspects of the petrography and mineralogy of the major lithologies of the "Anabama Complex" and surrounding area. Hand specimen descriptions and detailed thin section descriptions are documented in Appendix 1. Mineral compositions are tabulated in Appendix 2 and sample locations are shown in Appendix 5 and on Figures 22,23 and 24.

3.2 Anabama Granite

The Anabama Granite is coarse grained, holocrystaline and homogeneous, with major constituents of plagioclase (35 - 65 %), quartz (25 - 47 %), biotite (3 - 10 %) and potassium feldspar (4 - 20 %).

Plagioclase occurs as large subhedral grains (0.5 - 6 mm) with compositions which vary from andesine to oligoclase (Ab 54 - 74). Most grains exhibit brilliant examples of multiple twinning or concentric zoning. Concentrically zoned examples display variable compositions. Some grains occur with cores being more calcic than the rims, while others have more sodic cores. Minor sericitization of the plagioclase is common.

Large anhedral to subhedral quartz grains (0.5 - 5 mm) are present throughout the sections. Varying degrees of undulose extinction were observed, ranging from slight to quite strong.

Ferromagnesian minerals are present and include both biotite and hornblende.

Biotite occurs as light brown to dark brown subhedral grains, up to 5 mm in length. It is often hydrothermally altered to chlorite, muscovite and granular epidote ; and association with subhedral to euhedral hexagonal lozenge shaped apatite, subhedral to euhedral opaque grains, euhedral sphene, zircons and hornblende.

Zircons, up to 0.5 mm in size, are present as inclusions within biotite grains, complete with distinctive alteration haloes.

Hornblende (approximately Ca28:Mg40:Fe32) occurs as medium grained (1 - 2 mm) anhedral to subhedral, irregular to stubby prismic grains. It is dark green in colour, with some grains displaying simple twinning (Plate 8). The hornblende concentration decreases with increasing silica concentration.

Early crystalizing euhedral diamond shaped sphene, up to 6 mm long, are present in most sections (Plate 9). Pseudomorphs of opaques, usually titaniferous magnetite, after sphene, are seen in some sections.

Potassium feldspar is present as small anhedral to subhedral grains which display variable degrees of sericitization and remnant carlsbad twinning.

Mineral crystalization has tended to follow that of the Bowen's reaction series. Although plagioclase is in a seperate series to the Fe - Mg minerals, sphene, apatite and Na - Ca plagioclase all crystalized early, while twinned hornblende may have been as early as the plagioclase with biotite crystalizing slightly later, forming anhedral to subhedral grains. The crystalization of quartz and minor amounts of potassium feldspar, in the form of anhedral masses, composed the remaining grains.

3.3 Granophyre

The granophyre consists of fine grained quartz, potassium feldspar and plagioclase.

A spectacular granophyric texture (Plate 11), formed due to a complex eutectic intergrowth of quartz and microcline.

The limits of orthoclase is defined by minor sericitization and relict carlsbad twinning.

Fine ($\leq$ 0.5 mm) anhedral quartz and microcline along with small ($\leq$ 0.5 mm) subhedral plagioclase grains, form the general groundmass between the granophyric areas. Quartz displays non - undulose extinction.

Small subhedral needle like biotite, and opaques are rare.

3.4 Acid and Intermediate Dykes

Both the acid and intermediate dykes contain quartz, plagioclase and potassium feldspar as the dominant mineralogy. Acid dyke compositional variations were quartz (30 - 60 %), plagioclase (10 - 30 %) and potassium feldspar (25 - 36 %) ; while intermediate dyke variations were quartz (30 - 40 %), plagioclase (28 - 35 %) and potassium feldspar (20 - 25 %).

Acid dykes are predominantly fine grained, with subhedral plagioclase phenocrysts ($\leq$ 3 mm), oligoclase in composition (Ab 73 - 87). Multiple twinning and sericitization are characteristic features of the phenocrysts. Sample A981 - 40 also contains potassium feldspar phenocrysts, which display relict carslbad twinning.

The fine matrix consists of quartz and potassium feldspar. Potassium feldspar occurs as small subhedral elongate grains, while quartz occurs as both small (~ 0.5 mm) rounded regular grains and as a finer matrix filling.

Biotite, when present, occurs as small (≤ 1 mm) straw coloured subhedral grains disseminated throughout the section, with minor alteration to epidote in places.

Chlorite occurs as fine disseminations and as larger (≤ 1 mm) anhedral grains, often with a high potassium content (≤ 1 %).

Opaques are present as euhedral blocky grains (≤ 0.2 mm) - magnetite ; fine needle like grains - ilmenite ; and anhedral ruby red grains - rutile.

Intermediate dykes consist of a predominantly fine grained matrix of quartz and feldspars, which support subhedral plagioclase phenocrysts (≤ 2 mm) displaying slight sericitization and characteristic twinning.

Chlorite occurs as large (≤ 2 mm) irregular grains and as subhedral blades (≤ 1.5 mm long). Traces of epidote are seen intergrown with chlorite.

Opaques are present as subhedral to euhedral blocky shaped grains, and as small needle like grains of magnetite and ilmenite.

3.5 Microgranodiorite Dykes

Microgranodiorite dykes are fine to medium grained, holocrystalline and display anhedral to subhedral grains (≤ 2 mm).

The dominant mineralogy of the microgranodiorite dykes is quartz, plagioclase, potassium feldspar and biotite.

Anhedral to subhedral quartz grains vary in size, ranging up to 2.5 mm in diameter, and displaying slightly undulose to plain extinction. Quartz also forms complex intergrowths with plagioclase at their grain boundaries, comonly known as a myrmektitic texture. The presence of this texture may suggest a slow cooling history for this rock.

Plagioclase occurs as anhedral to subhedral grains (0.5 - 4 mm) which exhibit either multiple twinning or concentric zoning. Plagioclase compositions were found to be oligoclase (Ab 75 - 85) and alteration to sericite is observed.

Potassium feldspar occured as both microcline and orthoclase, forming subhedral to euhedral grains (≤ 3 mm). Microcline exhibits characteristic cross hatched twinning, while orthoclase displays simple carlsbad twinning. Commonly, perthitic textures of albite rods replacing orthoclase and anti - perthite textures of microcline replacing plagioclase is seen. According to Tuttle and Bowen (1958), perthitic textures are a result of cooling in a very dry environment.

The dominant ferromagnesian mineral present is small light brown subhedral to anhedral biotite, although hornblende is observed in sample A981 - 4. Zircons, complete with alteration haloes, are common inclusions within most biotite grains. Muscovite and epidote are seen as alteration products of biotite.

Small (≤ 0.5 mm) euhedral opaques of magnetite and ilmenite, occur randomly distributed throughout the sections.

3.6 Aplite Dykes

Aplite dykes contain quartz and potassium feldspar as the dominant mineralogy.

Quartz displays a bimodal distribution. Small (≤ 0.5 mm) rounded grains and larger (≥ 1 mm) irregular anhedral grains are present. The smaller grains exhibit straight extinction, while the larger grains display slight undulose extinction.

Potassium feldspar occurs as large (≤ 5 mm) subhedral orthoclase and microcline. Microcline exhibits characteristic tartan twinning and anti - perthite textures, while orthoclase displays simple carlsbad twinning and perthitic textures.

Plagioclase is present as smaller (1 - 4 mm) subhedral grains which display multiple twinning or concentric zoning.

Straw coloured biotite and small opaques occur only in trace amounts.

3.7 Quartz Porphyry

The dominant mineralogy of the quartz porphyry is essentially quartz, plagioclase and potassium feldspar.

Quartz and potassium feldspar form a fine granophyric texture, with a radiating appearance (Plate 10). Quartz and plagioclase occur as subhedral phenocrysts (≤ 2 mm) ; with plagioclase displaying multiple twinning and quartz non - undulose extinction.

Both muscovite (≤ 0.2 mm) and biotite (≤ 2 mm) subhedral to euhedral grains occur throughout the section. The occurence of muscovite is irregular, while biotite grains tend to aggregate together.

Opaques are rare.

3.8 Dacite Porphyry

The dacite porphyry consists primarily of a very fine grained originally glassy matrix, supporting plagioclase phenocrysts (Plate 12).

Small (0.2 - 4 mm) subhedral plagioclase phenocrysts are labradorite to oligoclase in composition (Ab 49 - 72). Some cores display more sodic compositions than the rims, while some grains display more calcic cores. These phenocrysts exhibit both multiple twinning and concentric zoning.

Very fine grained quartz and biotite dominate the groundmass. This fine grained biotite gives the rock a dark grey / black appearance. Larger subhedral biotite grains and small subhedral to euhedral opaques are rare.

3.9 Lamprophyre Dyke

This rock type consists of a fine grained matrix, supporting dominantly biotite and phlogopite phenocrysts.

Biotite (Mg # 50 - 65) and phlogopite (Mg # > 80) typically occur as small ($\leq$ 1 mm) elongate subhedral to euhedral phenocrysts. Biotite is distinguishable from phlogopite by a much lighter colour under transmitted light (Plate 13). Plate 13 indicates that both the biotite and phlogopite phenocrysts are aligned to a flow foliation, with biotite being light brown while phlogopite is dark brown to orange in colour. Phlogopite grains often display zoning, becoming darker and more magnesium rich towards the rims. It is, therefore, interpreted that both biotite and phlogopite occur as primary mineral phases. There is no textural evidence that suggests that the biotite is present as a replacement of phlogopite.

Chlorite occurs as light green potassium rich ($\leq$ 3 %) anhedral masses which, together with calcite, appear to have replaced what may have been round olivine phenocrysts ($\leq$ 3 mm) (Plates 14a and 14b). Calcite displays high order birefringence, occasional twinning and is often replacing chlorite.

The groundmass is predominantly fine grained quartz, plagioclase, which is oligoclase to albite in composition (Ab 73 - 97), and potassium feldspar.

Very small ($\leq$ 0.1 mm) subhedral to euhedral opaques are disseminated throughout the section (Plate 13). Compositions vary from magnetite to titaniferous magnetite to chromite.

Petrographically, the lamprophyre samples from this study are very similar to the Truro lamprophyre samples described by Morris (1991).

3.10 Metasediments

Metasedimentary thin sections are dominated by quartz, muscovite and sericite, which define a prominant foliation.

Quartz occurs as small (≤ 0.1 mm) anhedral grains which display slight undulose extinction. Quartz is also present as larger recrystalized and rotated grains in some sections (Plate 15).

Muscovite forms subhedral elongate grains, often aggregated together to form schlieren (≤ 0.5 mm). The muscovite, together with opaques in some sections, define a prominant foliation and sometimes weakly developed crenulation cleavage (Plate 15).

Remnant, possibly andalusite porphyroblasts (≤ 10 mm), display primary, sometimes rotated, fabrics. These porphyroblasts have undergone retrogression to quartz and very fine grained sericite.

Various accessory minerals such as epidote, biotite and tourmaline are also seen.

Plate 1 - Typical diamond drill core sample of the Anabama Granite. This sample displays the abundance of plagioclase and biotite within the granite. Sample A981 - 154, DDH - 5, depth 120.3 m.

Plate 2 - Typical field outcrop of Anabama Granite displaying weakly developed near vertical foliation. Photo was taken on the northern slopes of Anabama Hill.

Plate 3 - Hornblende bearing xenolith within an outcrop of coarse, massive unfoliated Anabama Granite, approximately 1.5 km north of Boulder Dam.

Plate 4 - The northern contact between the Anabama Granite and host Adelaidean metasediments with the granophyre occurring at the interface. Bag in the centre of the plate is approximately 50 cm tall.

Plate 5 - Hand specimen from adjacent to a small granitic intrusion north of the main body, approximately 1.5 km north of Boulder Dam. Note the folding of metasediments and small granitic veins. Sample A981 - 142.


1
0
2 cm


4


2


3


5
0
5 cm

Plate 6 - Dacite Porphyry dyke crosscutting the Anabama Granite, approximately 100 m north of the tank SW of Netley Gap Well.

Plate 7 - Dacite porphyry dyke at the tank SW of Netley Gap Well containing xenoliths of greisen. Indicating the intrusion of the dacite porphyry post dates the hydrothermal alteration of the granite.

Plate 8 - Photomicrograph showing a typical lozenge shaped apatite crystal from within the Anabama Granite. Crossed polars. Sample A777 - 179.

Plate 9 - Photomicrograph of a typical section of Anabama Granite showing twinned hornblende (H), euhedral sphene (S) and apatite (A). Crossed polars. Sample A981 - 153.

Plate 10 - Photomicrograph of the quartz porphyry showing the radiating granophyric texture. Crossed polars. Sample A981 - 100.

Plate 11 - Photomicrograph of the granophyre showing the spectacular granophyric intergrowth of quartz and feldspars. Crossed polars. Sample A981 - 54.

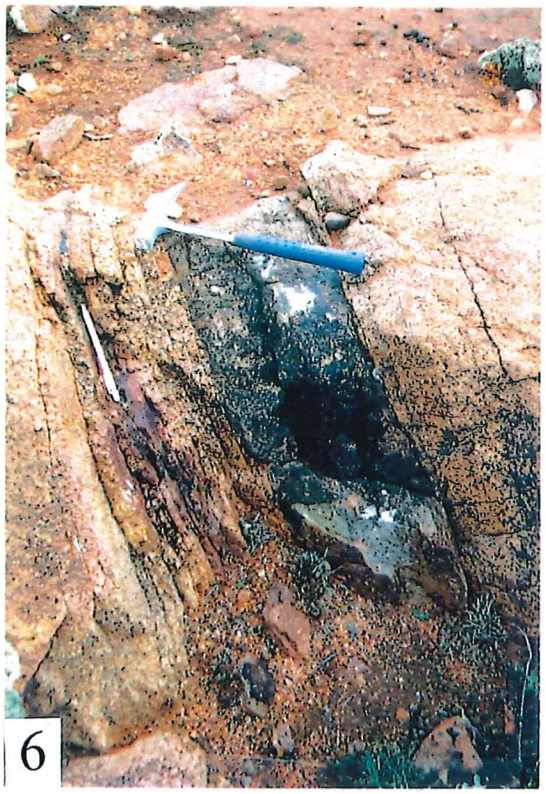

6

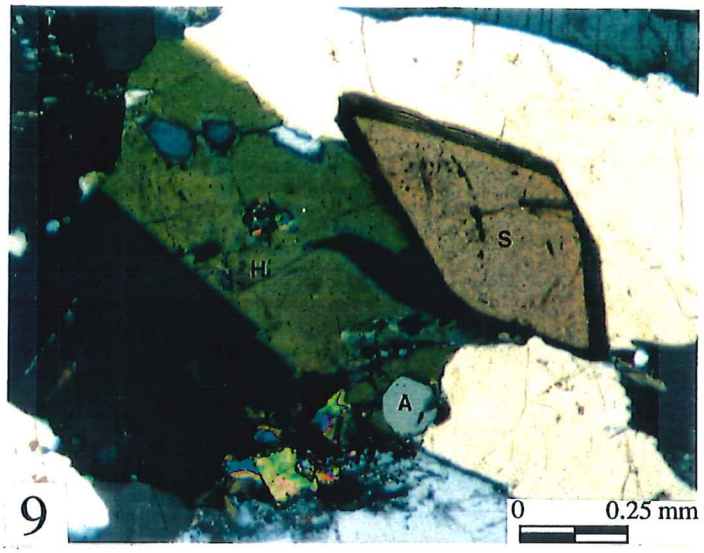

9

7

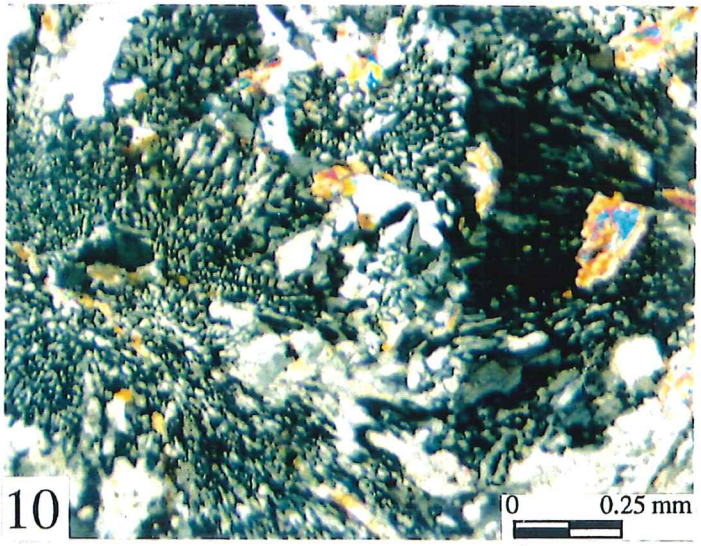

10

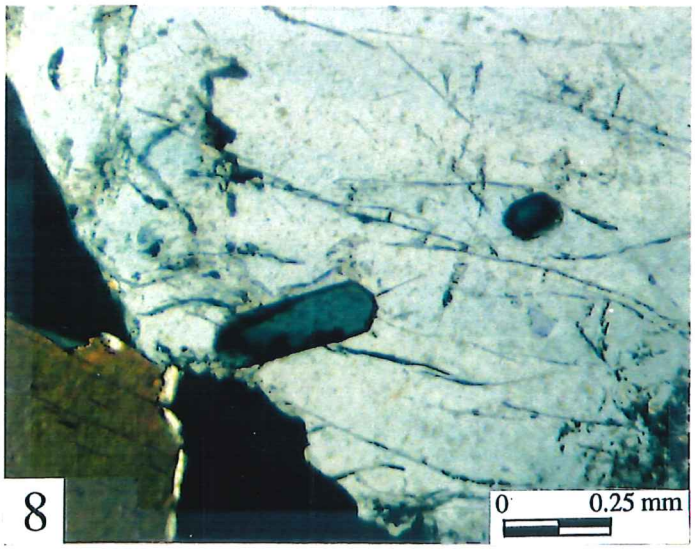

8

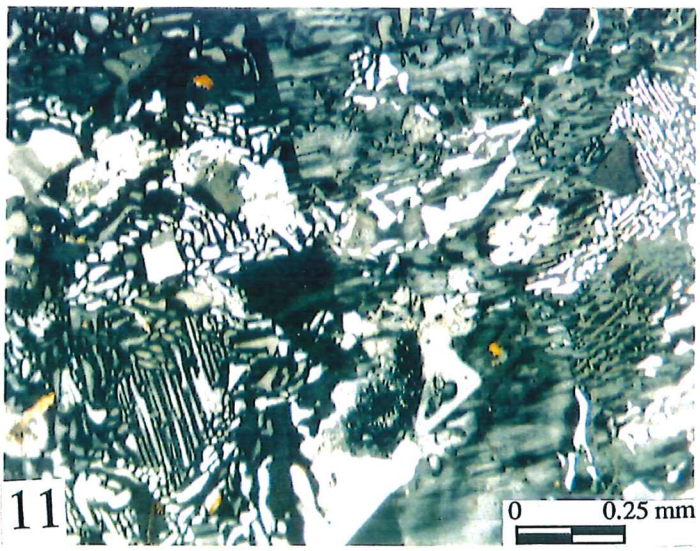

11

Plate 12 - Photomicrograph of plagioclase phenocrysts (P) supported by a very fine grained biotite, quartz and feldspar rich matrix within the dacite porphyry. Crossed polars. Sample A981 - 45.

Plate 13 - Typical photomicrograph for the lamprophyre dyke showing flow oriented biotite (bt) and darker phlogopite (ph) phenocrysts. Also shown are the very fine disseminated opaque grains. Normal light. Sample A981 - 35.

Plate 14a - Photomicrograph taken under normal light showing dark phlogopite phenocrysts (ph) and round remnant olivine grains which have been replaced by calcite (Ca) and chlorite (Cl). Sample A981 - 35.

Plate 14b - Photomicrograph as in plate 14a but under crossed polars.

Plate 15 - Photomicrograph of a metasediment showing recrystalized and deformed quartz phenocrysts with a prominent cleavage and often crenulation cleavage development. Sample A981 - 122.

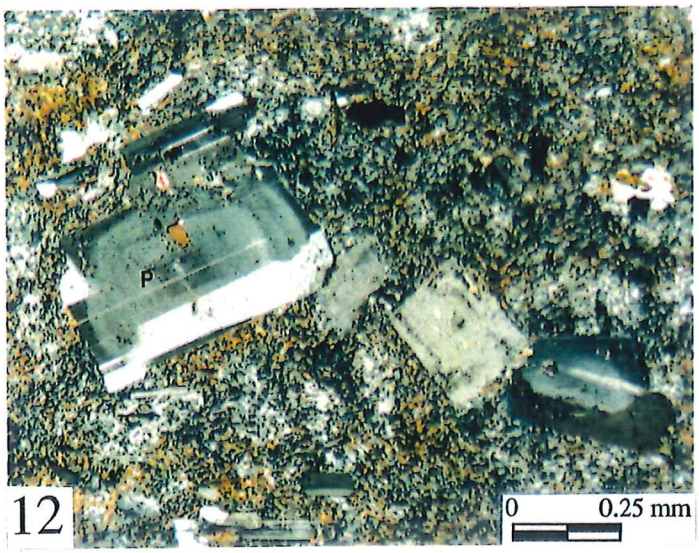

12

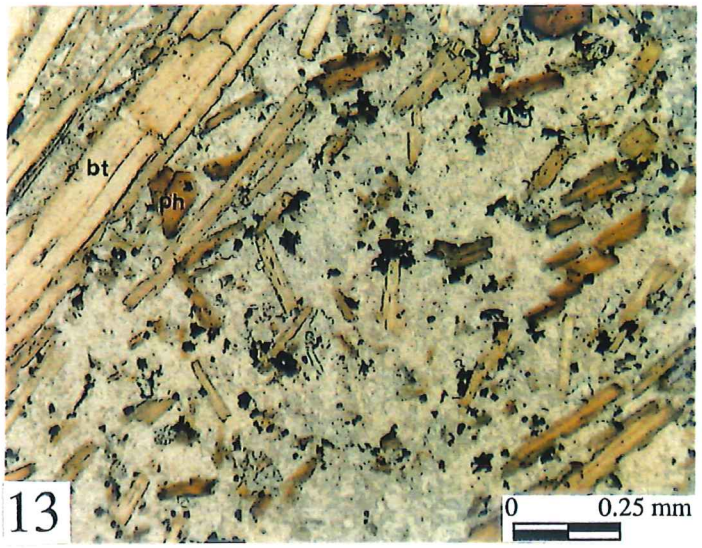

13

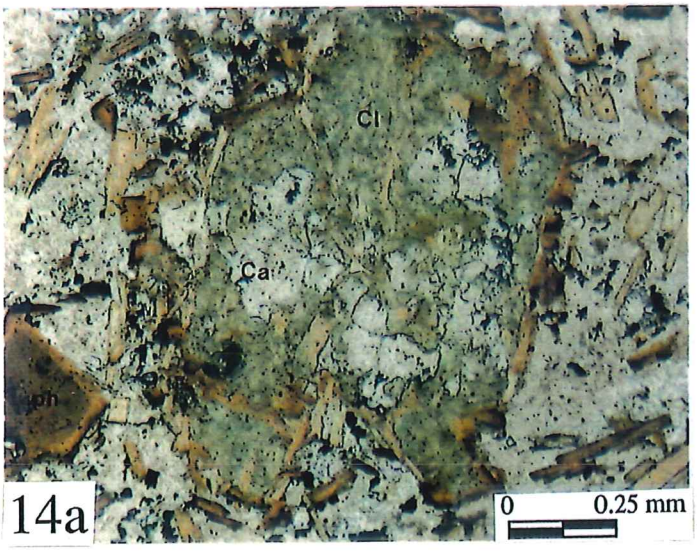

14a

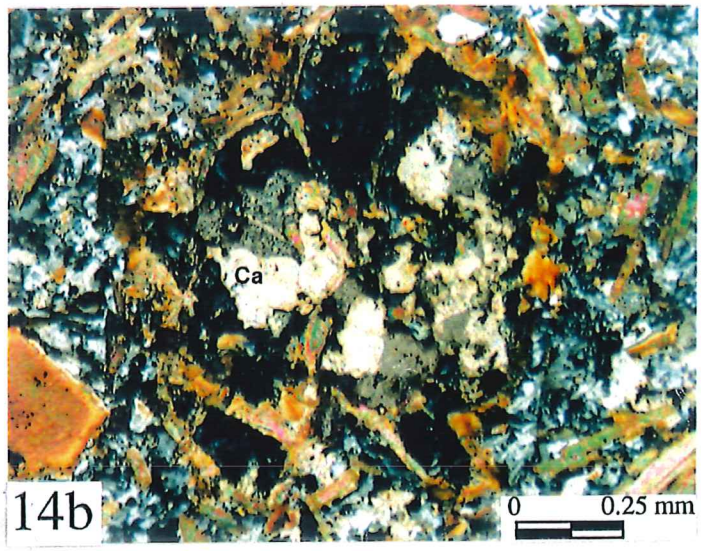

14b

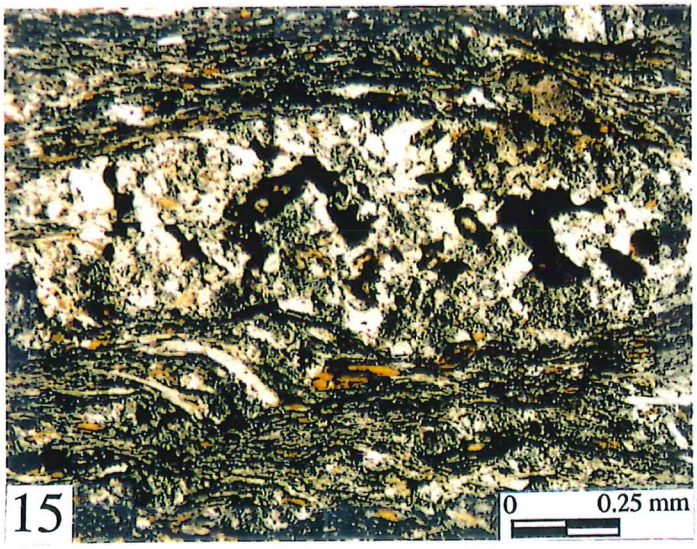

15

CHAPTER 4 - GEOCHEMISTRY

4.1 Introduction

The following chapter discusses results obtained from geochemical investigations. All major element, trace element and normative compositions mentioned are tabulated in Appendix 3. Individual mineral chemistries are listed in Appendix 2.

4.2 Anabama Granite

Although often documented in the literature as the "Anabama Granite", strictly, it is a granodiorite to tonalite to quartz monzodiorite / quartz diorite as defined by the classification of Streckeisen (1976), (Figure 4). However, for the sake of not diverting from the literature and for ease of discussion, it shall be referred to as the "Anabama Granite" throughout this paper.

The Anabama Granite displays a reasonable range in silica contents (60.42 - 60.88 %), as well as high aluminium (ave. 17.08 %), sodium (ave. 4.06 %) and calcium (ave. 4.1 %) contents. All samples analysed displayed a molar Al_2O_3 / (CaO + Na_2O + K2O) < 1.1 (Appendix 3), which, together with Na_2O contents > 2.2 %, classifies the Anabama Granite as I - type, using criteria established by Chappell and White (1974). However, all but one sample shows normative corundum rather than diopside (Appendix 3), which is more an S type characteristic.

Harker variation diagrams (Figures 8 and 9) for both major and trace elements, display the compositional variation within the Anabama Granite. For increasing SiO_2 contents the Anabama Granite displays increasing trends in some trace elements, such as Ba, Nd, La, Y and Zr. Trace elements with a negative correlation with SiO_2 are V, Sc, Sr, Ni, and Ga. Other trace elements display varied relationships with respect to SiO_2. Major elements such as Al, Ca, Fe, K, Mg and Ti display obvious decreasing linear trends with increasing SiO_2 content. Mn, Na and P show a more complex relationship but with overall decreases with increasing SiO_2.

Figure 6 shows the normative compositional variation of the Anabama Granite in the Q - Ab - Or ternary. It also shows that the Anabama granite plots away from the minimum melt positions of Tuttle and Bowen (1956).

Figure 7, after Kleeman (1965), shows that the Anabama Granite plots well away from the thermal trough. The Anabama Granite is also compared with other lithologies from the area in this diagram.

The Harker variation diagrams are consistent with the fractional crystallization of plagioclase and hornblende and / or biotite. Experimental work on granitic systems by Wyllie (1977) has shown for tonalitic to granodioritic compositions, hornblende and plagioclase will be liquidus phases for a large portion of their cooling history (approx. 1000° - 650°C). Barker et al. (1986) have also used hornblende and plagioclase fractionation to explain the variations in a graodioritic suite. Figure 5 shows a slight positive correlation between K / Rb and SiO_2, which, according to Taylor (1965), suggests that biotite may also play a role in fractional crystalization.

Modelling of major and trace elements during fractional crystallization (Appendix 4) of the Anabama Granite was undertaken. Results indicate that the fractional crystallization of a changing proportion of biotite, hornblende and plagioclase produce the chemical trends odserved in the Harker diagrams. Modelling of major elements proved quite successful, while modelling of trace elements left a little to be desired. This may be, as stated by Turner (1986), a result of the use of inadequate distribution coefficients for the trace elements or the failure to take account of minor phases with very high trace element K_D values (eg. apatite and zircon).

4.2.1 Mineral Chemistry

Biotites within the Anabama Granite display a limited range in compositions. Mg # varies from 52 - 55, indicating the biotites are neither magnesium nor iron rich. This is also displayed in Figure 10. Ti concentrations are generally quite high and range from 2 - 3.5 %. Figure 10 also shows the Anabama Granite and several other lithologies from within the study area. Similarities between the biotites from the microgranodiorites and the dacite porphyry are noticeable.

Plagioclase chemistries, for most lithologies, are displayed in Figure 11. The Anabama Granite displays quite a variable composition, Ab 54 - 74. The dacite porphyry plagioclase compositions display a tendency to form closer to the anorthite end member, while the acid dykes and microgranodiorite dykes tend to form closer to the albite end member.

4.2.2 Comparative Granite Geochemistry

Greater interest and research into the granites of western Victoria and the southern Adelaide Fold Belt, in particular, has substantially increased over the last ten to fifteen

years - for example, Milnes et al (1977), Mancktelow (1979), Moeller (1980), Turner (1986), Morrison (1988), Foden et al (1990) and Sandiford et al (1992) to mention a few.

These studies, together with many more, have provided an ever increasing isotopic and geochemical database of information. Consequently the classification of two isotopically and geochemically distinct groups of granites within the Adelaide Fold Belt has occurred :

(1) an older suite of dominantly I - type granites, with variably developed foliations and ages between 516 - 490 Ma, Sandiford et al. (1992); and,

(2) a younger suite of undeformed A - type granites associated with mafic magmas, with ages between 490 - 480 Ma, Sandiford et al. (1992), Turner et al. (1992).

Figures 8 and 9 show the comparative geochemistry between these two distinct groups through representative samples. The younger group of A - type granites are generally far more siliceous and depleted in all other major elements.

The Anabama Granite when compared to other Delamerian granites of the southern Adelaide Fold Belt, Figure 1b, is compositionally very similar with the Reedy Creek granodiorite and less similar to the Wando granodiorite of western Victoria. Both lithologies form part of the older I - type granites, and therefore, the Anabama Granite should also be classified as an older I - type granite.

Also plotted on Figure 8 is an average composition of a typical I - type granite suite - the Moruya Batholith, of New South Wales (Griffin et al., 1978). In comparison to the Anabama Granite, the average Moruya Batholith sample displays comparable SiO_2, CaO, Fe_2O_3, MgO, Na_2O and TiO_2 concentrations. It does, however, show a slightly lower Al_2O_3 concentration, significantly lower K_2O and P_2O_5 concentrations and slightly higher MnO concentrations. The range of compositions seen within the Moruya Batholith is slightly larger than those for the I - type granites of South Australia, but the trends shown by individual elements with increasing silica concentrations are very similar.

4.3 Granophyre

The main granophyre sample is A981 - 54. This sample contains 74.94 % SiO_2, low Al_2O_3 (13.54 %) and low Fe_2O_3 (0.45 %). A large potassium feldspar content is indicated by the high K_2O concentration (6.55 %). This sample also displays a high Rb / Sr ratio of 0.79 and a high Ba content (2196 ppm).

According to Barker (1983), granophyres contain roughly equal amounts of normative q, ab, and or, and therefore correspond compositionally to liquid at the minimum temperature on the solidus in the system $NaAlSi_3O_8$ - $KAlSi_3O_8$ - SiO_2, eutectic

intergrowth. Figure 6 shows such a diagram with the granophyre sample plotted. The granophyre sample does not plot exactly on the minimum temperature point, but does plot on the solidus for 3 k bars pressure at about 710 degrees C. Therefore, this gives a restriction on the depth from the surface at which the Anabama Granite was emplaced. The Anabama Granite was probably emplaced to within 9 - 10 km of the surface. These pressures and temperatures are also comparable with those needed for andalusite mineral growth seen in the metamorphic aureole.

4.4 Acid and Intermediate Dykes

Generally, the acid and intermediate dykes within the the field area have similar chemistries to that of the Anabama Granite. The major and trace elements are plotted against SiO_2 in Figures 8 and 9.

SiO_2 contents of the acid dykes vary from 68.92 % to 71.83 % - slightly more acidic than the most acidic sample of Anabama Granite. Al_2O_3, Na_2O and K_2O concentrations are all comparable with those measured for the Anabama Granite. However, TiO_2, Fe_2O_3, MnO, MgO, CaO and P_2O_5 concentrations are all down on the Anabama Granite concentrations. Significant trace element trends when compared to the Anabama Granite indicate lower V, Rb, Ce and Zr with increased Sr concentrations.

The trends discussed here and observed in Figures 8 and 9 may be the result of fractionation processes. Fractional crystallization modelling (Appendix 4) indicates that the acid dykes' chemistry can result from fractional crystallization of the most mafic Anabama Granite sample. Suggesting that the acid dykes are related to the Anabama Granite.

The intermediate dykes have chemistries similar to those of the Anabama Granite. SiO_2 contents range from 61.6 % to 64.55 % and only TiO_2, Fe_2O_3 and K_2O concentrations differing from those measured for the Anabama Granite samples.

Trace element geochemistry indicates that sample A981 - 47 has high Zn (118 ppm) and Sr (1116.9 ppm) contents and a relatively low Ba content (655 ppm). Sample A981 - 37, however, displays low Sr (305 ppm) and high Ba (1470 ppm) concentrations.

The normative compositions of the acid and intermediate dykes are plotted on Figure 7. This shows that these dyke rocks plot away from the field of the Anabama Granite and from the thermal trough, but towards the albite apex of the diagram.

Major and trace element modelling (Appendix 4) shows that the intermediate dykes may also form as a result of fractional crystalization with respect to the Anabama Granite. This indicates that the intermediate dykes observed are related to the Anabama Granite.

Loss on ignition values provide further evidence in support of the acid and intermediate dykes being fractionation products of the Anabama Granite. The loss on ignition for these dyke rocks is seen to be greater than those observed for the Anabama granite samples. For one intermediate dyke the value approached 4 %. This suggests a concentration of the more volatile components into these melts, which might be expect with the aforementioned model of formation.

4.5 Microgranodiorite Dykes

The microgranodiorite dykes are geochemically different to the Anabama Granite. Suggesting that the microgranodiorites do not constitute part of the recognized comagmatic series of granite and acid and intermediate dykes.

Some obvious major element trends are observed with increasing SiO_2 contents. Al_2O_3, CaO and Na_2O are seen to decrease while K_2O increases - a rise which may be evident as an increase in potassium feldspar, with respect to plagioclase, in more siliceous samples.

Trace element trends with increasing SiO_2 are increasing Rb and decreasing Sr concentrations.

The microgranodiorite dykes on an An - Ab - Or diagram (Figure 7) showed a trend towards the thermal trough of Kleeman (1965) with increasing SiO_2. Thus implying that the more siliceous microgranodiorite dykes represent minimum or near minimum melts.

4.6 Dacite Porphyry

The dacite porphyry dykes exhibit SiO_2 contents in a range from 68.5 % to 70.15 %, along with reasonable Al_2O_3 contents (15.2 - 16.1 %), CaO contents (2.58 - 3.47 %) and high Na_2O contents (4.56 - 4.8 %).

When plotted on Figure 7 the dacite porphyry dykes plot away from the thermal trough of Kleeman (1965) and near the field of the Anabama Granite.

Trace element considerations show low Rb, Ba and Zr contents with extremely high Sr contents (582.6 - 810.9 ppm). Rb / Sr ratios are in the order of 0.06 - 0.11. The lower Ba and Zr contents may reflect a more primitive source region of the dacite porphyry than for the Anabama Granite. The slightly more acidic nature of this rock type, however, indicates that it may have undergone a completely different thermal history to that of the Anabama Granite, - a point discussed further in Chapter 6 with the assistance of isotopic evidence.

4.7 Lamprophyre

The lamprophyre clan is a genetic term which includes kimberlites, lamproites and lamprophyres. From these three main sub-groups stem many other forms of classification and nomenclature of ultrapotassic igneous rocks, based on petrological and geochemical characteristics.

The lamprophyre petrology and geochemistry, when compared to all other lithologies within the area, is unique and distinctive.

Using the classification of Rock (1987), the samples analysed are of the calc - alkaline lamprophyre (CAL) variety, with further classification as a minette.

SiO_2 compositions are intermediate (ave. 55.29 %), with high TiO_2 (ave. 1.31 %), Fe_2O_3 (ave. 6.27 %), MgO (ave. 6.62 %), CaO (ave. 3.63 %), K_2O (ave. 7.11 %) and P_2O_5 (ave. 1.04 %). Both Al_2O_3 (ave. 13.12 %) and Na_2O (ave. 2.19 %) concentrations are reasonably low.

The trace element chemistry is very interesting. All indicators point towards a primative and possibly primary status for the lamprophyre, with nearly all trace elements analysed showing elevated values - tabulated in full in Appendix 2. Examples include Cr (ave. 361 ppm), Ni (ave. 140 ppm), V (ave. 178 ppm), Ba (ave. 1574 ppm), Zr (ave. 755 ppm), Th (ave. 103.5 ppm) and the LRE elements. Rb /Sr ratios are extremely high, at approximately 1.15.

Figure 10 shows the biotite and phlogopite mineral chemistries plotted on the Mg - Fe - Al ternary. There is a general trend between the biotites which have approximately equal amounts of Mg and Fe to the phlogopites which are Mg rich. Feldspar compositions are plotted on Figure 11.

Listed in Appendix 2 are average calc - alkaline lamprophyre analyses from Morris (1991) on the Truro Lamprophyres (32 samples) and from Rock (1987) on world wide examples (754 samples). It is interesting to note the similarities between the three sets of data. Examples from this study, however, show elevated K_2O values in comparison to data from Morris (1991) and Rock (1987) with lower CaO values with respect to the data from Rock (1987).

Further similarities between the sets of data include the very high Cr and Ni, implying equilibrium with an ultramafic peridotite source - but with LIL and high field strength elements, such as Ba and Rb. The data also shows very high Zr, with the Zr / Nb ratio being quite high.

Figure 12 shows a comparative plot between the lamprophyre of this study and those documented by Morris (1991) and Rock (1987). All three groups plot well within

the field of subduction and post collision related activity and well away from the locations remote from subduction field. Interestingly, Rock (1987) was able to show a strong correlation between CAL's and granitic igneous activity associated with orogenic belts. Therefore, it is suggested that the lamprophyres, associated with many granitic bodies of the Adelaide Fold Belt, may be sampling deep mantle material which was responsible for the heat influx, resulting in the generation of granitic melts.

FIGURE 3 - Rf / Ø plot for the strain analysis of deformed metasediments in the x/z plane.

FIGURE 4 - Normative, igneous rock classification diagram after Streckeisen (1976). Anabama Granite samples are shown to plot in the fields of Granodiorite (4), Tonalite (5), Quartz monzodiorite (9) and Quartz diorite (10). Typical granite plot in the fields of (2) and (3).

FIGURE 5 - A plot of K /Rb versus SiO_2 for the Anabama Granite showing a slight positive correlation indicative of biotite fractionation.

FIGURE 6 - Q - Ab - Or ternary diagram showing the Anabama Granite plotted as closed circles and the granophyre sample plotted as an open square. The granite samples plot away from the thermal minimum while the granophyre plots on the 3 kbar eutectic at approximately 710°C (after Tuttle and Bowen, 1958).

FIGURE 7 - An - Ab - Or ternary plot of normative compositions for selected lithologies. Most lithologies plot well away from the thermal trough of Kleeman (1965). The microgranodiorites form a linear trend towards the trough, as shown, with increasing SiO2 concentrations.

Legend for Figure 7

- ● Anabama Granite
- ■ Acid dyke
- □ Intermediate Dyke
- ○ Dacite porphyry
- ◇ Microgranodiorite dyke

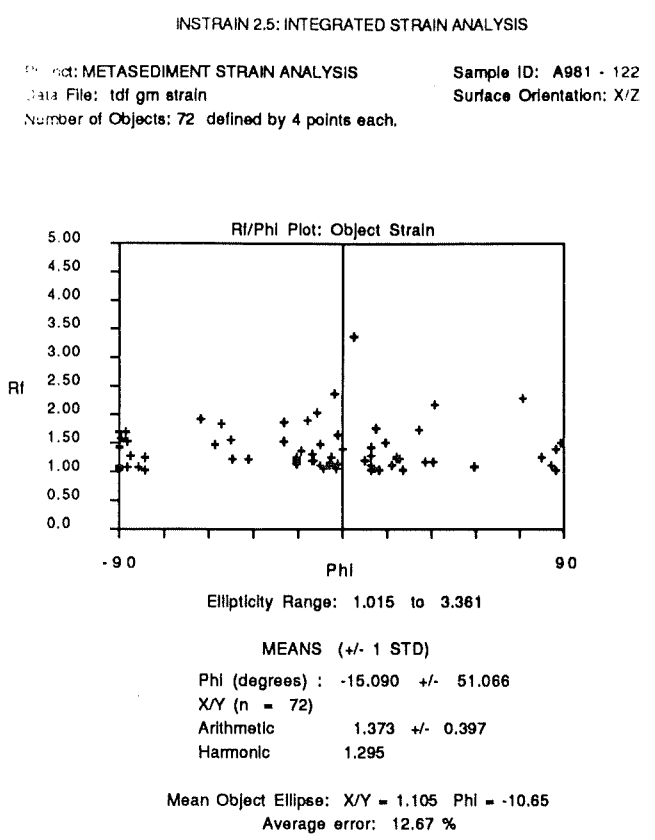

FIGURE 3

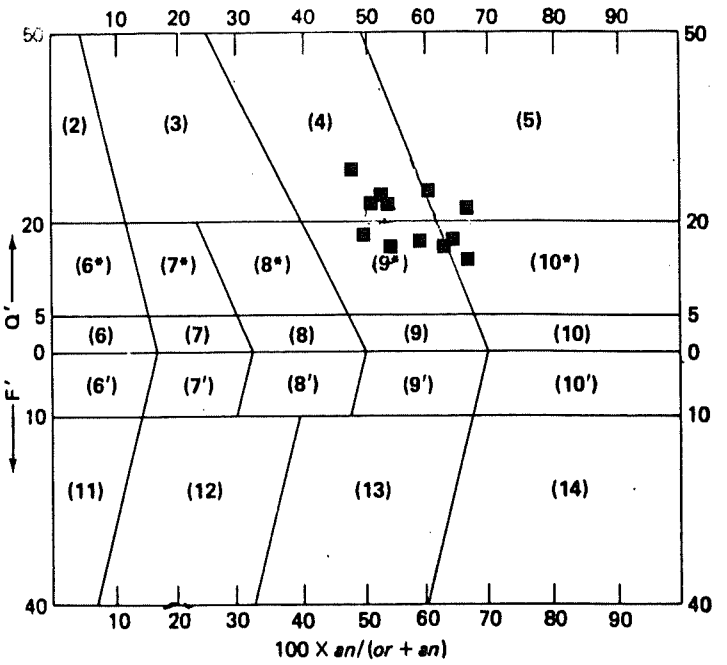

FIGURE 4

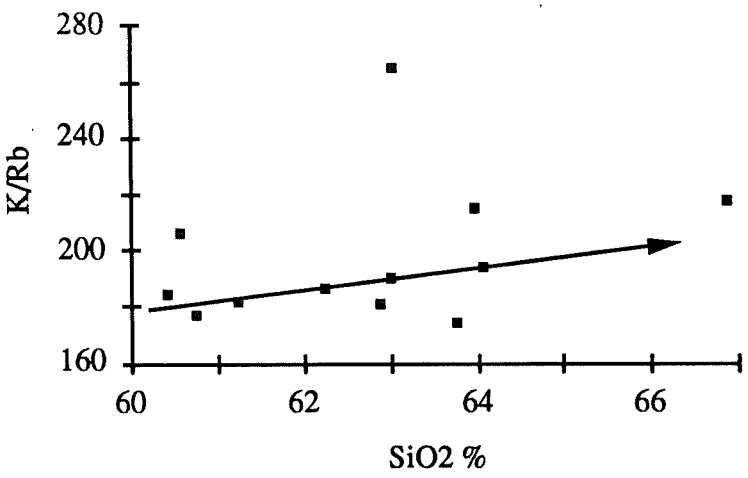

FIGURE 5

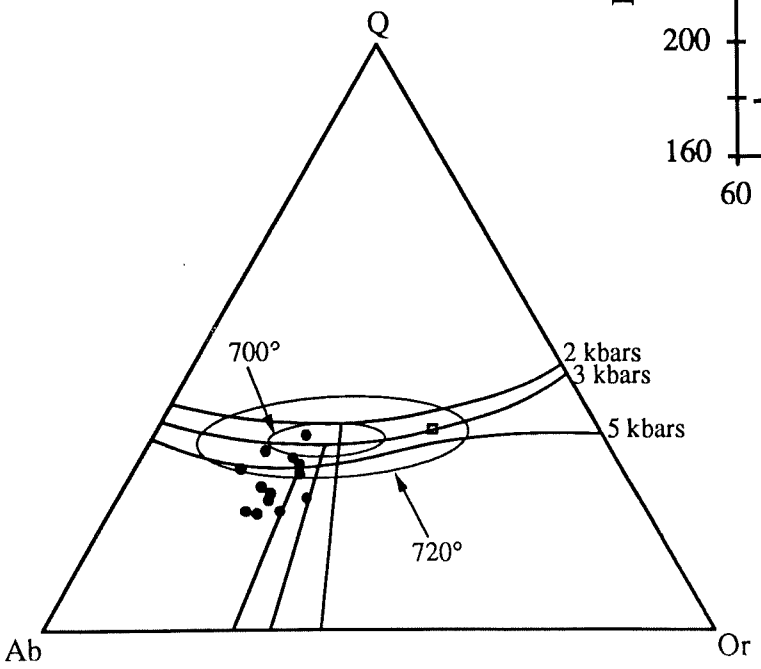

FIGURE 6

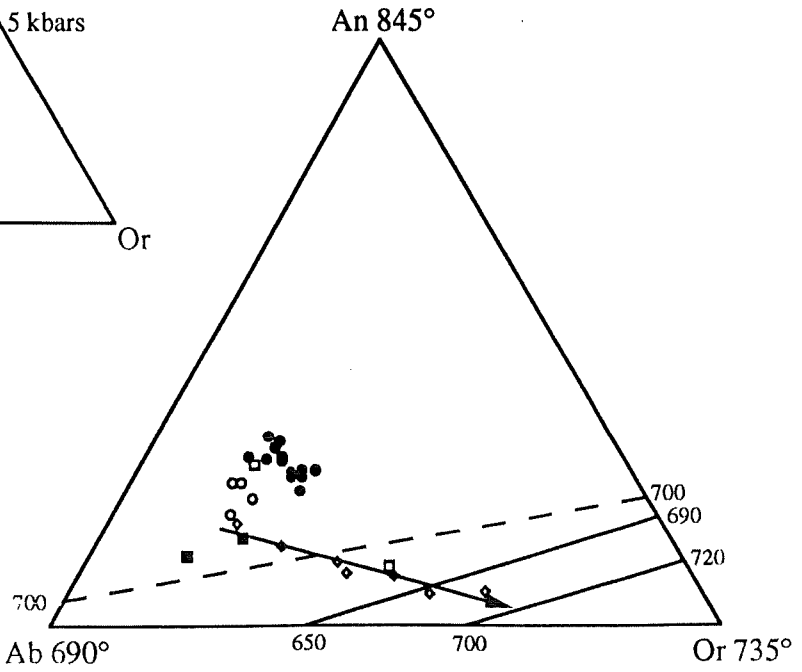

FIGURE 7

FIGURE 8 - Major element variation diagrams for the Anabama Granite with comparisons made with other lithologies from the Anabama region, Delamerian granites of the southern Adelaide Fold Belt, SE South Australia and western Victoria and with the Moruya Batholith of the Lachlan Fold Belt.

FIGURE 9 - Trace element variation diagrams as for Figure 8.

Legend for Figures 8 and 9

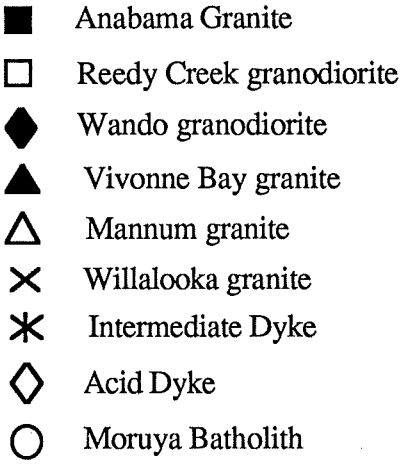

FIGURE 10 - Mg - Fe - Al ternary plot showing mica chemistry comparisons and trends. The Anabama Granite micas are plotted as open circles, the lamprophyre micas as closed circles, the dacite porphyry as closed squares and the microgranodiorite dyke as open diamonds.

FIGURE 11 - An - Ab - Or ternary plot of feldspar mineral chemistries. The Anabama Granite feldspars plot as open circles, the microgranodiorite dyke as open diamonds, the acid dyke as closed diamonds and the dacite porphyry as closed squares.

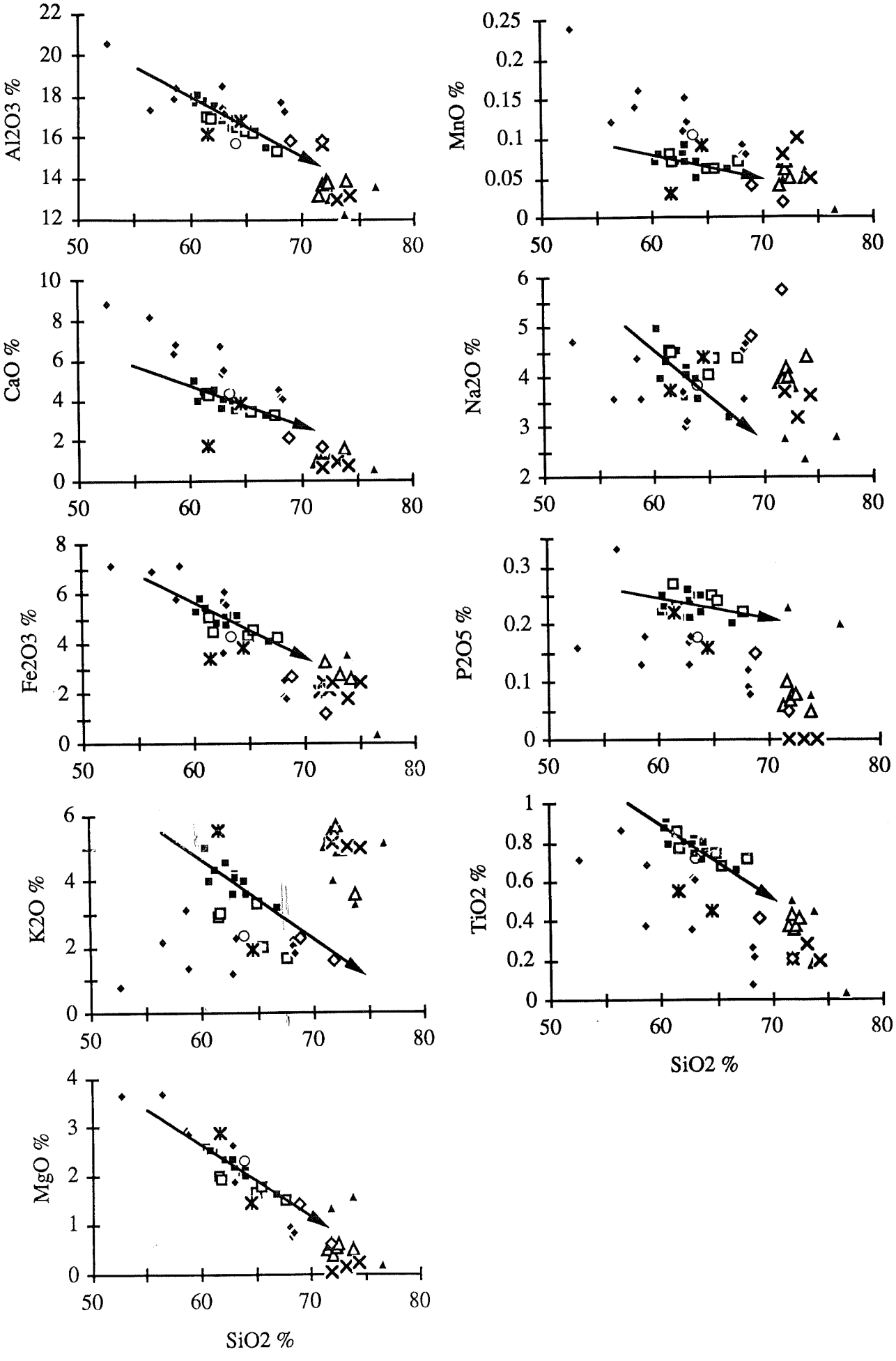

FIGURE 8

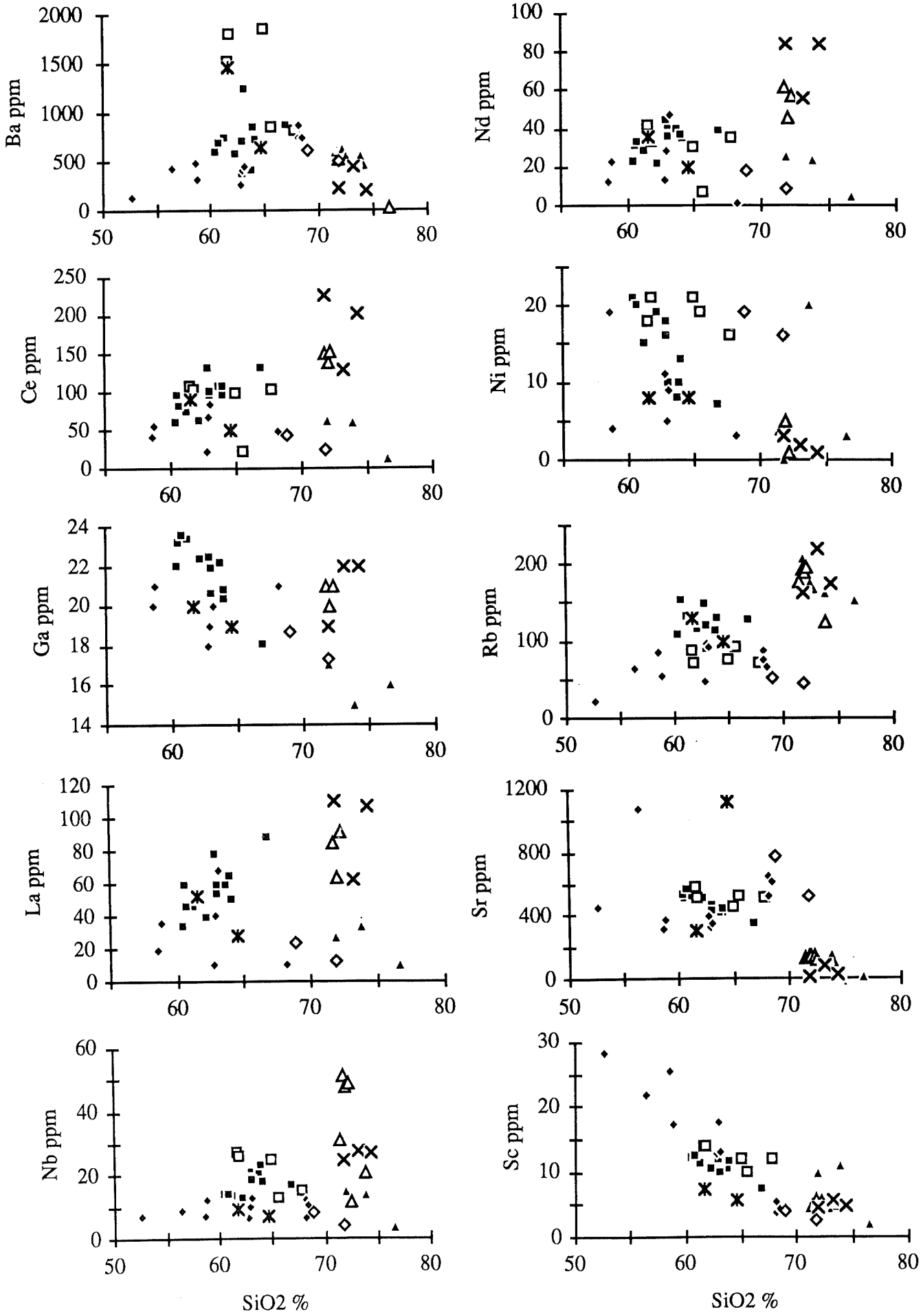
Ba ppm
2000
1500
1000
500
0
50
60
70
80
Nd ppm
100
80
60
40
20
0
60
70
80
Ce ppm
250
200
150
100
50
0
60
70
80
Ni ppm
20
10
0
60
70
80
Ga ppm
24
22
20
18
16
14
60
70
80
Rb ppm
200
100
0
50
60
70
80
La ppm
120
100
80
60
40
20
0
60
70
80
Sr ppm
1200
800
400
0
50
60
70
80
Nb ppm
60
40
20
0
50
60
70
80
SiO2 %
Sc ppm
30
20
10
0
50
60
70
80
SiO2 %

FIGURE 9

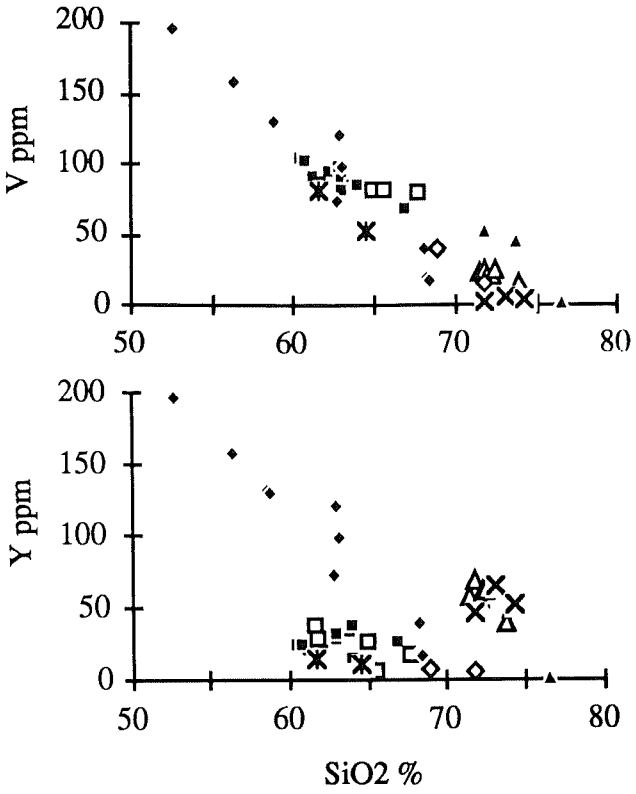

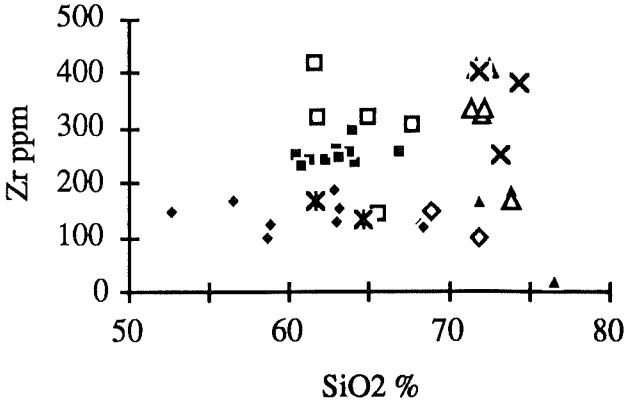

FIGURE 9 cont.

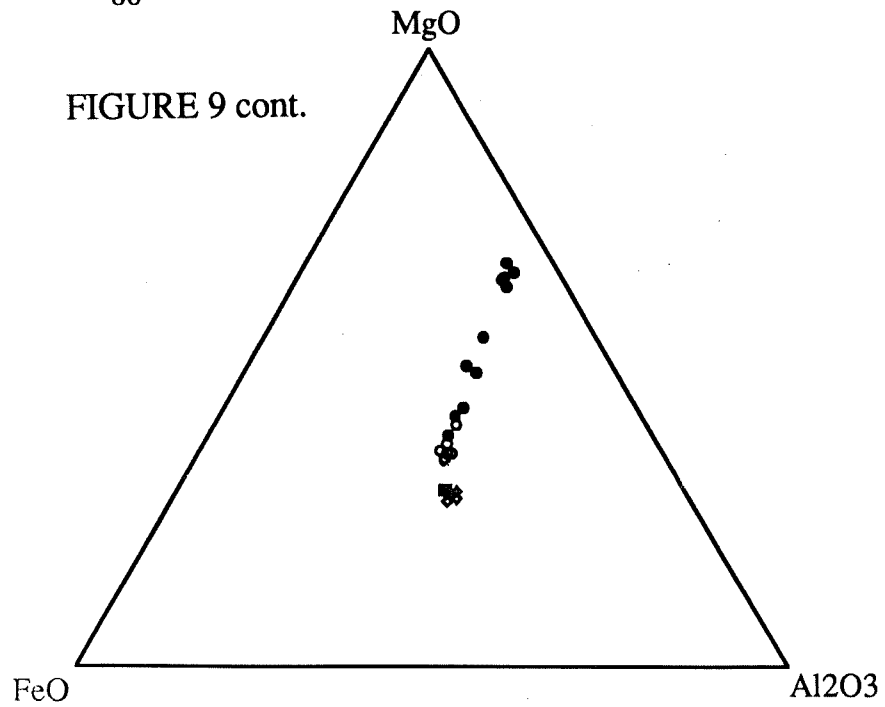

FIGURE 10

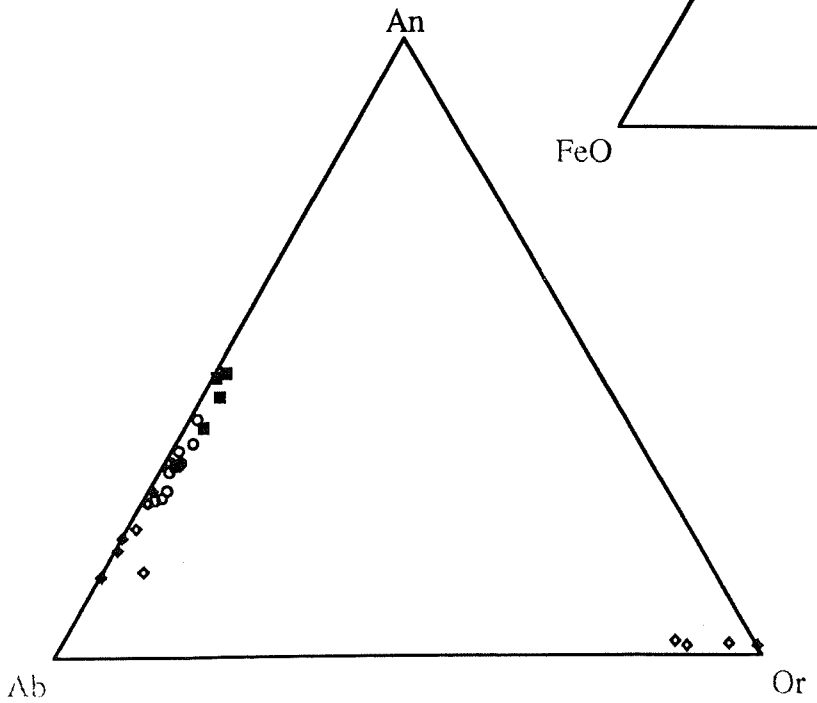

FIGURE 11

CHAPTER 5 ISOTOPE GEOLOGY AND GEOCHRONOLOGY

5.1 Introduction

This study involved the investigation of the Anabama Granite, the dacite porphyry and the lamprophyre dyke for rubidium / strontium and neodynium / samarium isotopic compositions. All isotopic data obtained during this study were determined on a Finnigan - Mat 261 mass - spectrometer.

Previous investigations into the isotopic compositions of the Anabama Granite and associated igneous activity are limited. Only rubidium and strontium analysis has been undertaken with the aim of obtaining an age of emplacement for the Anabama Granite. Webb (1976) used drill core samples to form an eight point isochron with an age of 539.2 Ma*, Table 1a. Compston et al (1966) used mineral separates - plagioclase, microcline and biotite - and a whole rock to form a five point isochron giving an age of 463.0 Ma*, Table 1a. The sample used was collected from a surface outcrop approximately 8 km SE of Netley Gap Homestead, and its description includes "The plagioclase is albite; many grains are sericitized and some altered to epidote" (Compston et al, 1966, p 270). This sample was clearly not fresh, and therefore, the age calculated questionable.

5.2 Anabama Granite

Isotopic compositions of the Anabama Granite indicate low initial $^{87}Sr / ^{86}Sr$ ratios in the range 0.70687 - 0.70827. This coupled with quite high initial ε Nd in the range -4.9 - -5.7 makes the Anabama Granite isotopically similar to the Reedy Creek granodiorite. Nd model ages for the Anabama Granite range between 1.32 and 1.55 Ga, which falls well within and towards the young end of the model age range for granites within the southern Adelaide Fold Belt.

Five samples were analysed for rubidium and strontium with the aim of forming an isochron for the Anabama Granite. The results were somewhat speculative. Considerations of plots similar to Figure 13, suggest that there may in fact be at least three seperate granitic associations with the same age, but with different initial $^{87}Sr / ^{86}Sr$ ratios. Consequently the possibility arises that several parallel isochrons, which give a younger age than that shown in Figure 14a, Table 1b, may be required to explain the data observed.

---

* ages recalculated using original data and Rb 87 $\lambda = 1.42 * 10^{-11}$

The age of the Anabama Granite was determined in this study as 625.6 ± 218 Ma if all data are grouped and considered to belong to the same isochron (Figure 14a). Also shown on Figure 14a are several parallel isochrons with ages of 500 Ma, indicating the possible range of initial isotopic compositions represented by the data from this study.

5.2.1 Isotopic Comparisons

Isotopic comparisons are made here between the Anabama Granite, the Victor Harbor granite of the Southern Adelaide Fold Belt, the Granite Harbour granites and Admiralty Intrusives of Antartica, and, the Berridale and Kosciusko suites of the Lachlan Fold Belt. All data are tabulated in full in Tables 1b, 1c, 2a and 2b.

Figure 16a shows the isotopic differences between the Anabama granite, the Victor Harbor granite and the Granite Harbour granite at 500 Ma. It is clear that the Anabama Granite represents more of a mafic component than either of the other two suites. The Anabama Granite displays lower 87Sr / 86Sr ratios and higher ε Nd values. Differences between the three suites is also seen in Figure 18a and Figure 18c.

The Anabama Granite is compared, indirectly, with the Admiralty Intrusives and the Berridale and Kosciusko suites in Figure 16b, plotted at 400 Ma. This diagram shows the Anabama Granite, at 400 Ma, has isotopic compositions more like the granites of the Lachlan Fold Belt, than those of the Admiralty Intrusives. More significanlty, the difference between the trend of the Admiralty Intrusives and the Berridale and Kosciusko suites is of importance with the difference due to varying ε Nd values with respect to the 87Sr / 86Sr ratio. Such a difference may be accountable by the two different suites being the result of melting of two completely different source regions.

5.3 Dacite Porphyry and Lamprophyre Dyke

The dacite porphyry and lamprophyry dykes were chosen for more detailed isotopic analysis. The dacite was chosen because of its clear crosscutting field relationships with respect to the Anabama Granite, while the lamprophyre was chosen because of its unusual nature.

The dacite porphyry occurs with a very low 87Sr / 86Sr ratio of 0.705854 ± 79 and a measured 143Nd / 144Nd ratio of 0.512212 ± 49, subsequently a Nd modal age of 1.13 Ga was determined.

The lamprophyre dyke, however, displays an extremely high 87Sr / 86Sr ratio of 0.737873 ± 36 and a low 143Nd / 144Nd ratio of 0.511653 ± 33. Nd modal ages were

slightly older than those calculated for either the granite or the daciteand determined as 1.74 Ga.

Both of the samples studied displayed reasonable concentrations of mica. The mica was extracted (using the methods described in Appendix 2) and analysed for Rb and Sr with the aim of constructing two point isochrons for each sample. This proved successful, with isotopic results outlined in Tables 1b and 1c.

The ages calculated for the lamprophyre and the dacite porphyry were 458.7 ± 18 Ma (Figure 14b) and 425.4 ± 13 Ma (Figure 14c) respectively. Both ages give some confinement to the total period of thermal activity in the region.

Three relatively fresh samples of Truro lamprophyre were submitted for K - Ar age determinations of mica phenocrysts, Morris (1991). The ages ranged from 478 ± 3 Ma to 481 ± 3 Ma, with a sample analysed in 1971 giving a K - Ar age of 458 Ma using modern constants. These ages compare favourably with those obtained for the lamprophyre in this study.

5.4 Discussion

The three rock types used for isotopic analysis in this study have displayed completely different isotopic signatures, suggesting differences in their histories.

Figure 15 shows the Sr isotope variation of the three rock types back in time. It is obvious, therefore, that the rock types represent sampling of three completely different sources at different times.

The lower isotopic ratio of the dacite tends to suggest that it evolved from a more primitive source than the Anabama Granite. However, the dacite porphyry displays a more siliceous whole rock chemistry than the granite, which indicates a larger degree or proportion of fractionation for the dacite. The dacite porphyry represents a larger proportion of a mafic end member composition and less of a crustal component when compared to the Anabama Granite. This difference in melt components is also reflected in Figure 16b, where the dacite plots closer to the mantle component on the mixing curve than the granite. The lower crustal influence is also indicated by the dacite's bulk chemistry. It displays lower trace element concentrations of Ba and Zr, which are generally thought to be indicative of crustal contamination.

Therefore, the dacite porphyry can not be thought of as a remelting product of the Anabama Granite or as a product of the remelting of the same source region.

SAMPLE	Rb ppm	Sr ppm	Rb / Sr	87Sr / 86Sr	87Rb / 86Sr
Compston et al. (1966)					
Whole Rock	139.8	140	0.99857	0.7251	2.874
Plagioclase	15.5	125.3	0.12370	0.7079	0.357
	16.2	128.1	0.12646	0.7071	0.364
Microcline	437.5	121.9	3.58901	0.7715	10.33
Biotite	889.8	10.2	87.23529	2.358	250.6
Webb (1976)					
Whole Rock	na	na	na	0.7126	0.806
"	na	na	na	0.7147	1.043
"	na	na	na	0.7145	1.15
"	na	na	na	0.7156	1.286
"	na	na	na	0.7575	6.877
"	na	na	na	0.7615	6.996
"	na	na	na	0.714	0.907
"	na	na	na	0.7152	1.277
na = not available					

Table 1a - Rb and Sr isotopic data for the Anabama Granite from selected authors.

SAMPLE	Nd ppm	Sm ppm	Sm / Nd	143Nd / 144Nd	147Sm / 144Nd
Lamprophyre					
A981 - 147	134.614	19.688	0.14625	0.511653	0.088469
Dacite Porphyry					
A981 - 86	29.325	4.589	0.1565	0.512212	0.094665
Anabama Granite					
A981 - 153	31.558	5.992	0.18986	0.512078	0.11485
A981 - 140	46.984	7.252	0.15434	0.512049	0.09336
A981 - 167	54.33	9.118	0.16783	0.512041	0.10151

TABLE 1b - Nd and Sm isotopic results for the Anabama Granite and the lamprophyre and dacite porphyry dykes.

SAMPLE	Rb ppm	Sr ppm	Rb / Sr	87Sr / 86Sr	87Rb / 86Sr
Lamprophyre					
A981 - 147 WR	316.49	303.563	1.04232	0.737873	3.0246
A981 - 147 Bt	-	-	-	0.81147	14.28238
Dacite Porphyry					
A981 - 86 WR	51.135	816.711	0.06261	0.705854	0.18111
A981 - 86 Bt	-	-	-	1.0036	49.32411
Anabama Granite					
A981 - 153	108.194	534.711	0.20234	0.71105	0.5886
A981 - 140	124.447	353.895	0.35165	0.715523	1.01819
A981 - 167	120.584	439.423	0.27441	0.713269	0.79438
A981 - 23	88.169	472.244	0.1867	0.711346	0.54037
A981 - 154	130.228	532.299	0.24465	0.711977	0.70814

TABLE 1c - Rb and Sr isotopic results for the Anabama Granite and the lamprophyre and dacite porphyry dykes.

SAMPLE	Nd ppm	Sm ppm	Sm / Nd	143Nd / 144Nd	147Sm / 144Nd
Granite Harbour Intrusives (Borg et al., 1987)					
ELR	36.6	6.8	0.18579	0.511144	0.1127
EOG	35.5	8	0.22535	0.511318	0.1355
ETC	32	6.1	0.19063	0.511125	0.1153
ANG25	28.31	5.81	0.20523	0.511152	0.1242
ANG27	51.37	9.94	0.19350	0.511107	0.1171
Victor Harbor Granite (Cock, 1992)					
V35a	45.321	11.227	0.24772	0.511863	0.1498
V35b	48.934	10.108	0.20657	0.511859	0.1250
V35c	44.141	9.110	0.20638	0.511863	0.1248
V35d	36.072	7.776	0.21557	0.511848	0.1209
Admiralty Intrusives (Borg et al., 1987)					
ANG3	31.78	8.28	0.26054	0.511611	0.1575
ANG10	39.81	8.17	0.20522	0.511432	0.1241
ANG11	27.49	5.44	0.19789	0.511344	0.1196
ANG14	40.27	7.67	0.19046	0.511258	0.1153
EMN	21.6	4.3	0.19907	0.511395	0.1207
ENS	17.1	3.2	0.18713	0.511519	0.1126
FAS	21.7	4.3	0.19816	0.511593	0.12
Berridale and Kosciusko Batholiths (McCulloch and Chappell, 1981)					
BB10	37.12	7.1	0.19127	0.511483	0.1157
BB110	33.18	6.58	0.19831	0.511514	0.1199
BB86	24.51	4.5	0.18360	0.511441	0.1111
BB42	8.98	2.9	0.32294	0.51164	0.195
BB104	34.39	6.86	0.19948	0.51152	0.1206
BB60	22.36	4.32	0.19320	0.511452	0.1168
BB62	42.26	6.92	0.16375	0.511596	0.0996
BB31	25.5	4.57	0.17922	0.511595	0.1083
BB74	28.48	5.59	0.19628	0.511282	0.1187
BB48	23.8	4.48	0.18824	0.511339	0.1138
BB61	18.42	6.52	0.35396	0.51116	0.1157
BB163	19.79	3.92	0.19808	0.511213	0.1198
KB22	17.96	3.75	0.20880	0.511393	0.1264
KB139	13.95	3.09	0.22151	0.511479	0.1338

TABLE 2a - Nd and Sm isotopic results for selected granites used in this study.

SAMPLE	Rb ppm	Sr ppm	Rb / Sr	87Sr / 86Sr	87Rb / 86Sr
Granite Harbour Intrusives (Borg et al., 1987)					
ELR	135.6	274.8	0.49345	0.72338	1.4271
EOG	93.9	254.4	0.36910	0.71747	1.0672
ETC	136.5	242.1	0.56382	0.72315	1.6306
ANG25	176.2	136.2	1.29369	0.74417	3.7481
ANG27	213.1	185	1.15189	0.73569	3.3346
Victor Harbor Granite (Cock, 1992)					
V35a	237.686	108.410	2.19248	0.763095	6.28955556
V35b	259.555	104.413	2.48585	0.769102	7.13108556
V35c	247.093	95.918	2.57608	0.770948	7.39003889
V35d	223.387	111.526	2.00300	0.759091	5.74594444
Admiralty Intrusives (Borg et al., 1987)					
ANG3	139	197.6	0.70344	0.71818	2.033
ANG10	196	136.8	1.43275	0.73873	4.1472
ANG11	188.4	131.8	1.42944	0.73607	4.1394
ANG14	256.2	127.9	2.00313	0.74995	5.8091
EMN	91.1	240.2	0.37927	0.7152	1.0962
ENS	85.8	256	0.33516	0.71123	0.9679
FAS	117.6	181.8	0.64686	0.71604	1.8694
Berridale and Kosciusko Batholiths (McCulloch and Chappell, 1981)					
BB10	189	191	0.98953	0.72352	2.86
BB110	195	175	1.11429	0.72555	3.24
BB86	86	252	0.34127	0.71203	0.98
BB42	201	33	6.09091	0.80803	17.64
BB104	172	131	1.31298	0.72906	3.79
BB60	104	264	0.39394	0.71357	1.14
BB62	119	189	0.62963	0.71617	1.81
BB31	176	121	1.45455	0.72986	4.23
BB74	125	243	0.51440	0.71763	1.49
BB48	126	231	0.54545	0.71711	1.57
BB61	130	139	0.93525	0.72691	2.69
BB163	125	123	1.01626	0.72948	2.94
KB22	89	254	0.35039	0.71362	1.01
KB139	38	256	0.14844	0.70902	0.43

TABLE 2b - Rb and Sr isotopic results for selected granites used in this study.

FIGURE 12 - Nb v Zr comparative plot for the lamprophyres of this study and an average Truro lamprophyre (Morris, 1991) and an average world wide example (Rock, 1987). The diagram shows that all three examples plot well within the subduction and post - collision field. Diagram after Thompson and Fowler (1986).

FIGURE 13 - Zr v Rb / Sr for the Anabama Granite showing several trends within the data which leads to the suggestion that Anabama Granite isochron of Figure 14a is in fact several parallel isochrons with varying initial Sr ratios.

FIGURE 14a - 5 point isochron for the Anabama Granite. Also shown are several parallel isochrons at 500 Ma indicating the possibility for a variable initial Sr ratio.

FIGURE 14b - 2 point whole rock and mineral isochron for the lamprophyre dyke.

FIGURE 14c - 2 point whole rock and mineral isochron for the dacite porphyry dyke.

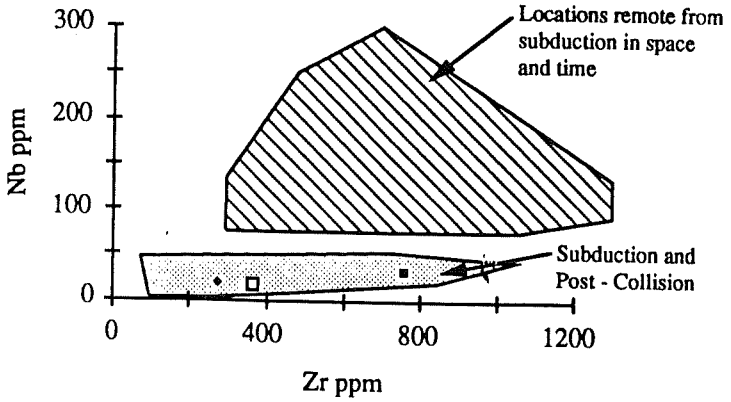

FIGURE 12

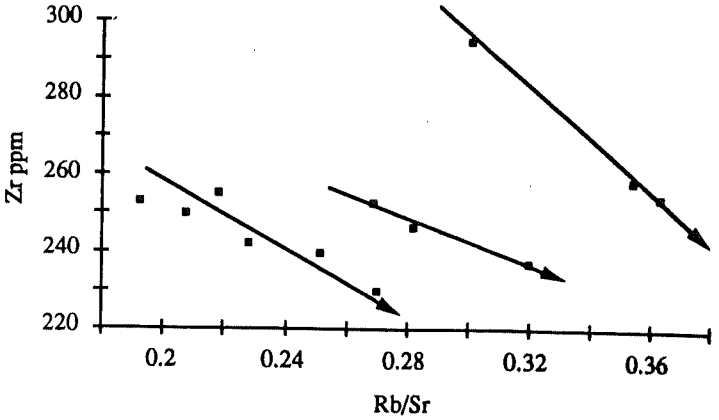

FIGURE 13

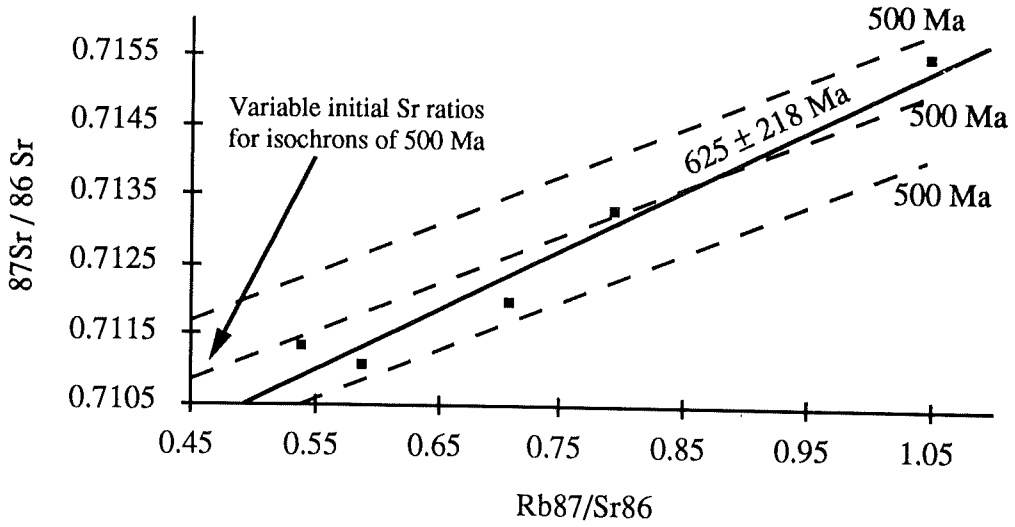

FIGURE 14a

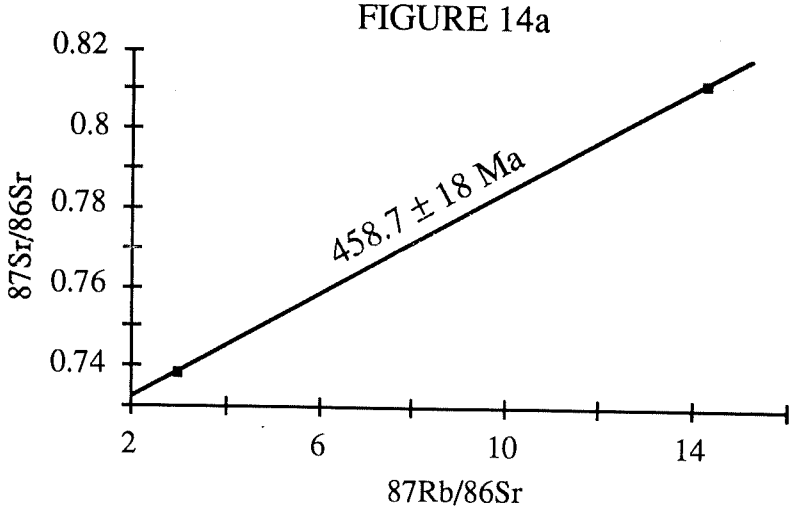

FIGURE 14b

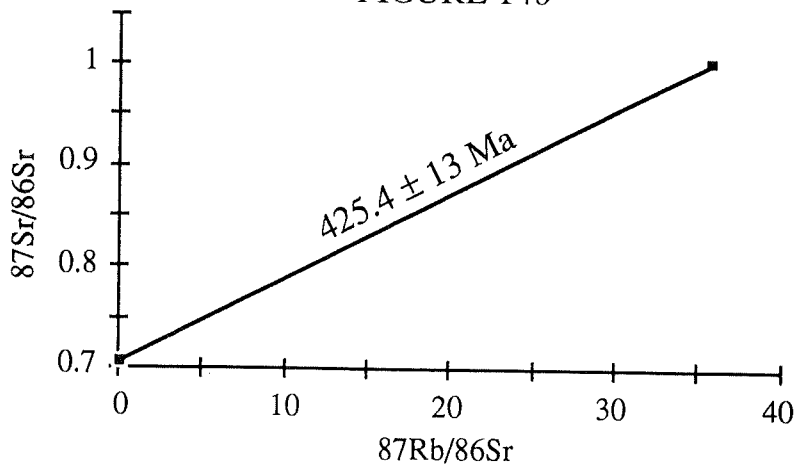

FIGURE 14c

CHAPTER 6 PETROGENESIS and DISCUSSION

It is proposed that the Anabama Granite was formed through a combination of assimilation of the wall rocks on ascent and fractional crystallization of a mantle derived parent, namely a Delamerian basalt.

Figure 16a shows a simple mixing curve between an average Delamerian mafic and an average Archean crustal composition at 500 Ma. The Anabama Granite samples plot very near this curve, approximately between 12 - 14 %. Thus, implying that the Anabama Granite mostly represents primitive Delamerian mafic, contaminated by 12 - 14 % Archean crustal material. In contrast, plotted on Figure 16a, is the Victor Harbor granite and the Granite Harbour granite. Both these suites plot near the same mixing curve as the Anabama Granite, suggesting that they too are mixtures of the same source regions, but in different proportions. The Victor Harbor granite and Granite Harbour granite, respectively, represent approximately 35 % and 15 - 30 % Archean crustal contamination of a Delamerian mafic.

However, it is more probable that both contamination (mixing) and fractional crystallization occur simultaneously. Fractional crystallization modelling, Appendix 4, indicates that it is possible the Anabama Granite composition was formed by the fractional crystallization of an average Delamerian basalt. The results suggest that approximately 40% fractional crystallization is required, along with the removal of augite and orthopyroxene and the addition of approximately 82 % of an average Archean crustal composition. Pure fractional crystallization, as shown, approaches the major element chemistry necessary but does not explain the occurrence of the isotopic shift observed. Therefore, some proportion of assimilation, together with fractional crystallization, is required to produce the observed chemistry and isotopic signatures.

Figures 17a and 17b illustrate the variation of selected trace elements as a function of isotopic composition at 500 Ma. Both diagrams display curves of varying r values, where r is the ratio of assimilation rate to fractionation rate. It is demonstrated in both diagrams that the Anabama Granite represents low r values (r = 0.18 - 0.2), indicating that fractional crystallization is the dominant process. In contrast, the Victor Harbor granite, potentially the product of the same end members as the Anabama Granite, has assimilation as the dominant process (r = 0.5 - 0.57).

These results are consistent with those obtained by Sandiford et al. (1992), for trends observed within the younger and older granite suites of the southern Adelaide Fold Belt. On the basis of these results it is difficult to classify the Anabama Granite as a member of the younger or older granite suites since it plots within a region where these

fields overlap. Nevertheless it does plot closer to the younger granite field of Sandiford et al. (1992).

The shifts in r values between the two different suites may represent and correlate with changes in the tectonic regime of the Adelaide Fold Belt. Interestingly, the younger granite suite has the smallest crustal component and greatest mantle influence, and is generally located east of the older granite suite. Many authors, including Preiss (1987), have noted that the Kanmantoo trough sediments represent flysch - like sediments deposited into a marginal sea to the east of the Adelaidean sediments during an extensional phase of the belt's history. This extensional phase may be related to a subduction zone to the east, which resulted in back arc spreading in the region of the Kanmantoo trough. It has also been recognized that the Kanmantoo sediments thin towards the east, and therefore, likely that the rift axis lies somewhere to the east of the Adelaide Fold Belt under the present Murray Basin (Figure 1b). Evidence in support of this notion is present in the aforementioned r values. The vicinity nearest to the rift axis is the area of thinest crust, which coincides with the area of granite magmatism with the least crustal contamination. Recent studies into the mafic suites of rocks beneath the Murray Basin, by Rankin et al. (1991), have shown that there are large volumes of basalt below the eastern Murray Basin extending into the NW of Victoria. It is postulated by Rankin et al. (1991), that these mafic rocks represent the subsurface extension of the Stavely Greenstone Belt of western Victoria. Therefore, it is interpreted that the Anabama Granite represents the most northern extent of the Delamerian back arc spreading, though is was more subdued, since no evidence for Delamerian sedimentation exists in the area, or if it did occur, has subsequently been removed.

The fractional crystallization model of granite genisis, as outlined for the Anabama Granite and granites from the southern Adelaide Fold Belt, Antarctica and the Lachlan Fold Belt, is in stark contrast to the restite model of granite genesis proposed for the Lachlan Fold Belt by White and Chappell (1977). In their model, White and Chappell (1977) proposed that I - type granites do not form directly from basaltic mantle melts. Instead, they suggest that basaltic melts are emplaced into the lower crust at an earlier stage and later partially remelted (ultrametamorphism) to form melts of granitic composition. These melts, together with unmelted residuum (restite), then move towards the surface where crystallization occurs. White and Chappell (1977) explain the straight - line variation diagrams of most granitic suites as a progressive separation of residuum and melt during crystallization.

The restite model requires at least two periods of heat influx: firstly, to emplace the basaltic melts into the lower crust, and secondly, to cause remelting and granite genesis. It

is difficult to account for the granite genesis of the Adelaide Fold Belt using the restite model because of the multiple heating required. The short time scales involved in the granite generation and Delamerian Orogeny of the southern Adelaide Fold Belt suggests that only one thermal event could be responsible, since it has been shown extensively that granites of the southern Adelaide Fold Belt and the Anabama Granite are most likely products of Delamerian basalt fractionation. Consequently, there could not have been enough time for a Delamerian basalt to be emplaced into the lower crust, cooled and then remelted to give the Cambro / Ordovician granites observed.

Similarities in the contact relationships between the Anabama Granite, the Victor Harbor granite (Cock, pers comm., 1992) and the Reedy Creek granodiorite (Foden, pers comm., 1992), suggest a similar mechanism of emplacement for all three bodies. All three contacts are relatively intact and show little evidence of perturbations of granite material into the host rock or mingling with the host at the interface. The contact between the Anabama Granite and the Adelaidean host rocks dips down to the NNW, back under the Adelaidean metasediments ; the Victor Harbor granite contact dips to the NW, back under Kanmantoo sediments, while the Reedy Creek granodiorite contact dips down to the W. In relation to the sigmoidal shape of the Adelaide Fold Belt, all three bodies display similar relationships. It is suggested that the intrusion of the Anabama Granite, Victor Harbor granite and the Reedy Creek granodiorite were controlled by large scale basement faults. Therefore, rather than being of a plutonic nature, the ascent of the granites is more likely to have occurred through fracture propagation, as proposed by Clemens and Mawer (1992). The Victor Harbor granite and Reedy Creek granodiorite most probably intruded along normal faults, which controlled the formation of the Kanmantoo trough, but were later rotated to become west dipping reverse faults during the Delamerian compressional event. The Anabama Granite is most likely to have intruded along the Anabama fault, a large bounding fault of the Adelaidean metasediments. This fault was probably formed during the Adelaidean time, when rifting of Middle Proterozoic basement and sedimentation of the Adelaidean sediments was occurring. The Anabama fault may have been slightly reactivated during Delamerian time, allowing the fracture propagation of the Anabama Granite towards the surface. The weakness of the fault zone, which would allow relatively quick and shallow penetration of the granite body, along with the features associated with the formation of the Anabama Granite, provide support for the aforementioned model.

Many different sources of evidence support the Anabama Granite intruding the Adelaidean metasediments after being regionally deformed by the Delamerian Orogeny during Cambrian / Ordovician time. The Anabama Granite is seen to be locally crosscutting, with associated acid and intermediate dykes often crosscutting too. Thin

section observations of sediments from within the metamorphic aureole suggest two periods of deformation: an earlier flattening period followed by an influx of heat, porphyroblast growth, and subsequent deformation and rotation of the porphyroblasts ; and later, crenulation development due to the intrusive forces related to the Anabama Granite. This, along with the generally undeformed nature of the granite outcrop, concludes the Anabama Granite as post tectonic / post deformational.

Geochemical and isotopic comparisons, however, indicate the Anabama Granite is similar to the Reedy Creek granodiorite and less similar to the Wando granodiorite of western Victoria. These two granodiorites have previously been interpreted as being pre - to syn - tectonic. Consequently the Anabama Granite could also be interpreted as pre - to syn - tectonic. Evidence which may support this is present in the form of plots, refer to Figures 19a and 19b. In Figure 19a, the Anabama Granite plots clearly in the Pre Plate Collisional field ; whilst in Figure 19b, the Anabama Granite plots on the border of the Volcanic Arc granite field and the Within Plate granite field.

The Anabama Granite, therefore, could be interpreted to have formed in a pre - tectonic environment, ascended as deformation was occuring, and finally, emplaced after the regional deformation was concluded - or else, towards the final stages of folding. These observations have interesting consequences on the timing of deformation in the area, especially in relation to the southern Adelaide Fold Belt. The age of the Anabama Granite is uncertain, due mainly to the overprinting of hydrothermal alteration, but is probably in the range of 475 - 500 Ma. Hence, all deformation within the area must have been completed, or very near completion, by this time. A recent estimate of the timing for deformation in the southern Adelaide Fold Belt is 516 - 487 Ma, Sandiford et al. (1992), which may be consistent with the timing for the northern part of the fold belt where constraining features, such as deformed igneous plutons and crosscutting undeformed dykes like those found in the southern Adelaide Fold Belt, are absent.

Timing of thermal and igneous events in the Lachlan Fold Belt as represented by zircons from granitic intrusions is 390 Ma (Williams et al., 188) - 412 Ma (Chen et al., 1988). The onset of this activity corresponds approximately to the age obtained for the dacite porphyry in this study. It is, therefore, suggested that the dacite porphyry may represent a western extension of the thermal perturbations responsible for the production of granitic melts in the Lachlan Fold Belt, some 700 - 1000 km further to the east. The dacite porphyry is plotted on Figures 16b and 18b, where it is compared to the Lachlan Fold Belt samples. The dacite differs slightly from the Lachlan Fold Belt samples and this can be accounted for by a difference in source regions.

Evidence for the source of the thermal perturbation responsible for the melt generation comes from Borg and De Paolo (1990). They present isotopic evidence from Antarctia which indicates a west dipping subduction zone at around 500 Ma as proposed for the same time in the Adelaide Fold Belt, then a reversal in the subduction zone to east dipping by about 400 Ma, resulting in the granitic magmatism observed in the east of Australia and Antarctica at this time.

Field observations together with age determinations indicate that the dacite porphyry represents the last episode of igneous activity in the vicinity of the Anabama Granite. Between this and the time of emplacement of the Anabama Granite, were further episodes of hydrothermal and igneous activity. It is difficult to determine the relationship between the source of the later dykes and the Anabama Granite without further isotopic studies, but their presence says something about the persistent thermal perturbation in the area not expressed anywhere in the southern Adelaide Fold Belt.

FIGURE 15 - 87Sr / 86Sr v Time diagram showing the isotopic variation over time between the Anabama Granite, lamprophyre and the dacite porphyry. A representation of the basalt field is also shown with the dacite porphyry seen to plot nearest to it, indicating a more primitive source material than that for the Anabama Granite.

FIGURE 16a - ε Nd v 87Sr / 86Sr plotted at 500Ma. Simple mixing curve between an average Delamerian mafic rock and an average Archean crust composition. Values shown on the mixing curve are % of the Archean end member. The Anabama Granite is represented by the open squares, the Victor Harbor granite by the open diamonds and the Granite Harbour granites by the closed squares.

FIGURE 16b - ε Nd v 87Sr / 86Sr plotted at 400Ma. Simple mixing curve between an average Delamerian mafic rock and an average Archean crust composition. Values shown on the mixing curve are % of the Archean end member. The Anabama Granite is represented by the open diamonds, the dacite porphyry by the closed diamonds, the Admiralty Intrusives by the closed squares and the Berridale and Kosciusko suites by the open squares. It is interesting to note the difference in trends between the Admiralty Intrusives and Berridale and Kosciusko suites. This may be accounted for by slight differences in source materials.

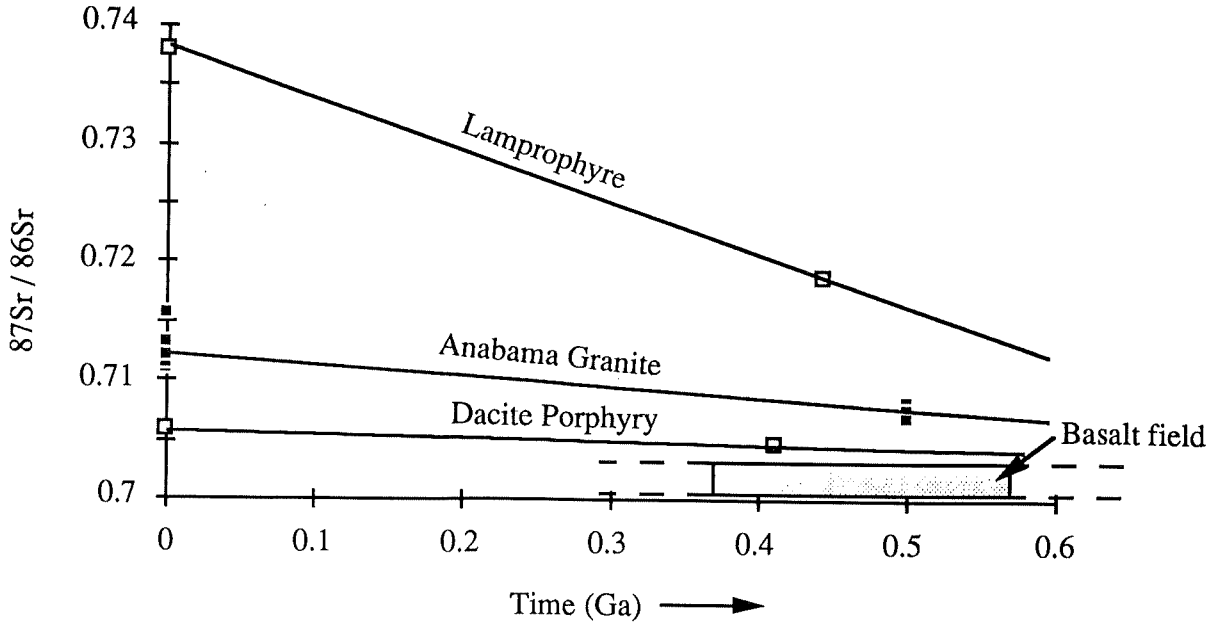

FIGURE 15

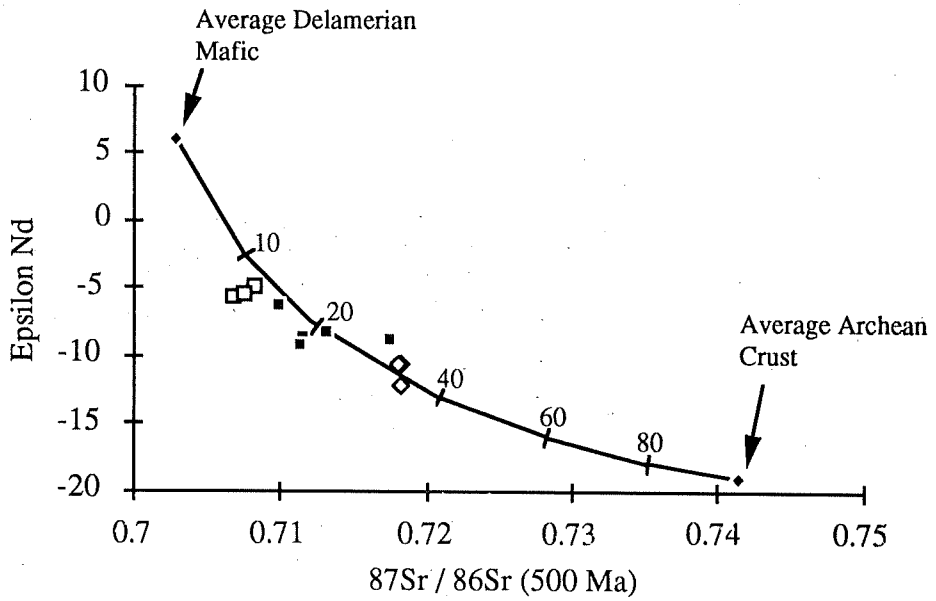

FIGURE 16a

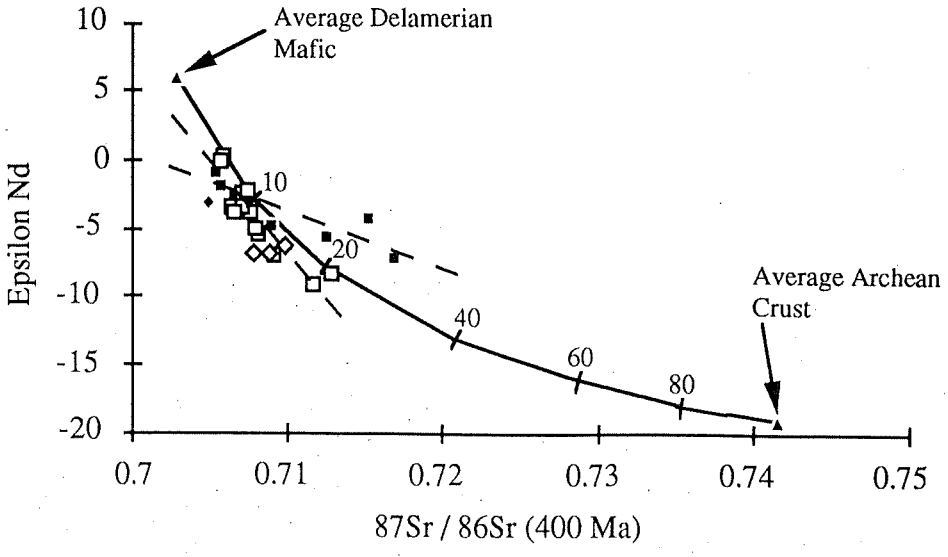

FIGURE 16b

FIGURE 17a - 143 Nd / 144 Nd v Nd ppm at 500 Ma. Samples plotted are the Anabama Granite - closed squares, and the Victor Harbor granites - open squares. Curves represent AFC trends involving a 500 Ma basaltic end - member and an average Archean crustal composition. r = assimilation rate / rate of crystallization. Parameters of the modelled curves are as follows : basaltic end - member, Nd = 5.8 ppm, 143Nd / 144Nd (500 Ma) = 0.51230, Sr = 120 ppm, 87Sr / 86Sr (500 Ma) = 0.7028, Zr = 50 ppm, Sm = 1.5 ppm ; crustal end - member Nd = 30 ppm, 143Nd / 144Nd (500 Ma) = 0.511135, Sr = 150 ppm, 87Sr / 86Sr (500 Ma) = 0.7119, Zr = 180 ppm, Sm = 7 ppm. Bulk distribution coefficients used are as follows : DNd = 0.0001 and 1.1, DSr = 0.005 and 2.5, DZr = 0.005 and 1.2. The dashed curve represents the younger granite suite of Sandiford et al. (1992) and the bold curve the older suite.

FIGURE 17b - Zr ppm v 143Nd / 144Nd at 500 Ma. The symbols and parameters used are as in Figure 17a. The bold curve here, however, represents the younger granite suite and the dashed curve the older suite. The Victor Harbor granites are represented by closed diamonds.

FIGURE 18a - Sm / Nd v ε Nd diagram displaying the differences between 500 Ma Anabama Granite - open squares, Victor Harbor granite - closed diamonds and Granite Harbour granite - closed squares. Also shown for comparison is the field of average Archean rocks and the average Delamerian mafic.

FIGURE 18b - Sm / Nd v ε Nd diagram at 400 Ma. Lithologies shown are the Admiralty Intrusives - closed squares, Berridale and Kosciusko suites - open squares and the dacite porphyry from this study - closed diamond.

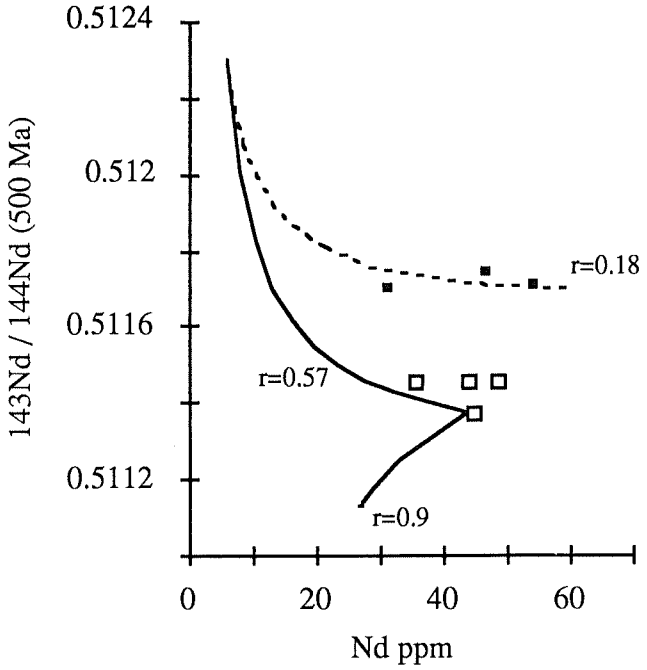

FIGURE 17a

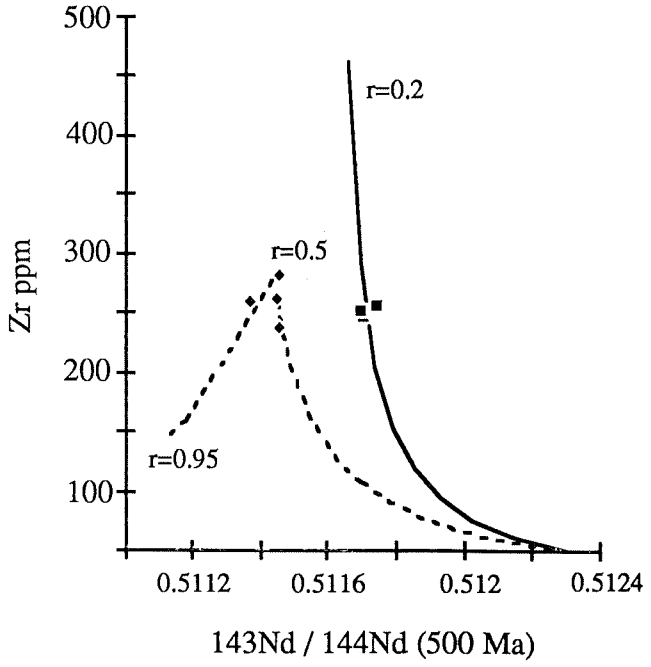

FIGURE 17b

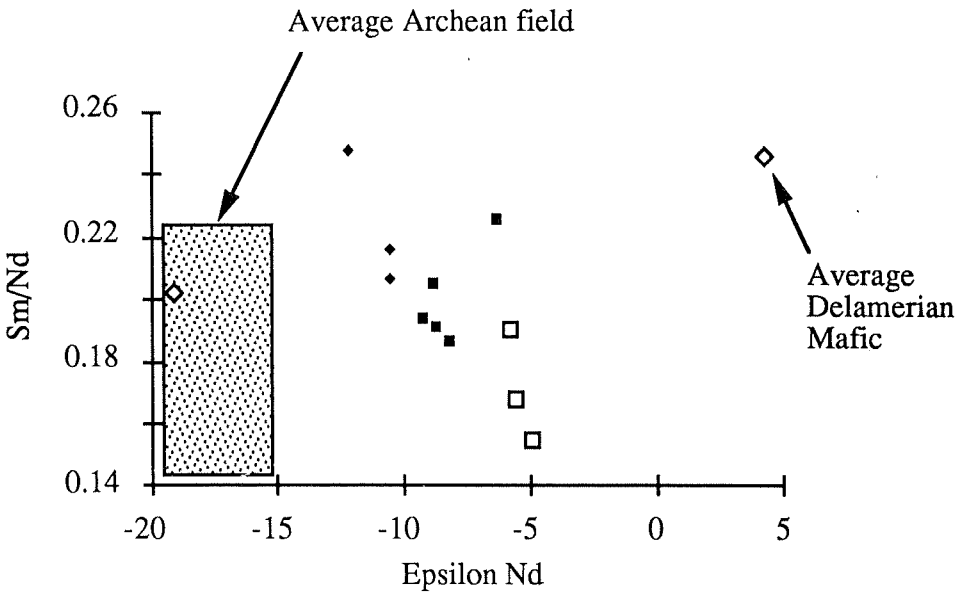

FIGURE 18a

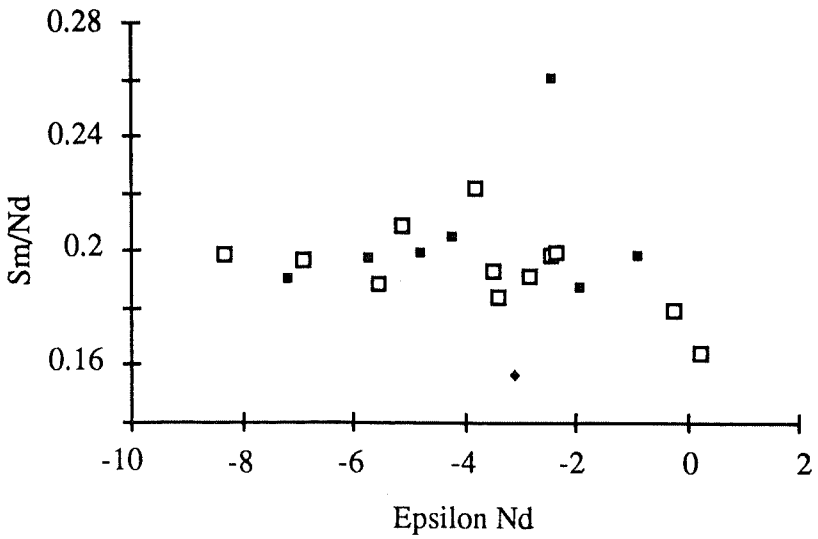

FIGURE 18b

FIGURE 18c - Rb / Sr v 87Sr /86Sr for 500 Ma granites. Average Delamerian mafic and Archean crust are as shown. A linear trend is observed between the Anabama Granite - closed squares and the Granite Harbour granites - open squares.

FIGURE 19a - Tectonic discrimination diagram after Bachelor and Bowden (1984). The Anabama Granite samples plot well within the pre - plate collision field (ppc). Other fields include the post - collision uplift (pcu), late - orogenic (lo), anorogenic (a) and syn - collision (sc) fields. R1 and R2 are represented by the following equations :

$$R1 = 4Si - 11 (Na + K) - 2 (Fe + Ti)$$

$$R2 = 6Ca + 2Mg + Al$$

FIGURE 19b - Tectonic discrimination diagram after Pearce et al. (1984). The Anabama Granite samples plot on the border between the Volcanic Arc granite and Within Plate granite fields.

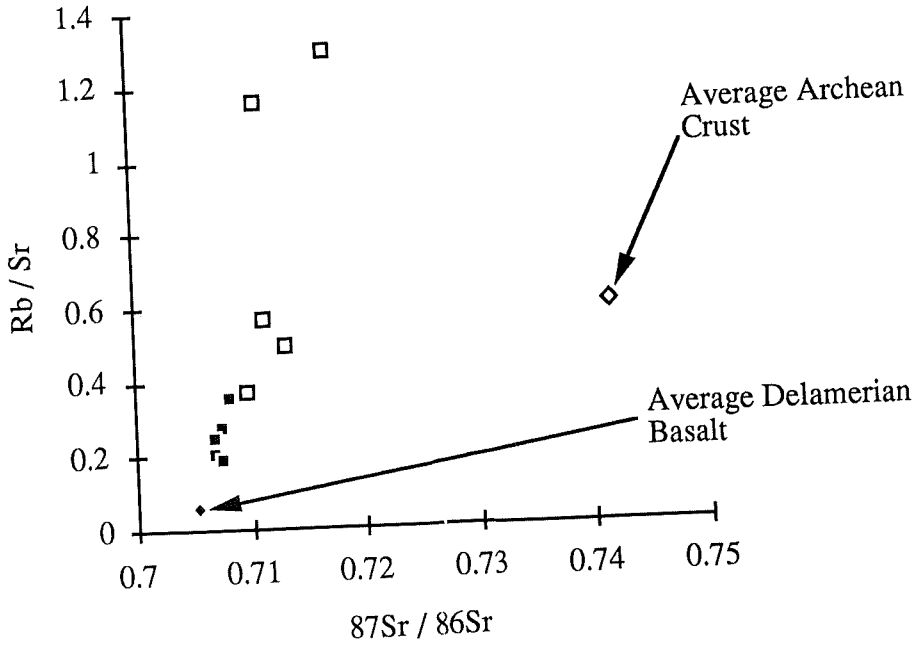

FIGURE 18c

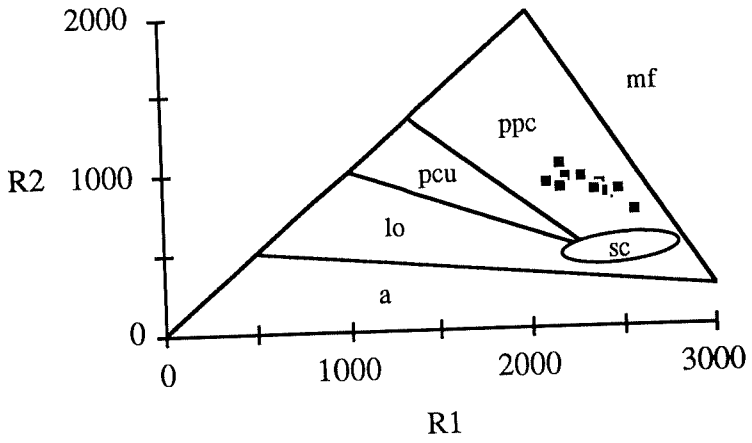

FIGURE 19a

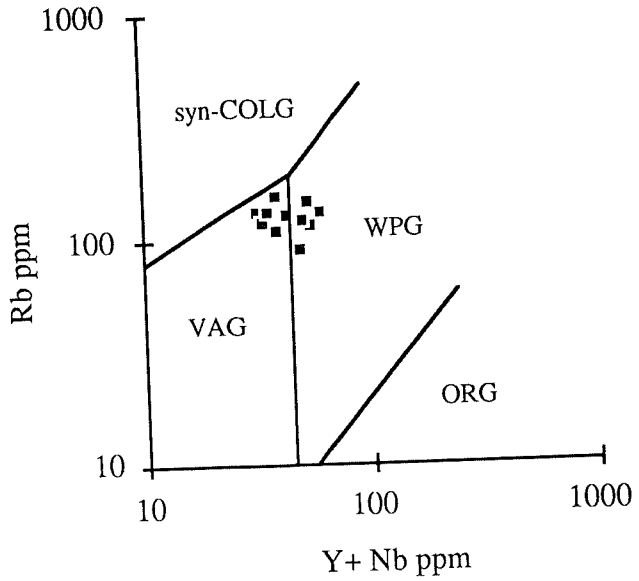

FIGURE 19b

CHAPTER 7 - GEOPHYSICS

7.1 Gravity Modelling

The Anabama Granite is the cause of a very large negative Bouguer gravity anomaly, Figure 20, which caught the attention of Tucker (1972). Interest in the gravity profile for the Anabama Granite stems from a quest to gain an idea about the shape, style, and possible dip of the granitic intrusion. The profile modelled was taken along a line equivalent to A - A' on figure 20.

Detailed density calculations for both the metasediments and granite were carried out by Tucker (1972). This resulted in the use of -0.1 gm/cm^3 as a density contrast between the granite and surrounding metasediments.

Modelling was carried out using POTENT, version 2.1, on an IBM compatable computer. POTENT is a forward modelling program designed for geophysical magnetic and gravity interpretation.

The resulting model for the shape of the Anabama Granite is shown in Figure 21.

This model suggests a granite body with a strike length of ~ 60 km, width of 12 - 15 km, and extending to a depth of 14 - 16 km. The southeastern margin of the granite appears to be steeply dipping, possibly slightly to the northwest. The northwestern margin, on the other hand, has a uniform dip of approximately 50 - 60° to the northwest, back under the Adelaidean metasediments. This notion is strongly supported by field evidence at the granite contact north of Netley Hill (Figure 27). Here, the granite contact is seen to dip at 55° to the northwest.

Gerdes (1973) suggested that the Anabama Granite has a vertical southern contact, a 70° north - dipping northern contact, and an origin at about 20 km depth. This further supports the modelling undertaken.

7.2 Problems with the modelling

Modelling of regional gravity data does have problems associated with it. Large station spacings and errors associated with elevation may create uncertainties with the results of any modelling undertaken.

Density considerations may also cause a problem. Both the models discussed previously assume a constant density contrast between the granite and the host rock and do not take into account any vertical density gradient which will exist naturally. Hence, one

would expect the density contrast between the granite and host rock to decrease with depth, thereby, affecting the size of the modelled body.

7.3 Conclusion

It can be concluded, from the model shown in Figure 21, that the shape of the Anabama Granite differs from the traditional plutonic nature assumed for most granitic intrusions. Instead, the Anabama Granite resembles a large dyke-like body, with only its upper most portion exposed. This supports evidence put forward in Chapter 2: that the body is shallow seated and only the top of a larger body, that is currently concealed beneath, can be seen. It also supports the model of fracture propagation as a mode of magma transport.

FIGURE 20 - Bouguer gravity anomoly over the Anabama Granite. The section taken for geophysial modelling was along the line A - A'.

FIGURE 21 - Geophysical gravity modelling of the Anabama Granite. Features to note are the depth extent of the body and the uniform dip of the body to the north west.

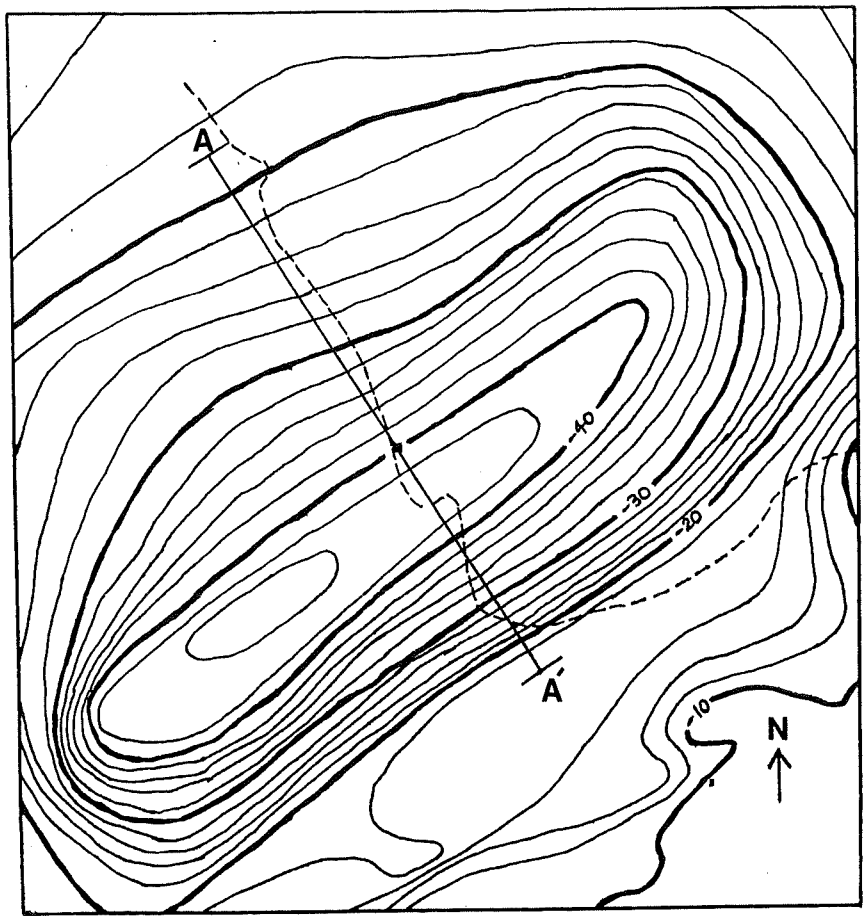

FIGURE 20

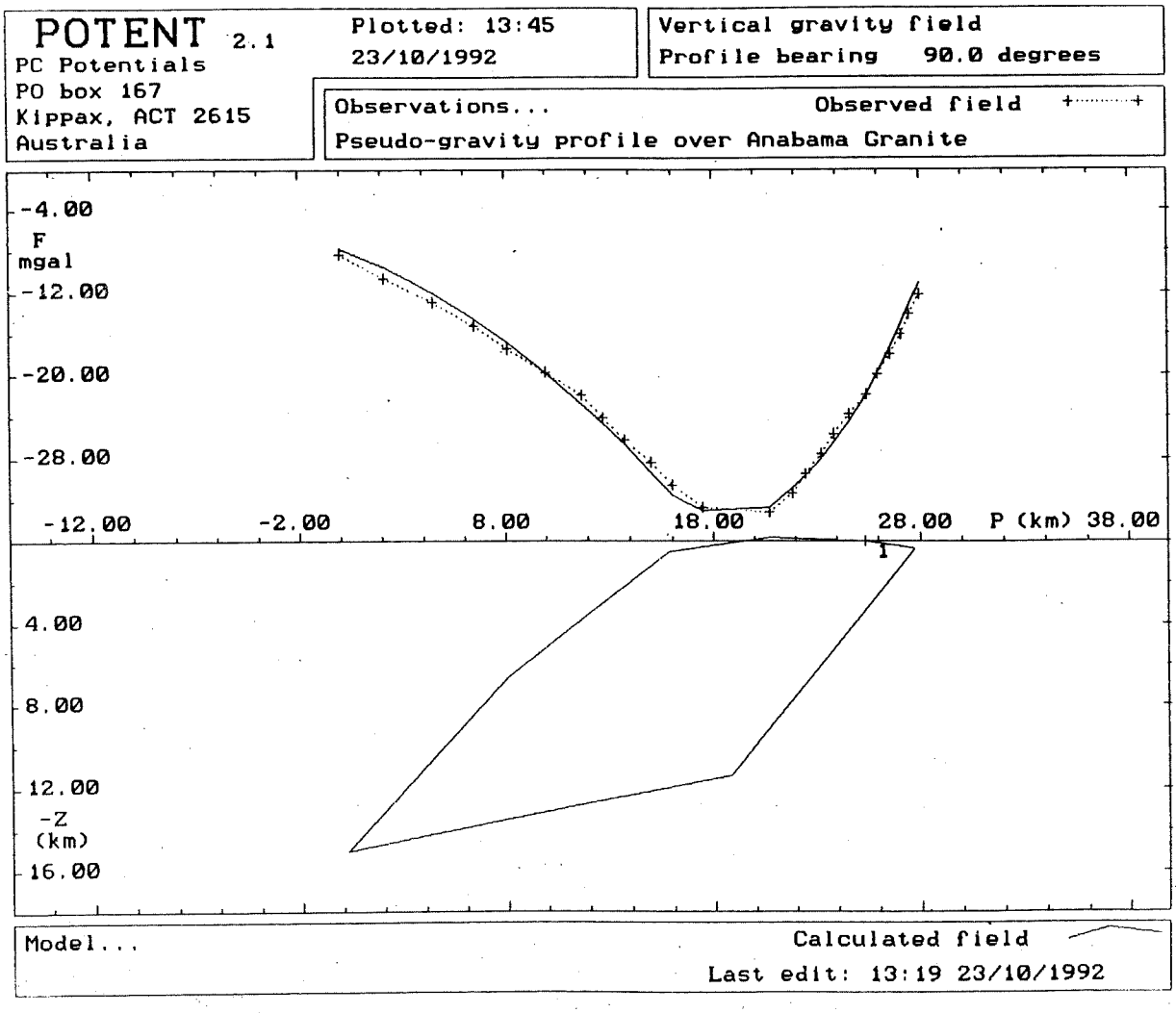

FIGURE 21

CONCLUSIONS

This study has shown that the Anabama Granite represents the site of multiple magmatic intrusions between Cambro / Ordovician - Silurian time. Episodes of hydrothermal alteration and crosscutting dykes indicate an ongoing thermal perturbation, over this period of time, which was responsible for the continued melt generation. Evidence for a long lived thermal source in the region of the southern Adelaide Fold Belt is not present, and therefore, the Anabama Granite represents an area of anomalous heat production and melt generation.

AFC modelling, of Nd - and Sr - isotopic data and some trace elements for the Anabama Granite, indicates that it formed as a result of direct fractionation of a delamerian basaltic melt with minor assimilation (r = 0.2) of an Archean crustal composition. Isotopic comparisons were made between the 500 Ma granites of Victor Harbor, the 400 Ma and 500 Ma granites of Antarctica and the 400Ma granites of the Lachlan Fold Belt, as well as the dacite porphyry and lamprophyre dykes from this study. Modelling reveals that it is possible to form all of the granites through the process of fractional crystallization, but with different parent materials; although, modelling also indicates that the granites asociated with the Adelaide Fold Belt and the 500 Ma granites of Antarctica represent fractionation of the same Delamerian basaltic material with differing amounts of assimilation of crustal material involved. Differences in the source regions, between the Anabama Granite and the dacite porphyry, is represented by differences in their isotopic signatures. The dacite porphyry represents a more primitive source than that proposed for the Anabama Granite, and therefore, does not represent a remelting of the Anabama Granite or its source region. The more siliceous nature of the dacite porphyry indicates that it more highly fractionated than the Anabama Granite. The dacite porphyry was dated at 425 ± 13 Ma, which corresponds to the onset of igneous activity in the Lachlan Fold Belt. Therefore, it is proposed that the dacite porphyry may represent the western margin of thermal perturbations affecting the Lachlan Fold Belt.

The lamprophyre dyke was dated at 457 ± 18 Ma, which approximately corresponds to dates obtained for lamprophyres near Truro. Geochemically, the lamprophyres from this study are similar to those of the Truro area, indicating that the two may be related and reflect a deeper mantle sampling towards the end or after the Delamerian Orogeny.

Similarities were observed between the geochemistry of the Anabama Granite and the Reedy Creek granodiorite of the southern Adelaide Fold Belt and the Wando granodiorite of western Victoria, and like them, the Anamabam Granite can be classified as

an I - type granite. Similarities were observed, and fractional crystallization modelling showed that the acid and intermediate dykes found within the study area are genetically related to the Anabama Granite. Tectonic plots indicate that the Anabama Granite was formed in a pre - deformational type environment, but field evidence and AFC modelling suggest that it is in fact post - deformation, but has intruded along the regional fabric of the host metasediments.

Geophysical gravity modelling of the Anabama Granite indicated that the granite extends to a depth of approximately 15 km and dips uniformly to the north west. This, together with field observations of the contact relationships of the Victor Harbor granite and Reedy Creek granodiorite, indicate that there may be a structural control to their emplacement. It was suggested that the granitic melts were transported to the surface by a means of fracture propagation along large basement faults. This is in contrast to the generally recognized plutonic mechanism of emplacement.

It is recommended that further, more detailed isotopic studies be carried out on all lithologies in the area, in an effort to establish the nature and timing of the various episodes of dyke activity recognized during the Cambro / Ordovician - Silurian time. It would also be of imopotance to establish the mechanisms and thermal regimes associated with these intrusions, whether it be an ongoing activity, as suggested in this study, or a series of rapid, closely spaced thermal perturbations.

REFERENCES

BARKER, D.S., 1983. Igneous Rocks. Prentice Hall. p 417.

BARKER, F., ARTH, J.G. & STERN, T.W., 1986. Evolution of the Coast batholith along the Skagway Traverse, Alaska and British Columbia, *American Mineralogist*, **71**, 632 - 643.

BATCHELOR, R.A. & BOWDEN, P., 1984. Petrogenetic interpretation of granitoid rock series using multicationic parameters. *Chemical Geology*, **48**, 43 - 55.

BLISSETT, A.H. & REED, J.A., 1973. Investigation of the Anabama copper and molybdenum prospect. *South Australia. Department of Mines and Energy. Open file Envelope*, 2988 (unpublished).

BORG, S.G., STUMP, E., CHAPPELL, B.W., McCULLOCH, M.T., WYBORN, D., ARMSTRONG, R.L. & HOLLAWAY, J.R., 1987. Granitoids of Northern Victoria Land, Antarctica : Implications of chemical and isotopic variations to regional crustal structure and tectonics. *American Journal of Science*, **287**, 127 - 169.

BORG, S.G. & DePAOLO, D.J., 1990. A tectonic model of the Antarctic Gondwana margin with implications for southeastern Australia : isotopic and geochemical evidence. *Tectonophysics*, **196**, 339 - 358.

BOYD, D., 1992. Personnel Communication. Department of Geology and Geophysics. University of Adelaide.

CHAPPELL, B.W. & WHITE, A.J.R., 1974. Two contrasting granite types. *Pacific Geology*, **8**, 173 - 174.

CHEN, Y.D., WILLIAMS, I.S. & COMPSTON, W., 1989. Dating zircons in mafic inclusions using ion microprobe. *Transactions American Geophysical Union,* **70**, pt 20, p 604.

CLEMENS, J.D. & MAWER, C.K., 1992. Granitic magma transport by fracture propagation.*Tectonophysics*, **204**, 339 - 360.

COCK, B.J., 1992. Aspects of granite genesis in the southern Adelaide Fold Belt : implications from case studies of Victor Harbor and Monarto. B.Sc. (Hons) thesis, University of Adelaide (unpublished).

COMPSTON, W., CRAWFORD, A.R. & BOFINGER, V.M., 1966. A radiometric estimate of the duration of sedimentation in the Adelaide Geosyncline, South Australia.*Journal of the Geological Society of Australia*, **13**, 229 - 276.

COX, K.G., BELL, J.D. & PANKHURST,R.J., 1979. The interpretation of igneous rocks, 450p.

CSR Ltd., 1982. EL 753, Anabama Hill. Reports for period 6/10/81 - 6/11/82. *South Australia. Department of Mines and Energy. Open file Envelope*, **4029** (unpublished).

EL - RAGHY, S., 1980. Anabama Hill Prospect, EL 173, 14/7/80, for Asarco (Aust.) Pty. Ltd. *South Australia. Department of Mines and Energy. Open file Envelope*, **3854** (unpublished).

FODEN, J.D., TURNER, S.P. & MORRISON, R.S., 1990. Tectonic implications of Delamerian magmatism in South Australia and western Victoria. *Journal of the Geological Society of Australia Special Publication* , **16**, 465 - 482.

FODEN, J.D., WILLIAMS, I., COMPSTON, W., TURNER, S.P. & MICHARD, A., 1992. The nature, timing and duration of the Delamerian - Ross Orogeny. In Prep.

FODEN, J.D., 1992. Personnel Communication. Department of Geology and Geophysics. University of Adelaide.

FORBES, B.G., 1991. 1:250 000 geological series - Explanatory Notes, OLARY, South Australia, Sheet SI/54-2 International Index. *South Australian Department of Mines and Energy* Rpt. Bk. 91/137.

GERDES, R.A., 1973. Anabama Fault Project.*South Australian Department of Mines and Energy* Rpt. Bk. 73 / 75.

GRIFFIN, T.J., WHITE, A.J.R. & CHAPPELL, B.W., 1978. The Moruya Batholith and geochemical contrasts between the Moruya and Jindabyne suites. *Journal of the Geological Society of Australia*, **25**, pt 4, 235 - 247.

HIGUCHI, H. & NAGASAWA, H., 1969. Partition of trace elements between rock - forming minerals and the host volcanic rock. *Earth and Planetary Science Letters*, **7**, 281 - 287.

KLEEMAN, A.W., 1965. The origin of granitic magmas. *Journal of the Geological Society of Australia*, **12**, pt 1, 35 - 52.

MANCKTELOW, N.S., 1979. The structure and metamorphism of the southern Adelaide fold belt. Ph.D. thesis, University of Adelaide (unpublished).

McCULLOCH, M.T. & CHAPPELL, B.W., 1981. Nd isotopic characteristics of S - and I - type granites. *Earth and Planetary Science Letters*, **58,** 51 - 64.

MILNES, A.R., COMPSTON, W. & DAILY, B., 1977. Pre- to syn-tectonic emplacement of Early Palaeozoic granites in southeastern South Australia. *Journal of the Geological Society of Australia*, **24**, 87 - 106.

MIRAMS, R.C., 1961. Field relationships of the Anabama Granite. *Royal Society of South Australia. Transactions*. **85**, 121 - 154.

MOELLER, T., 1980. The petrology and geochemistry of the Reedy Creek granitoids and migmatites. B.Sc. (Hons) thesis, University of Adelaide (unpublished).

MORRIS, B.J., 1977. EL 173 - final report. An investigation of copper and molybdenum mineralisation at Anabama Hill and the Cronje Dam copper

prospect (OLARY 1 : 250 000). *South Australia.Department of Mines. Report Book,* 77/51.

MORRIS, B.J., 1991. Kanmantoo trough geological investigations. Karinya syncline. Truro lamprophyres. *South Australia.Department of Mines and Energy. Report Book,* 91/29.

MORRISON, R.S., 1988. Igneous intrusive rocks of the Adelaide Geosyncline. Ph.D. thesis, University of Adelaide (unpublished).

MORRISON, R.S. & FODEN, J.D., 1990. A zoned Middle Cambrian pluton in the Peake and Denison Ranges, South Australia. *Journal of the Geological Society of Australia Special Publication* **16**, 450 - 464.

NAGASAWA, H. & SCHNETZLER, C.C., 1971. Partitioning of rare earth alkali and alkaline earth elements between phenocrysts and acid igneous magma. *Geochim. Cosmochim. Acta.* **35**, 953 - 968.

PEARCE, J.A., HARRIS, N.B.W. & TINDLE, A.G., 1984. Trace element discrimination diagrams for the tectonic interpretation of granitic rocks. *Journal of Petrology*, **25**, 956 - 983.

PREISS, W.V., (Compiler),1987. The Adelaide Geosyncline - late Proterozoic stratigraphy, sedimentation, palaeontology and tectonics. *South Australia. Geological Survey. Bulletin* **53**.

RAMAKRISHNAN, M. & BHATTACHARYYA, S., 1985.Contact metamorphic granophyres of partial melting origin adjacent to dolerite dykes in Karnataka. *Journal of the Geological Society of India*, **26**, 95 - 102.

RANKIN, L.R., CLOUGH, B.J. & GATEHOUSE, C.G., 1991. Mafic suites in basement beneath the Murray Basin : New data for the early Palaeozoic history of the Tasman Orogenic Province. *South Australia.Department of Mines and Energy. Report Book,* 91/44.

RICHARDS, N.C., 1980. Copper and molybdenum mineralisation associated with the Anabama Granite, Olary region, S.A. B.Sc. (Hons) thesis, University of Adelaide (unpublished).

ROCK, N.M.S., 1987. The nature and origin of lamprophyres: an overview. *Alkaline Igneous Rocks* , FITTON, J.G. & UPTON, B.G.J. (eds) Geological Society Special Publication, **30**, 191 - 226.

SANDIFORD, M., FODEN, J.D., ZHOU, S. & TURNER, S.P., 1992. Granite genesis and the mechanics of convergent orogenic belts with application to the Southern Adelaide Fold Belt. *Transactions of the Royal Society of Edinburgh : Earth Sciences*, **83**, 83 - 93.

STRECKEISEN, A., 1976. To each plutonic rock its proper name. *Earth Science Reviews*, **12**, 1 - 33.

TAYLOR, S.R., 1965. The application of trace element data to problems in petrology. *Physics and Chemistry of the Earth*, **6**, 133 - 213.

THOMPSON, R.N. & FOWLER, M.B., 1986. Subduction - related shoshonitic and ultrapotassic magmatism : a study of Siluro - Ordovician syenites from the Scottish Caledonides. *Contributions to Mineralogy and Petrology*. **94**. 507 - 522.

TUCKER, D.H., 1972. Magnetic and gravity interpretation of an area of Precambrian sediments in Australia. Ph.D. thesis, University of Adelaide (unpublished).

TURNER, S.P., 1986. Early Palaeozoic plutonism in western Victoria and eastern South South Australia : Implications. B.Sc. (Hons) thesis, University of Adelaide (unpublished).

TURNER, S.P., FODEN, J.D. & MORRISON, R.S., 1992. Derivation of some A - type magmas by fractionation of basaltic magma : An example from the Padthaway Ridge, South Australia. *Lithos*, **28,** 151 - 179.

TUTTLE, O.F. & BOWEN, N.L., 1958. Origin of granite in the light of experimental studies in the system $NaAlSi_3O_8$ - $KAlSi_3O_8$ - SiO_2 - H_2O. *The Geological Society of America Memoir* , **74** ,

WEBB, A.W., 1976. Geochronology of the granitic rocks of south - eastern South Australia. *Amdel. Report.* **1138.**

WEBB, R., 1992. The geology and mineralization in the vicinity of the Gibraltar 1 drill site, NW of Tarcoola S.A. B.Sc. (Hons) thesis, University of Adelaide (unpublished).

WHITE, A.J.R. & CHAPPELL, B.W., 1977. Ultrametamorphism and granitoid genesis, *Tectonophysics*, **43**, 7 - 22.

WILLIAMS, I.S., CHEN, Y., CHAPPELL, B.W. & COMPSTON, W., 1988. Dating the sources of Bega Batholith granites by ion microprobe. *Abstracts Geological Society of Australia*, **21** p 424.

WYLLIE, P.J., 1977. Crustal anatexis : an experimental review. *Tectonophysics*, **43,** 41 - 71.

APPENDIX 1

HAND SPECIMEN AND THIN SECTION DESCRIPTIONS

Appendix 1 - Hand Specimen and Thin Section Descriptions

The following appendix presents hand specimen and thin section descriptions for (most of) the lithologies mentioned in this study. Estimates of mineral proportions for every thin section are tabulated for each lithology and the descriptions given are representative of a typical description for that lithology. All sample numbers have the prefix A981, unless stated otherwise.

The mineral chemistries used are documented in Appendix 2. The abbreviations are as follows :

HS - Hand Specimen
TS - Thin Section
PTS - Polished Thin Section

ANABAMA GRANITE

Sample No.	18	96	23	26	153	777/179
quartz	30	30	40	47	30	25
plag.	40	55	35	40	55	60
kspar.	20	4	15	10	5	5
biotite	9	10	7	3	7	8
hbl.	-	tr	2	tr	2	1
sphene	1	1	1	tr	1	1
accessory*	tr	tr	tr	tr	tr	tr

* accessory phases include opaques, zircons, muscovite, sericite, epidote, chlorite and apatite.

18 - Anabama Granite

HS - A coarse - grained, slightly foliated, biotite rich granodiorite.

TS - Plagioclase and quartz form the dominant minerals within this section.

Plagioclase occurred as large (0.5 - 5 mm) subhedral grains, with most displaying characteristic multiple twinning. Occasionally, myrmekitic textures were seen at some grain boundaries. Minor sericitization of some grains has occurred.

Quartz was present as large (0.5 - 4 mm) anhedral to subhedral grains, which generally exhibited slight undulose extinction.

Potassium feldspar occurred as large (2 - 5 mm) anhedral to subhedral grains, with evidence of carlsbad twinning. Minor sericitization of the potassium feldspars had also occurred.

The only ferromagnesian mineral present was light brown to brown subhedral biotite grains, up to 3 mm in length and randomly oriented. Hydrothermal muscovite and chlorite were seen to replace biotite, and epidote with chlorite. Zircon grains, up to 0.5 mm long, were seen as inclusions within biotite, often complete with obvious alteration haloes.

Subhedral to euhedral diamond shaped sphene crystals (0.5 - 1.5 mm) were present, often associated with opaques.

153 - Anabama Granite

HS - A coarse - grained granodiorite with quartz, plagioclase, biotite, hornblende, potassium feldspar and sphene as the observable mineralogy.

PTS - This section was predominantly plagioclase and quartz.

Plagioclase was andesine in composition (Ab 61 - 69) and was present as large (0.5 - 6mm) subhedral crystals, which displayed either multiple twinning or concentric zoning.

Quartz was present as generally large (1 - 5 mm), irregular anhedral grains, which exhibited slight undulose extinction.

Potassium feldspar occurred in minor amounts as small subhedral grains, characterised by sericite alteration.

Often large ($\leq$ 6 mm) subhedral to anhedral light brown, to dark brown biotite grains occurred throughout this section. Biotite was often altered to chlorite and epidote, and associated with anhedral hornblende and euhedral sphene. Subhedral to euhedral hexagonal apatite grains were also associated with these more mafic minerals.

Opaques (dispersed thruoghout the section), were present as subhedral to euhedral grains.

777 -179 - Anabama Granite (Richards, 1980)

HS - An unfoliated, coarse - grained, biotite granodiorite.

PTS - Plagioclase, quartz and biotite were the main constituents in this section.

Subidiomorphic plagioclase grains, showing multiple twinning and oscillatory zoning, displayed slight sericitization. The plagioclase composition varied from andesine to oligoclase (Ab 60 - 74), with some cores being more calcic and others more sodic in composition.

Anhedral quartz grains (≤ 5 mm) showed slight fracturing and displayed moderate undulose extinction.

The potassium feldspar displayed remnant carlsbad twinning, with some degree of sericite alteration.

Irregular subhedral biotite flakes (≤ 4.5 mm) clustered into aggregates with hornblende, sphene and apatite. Biotite alteration to chlorite and granular epidote were common. Equant, irregular, dark green hornblende grains (≤ 1.5 mm) often displayed simple twinning.

Sphene occurred as large (3 - 6 mm) euhedral diamond shaped crystals, which exhibited concentric zoning. The cores were generally richer in iron and poorer in titanium.

Opaques were generally subhedral to euhedral magnetite grains.

MICROGRANITE / GRANODIORITE

Sample No.	4	75	160
quartz	31	55	60
plag.	25	25	8
kspar.	41	17	30
biotite	3	3	2
hbl	3	-	-
epidote	2	tr	tr
accessory*	tr	tr	tr

* accesory phases include zircon, opaques, muscovite, chlorite and sericite

75 - Microgranodiorite

HS - A fine - grained quartz and plagioclase rich microgranodiorite with fine biotite grains.

TS - The microgranodiorite consisted of anhedral to subhedral grains, up to 2 mm in size.

Quartz and plagioclase were the dominant minerals, with intergrowths of the two forming myrmekitic textures at grain boundaries. The presence of this texture might suggest a slow cooling history for this sample.

Plagioclase occurred as subhedral grains, with predominantly multiple twinning but occasional oscillatory zoning.

Potassium feldspar occurred as both microcline and orthoclase, displaying cross hatching and simple twinning respectively. They showed minor alteration to sericite. Perthite textures within orthoclase were also observed in places.

Equant euhedral quartz grains (0.5 - 2 mm) exhibited straight to slightly undulose extinction.

The dominant mafic mineral is small (≤ 1 mm), light brown to brown, anhedral biotite grains, with zircon inclusions. Both epidote and muscovite were present as alteration products of biotite.

Opaques were present as small (≤ 0.2 mm), euhedral grains.

160 - Microgranite

HS - A fine - grained, grey, biotite microgranite.

PTS - This section was primarily composed of quartz, potassium feldspar, plagioclase and biotite.

Quartz occurred as small (≤ 2.5 mm), anhedral grains. Most grains exhibited straight extinction.

Potassium feldspar was present as subhedral to euhedral grains (≤ 1.5 mm), with often intense sericitization. Composition included microcline, with weak characteristic cross hatching, and more commonly, orthoclase (replaced by sericite), with remnant simple twinning.

Plagioclase was oligoclase (Ab 75 - 85) in composition and occurred as anhedral grains, which exhibited characteristic multiple twinning.

Biotite was present as small (≤ 0.5 mm), light brown to light green, subhedral to euhedral grains. Muscovite and chlorite were present as a hydrothermal alteration product of biotite.

Small (≤ 0.5 mm), euhedral opaque grains were disseminated throughout the section and varied in composition from magnetite to ilmenite.

ACID DYKES

Sample No.	30	32	34	40
quartz	30	35	35	60
plag.	20	20	30	10
kspar.	36	30	25	30
chl.	8	tr	-	1
biotite	-	2	-	-
sericite	5	10	8	-
opaques	tr	3	2	tr
epidote	1	tr	tr	tr

30 - Acid Dyke

HS - A fine - grained, grey to dark grey acid dyke, with small plagioclase phenocrysts.

PTS - This section was predominantly fine grained with remnant feldspar phenocrysts.

Subhedral (≤ 2.5 mm) plagioclase phenocrysts displaying remnant multiple twinning were severely sericitized. Plagioclase was oligoclase in composition (Ab 73 - 87).

Potassium feldspar and quartz account for the majority of the matrix. Potassium feldspar occurred as small subhedral elongate grains, while quartz occurred as both small (~ 0.5 mm), rounded regular grains and as finer matrix filling.

Epidote was present as small (~ 0.5 mm), granular anhedral grains, which appearred to be an alteration product of chlorite.

Anhedral chlorite was present as disseminations throughout the groundmass. Pale green under transmitted light, and, blue / grey under crossed polars, it often had a high potassium content (up to 1%).

Subhedral opaques were present and varied in composition from magnetite, to ilmenite, to rutile.

40 - Acid Dyke

HS - A fine - grained, pale grey to green acid dyke, with small feldspar phenocrysts and small needle - like grains.

TS - This section consisted of a fine - grained, predominantly equigranular quartz matrix, supporting feldspar phenocrysts up to 2.5 mm in size.

The feldspar phenocrysts were predominantly subhedral potassium feldspar, displaying characteristic carlsbad twinning. Plagioclase was also present as phenocrysts and displayed multiple twinning. Minor sericitization of the feldspars has occurred.

Chlorite occured as small (≤ 1 mm), irregularly shaped crystals disseminated throughout the section, and in places, was seen altered to epidote.

Anhedral opaque grains were rare.

INTERMEDIATE DYKES

Sample No.	33	37
quartz	30	40
plag.	35	28
kspar.	25	20
chlorite	8	10
opaques	2	1
sericite	tr	1
epidote	tr	tr

33 - Intermediate Dyke

HS - A fine - grained, brown to green intermediate dyke, with plagioclase phenocrysts.

TS - This section consisted of a fine grained matrix of quartz and feldspars, with plagioclase phenocrysts and large (≤ 2 mm), subhedral, irregular chlorite.

Subhedral plagioclase phenocrysts, up to 2.5 mm long, were quite numerous and often exhibited multiple twinning with minor sericitization.

Chlorite was characteristically light green in colour, and often showed minor alteration to epidote.

Opaques were present as subhedral to euhedral blocky grains, as well as, small needle - like crystals, probably magnetite and ilmenite respectively.

LAMPROPHYRE

Sample No.	35
quartz	5
plag.	30
kspar.	15
biotite	18
phlogopite	12
calcite	16
opaques	4
zircon	tr
apatite	tr

35 - Lamprophyre

HS - A fine grained grey rock with fine mica phenocrysts (≤ 2mm long) and mica aggregates (2 - 3 cm long). Sample effervesces with HCl.

PTS - Biotite, chlorite, calcite, quartz, plagioclase, potassium feldspar and opaques are the dominant minerals within this section.

Mica occurs in the section as diotite (Mg # 50 - 65) and as phlogopite (Mg # > 80). Both occur typically as small (≤ 1 mm) elongate subhedral to euhedral grains. Biotite is distinguishable from phlogopite by a much lighter colour under transmitted light. Biotite is light brown while phlogopite is dark brown to orange in colour.

Chlorite is present as light green, often potassium rich (≤ 3 %), anhedral grains which in places appear to be replacing phlogopite.

Carbonate is present as non - primary calcite. It is seen dispersed throughout the section and as a replacement of chlorite. The calcite displays high order birefringence and occasional twinning.

The groundmass is predominantly fine grained quartz, plagioclase, which is oligoclase to albite in composition (Ab 73 - 97), and potassium feldspar.

Very fine (≤ 0.1 mm) subhedral to euhedral opaques are present disseminated evenly throughout the section. They include magnetite and chromite.

APLITE DYKE

Sample No.	91
quartz	40
plag.	25
kspar.	35
biotite	tr
opaques	tr

91 - Aplite Dyke

HS - A medium grained quartz, potassium feldspar rich rock with minor platy biotite grains.

TS - Quartz and potassium feldspar are the dominant mineralogy within this section.

Quartz shows a bimodal distribution. Small (≤ 0.5 mm) rounded quartz grains and larger (≥ 1 mm) irregular anhedral grains. The smaller grains exhibit straight extinction while the larger grains show slight undulose extinction.

Potassium feldspar is present as large (≤ 5 mm) subhedral grains. Compositions vary from orthoclase to microcline which exhibits characteristic tartan cross hatching. Orthoclase exhibits carlsbad twinning with a perthitic texture. Microcline is also seen to form an anti - perthite texture with albite.

Plagioclase occurs as generally smaller (1 - 4 mm) subhedral grains which may exhibit typical multiple twinning or concentric zoning.

Pale straw coloured biotite and small opaques occur in trace amounts.

QUARTZ PORPHYRY

Sample No.	100
quartz	70
plag.	10
kspar.	17
biotite	2
muscovite	1
opaques	tr

100 - Quartz Porphyry

HS - A very fine grained bluey grey matrix with often large (3 - 5 mm) biotite grains ans slightly smaller quartz phenocrysts.

TS - This section is essentially composed of quartz, potassium feldspar and plagioclase with minor amounts of biotite and muscovite.

The dominant texture displayed within the section is a fine granophyric intergrowth between quartz and potassium feldspar. The granophyric texture exhibits a radiating appearance. Both quartz and plagioclase also occur as subhedral phenocrysts ($\leq$ 2 mm), with the plagioclase exhibiting multiple twinning while quartz displays non - undulose extinction.

Muscovite is present as small ($\leq$ 0.2 mm) irregular anhedral grains disseminated throughout the section. Biotite occurs as small ($\leq$ 2 mm) subhedral to euhedral straw coloured grains, often aggregatin together.

Opaques are rare.

GRANOPHYRE

Sample No.	54
quartz	60
plag.	5
kspar.	35
biotite	tr
sericite	tr
opaques	tr

54 - Granophyre

HS - Pale pink to white to yellow rock with large (10 - 30 mm), potassium feldspar phenocrysts.

TS - The granophyre was predominantly fine grained quartz, potassium feldspar and plagioclase.

Quartz and microcline combined to form a spectacular granophyric texture, often replacing large (≤ 6 mm), subhedral microcline grains. Microcline was distinguished by it's characteristic tartan twinning.

Orthoclase was distinguished by minor sericitization and relict carlsbad twinning.

Small (≤ 0.5 mm), subhedral plagioclase together with small anhedral quartz and microcline formed the general groundmass. Quartz displayed non - undulose extinction.

Small (≤ 0.5 mm), subhedral needle like biotite and opaques are rare.

DACITE PORPHYRY

Sample No.	45
quartz	40
plag.	40
biotite	20
opaques	tr
chlorite	tr

45 - Dacite Porphyry

HS - A rock consisting of a dark grey to black matrix with large (≤ 5 mm) plagioclase phenocrysts.

PTS - Plagioclase occurred as the most obvious mineral within this section. It occurred as phenocrysts (0.2 - 2 mm), within a very fine grained glassy matrix. The phenocrysts were often subhedral to euhedral, tabular crystals, exhibiting either multiple twinning or concentric zoning. Compositions varied from labradorite to oligoclase (Ab 49 - 72).

The matrix consisted of very fine grained biotite and quartz. Subhedral to euhedral opaques were rare.

METASEDIMENTS

Sample No.	43	122
quartz	55	40
muscovite	35	25
sericite	7	5
feldspars	tr	tr
opaques	tr	30
biotite	tr	tr
tourmaline	3	tr

43 - Metasediment

HS - A light grey metasiltstone with small aligned porphyroblasts and a prominent cleavage.

TS - This section was dominated by a prominant foliation, defind by muscovite and quartz.

Muscovite formed subhedral elongate grains, often aggregated to form schlieren (≤ 0.5 mm).

Quartz was present as small (≤ 0.1 mm) recrystalized grains which displayed slight undulose extinction and evidence for equilibrium in the form of tripple point junctions.

Remnant porphyroblast textures were a striking feature of this section. It was uncertain as to what the porphyroblasts originally were and there was no evidence of a foliation having been developed within them. The porphyroblasts have retrogressed to primarily quartz and sericite.

Tourmaline was quite common as pale yellow anhedral grains, often within the fine groundmass. Opaques were rare.

122 - Metasediment

HS - A dark grey slaty siltstone with remnant deformed porphyroblasts.

TS - This section was generally fine grained with the dominant mineralogy being quartz, muscovite, sericite and opaques.

Quartz was present as very fine, recrystalized anhedral grains, which displayed slight to non - undulose extinction. Quartz also presented as rotated recrystalized porphyroblasts (≤ 3.5 mm). Plagioclase was rare and occurred as small anhedral grains in the groundmass.

Abundant muscovite and very fine opaques (possably sulphides) defined the prominant foliation and often well developed crenulation celavage.

Remnant, possibly andalusite porphyroblasts (≤ 10 mm), displayed primary, sometimes rotated, fabrics. These porphyroblasts had undergone retrogression to quartz and very fine grained sericite.

Various accessory minerals, such as epidote, biotite and tourmaline, were also present.

APPENDIX 2

ELECTRON MICROPROBE ANALYSES OF MINERAL COMPOSITIONS

APPENDIX 2 - Electron Microprobe Analysis

Several polished sections were coated with approximately 250 um of carbon. Analyses of up to 20 - 30 grains on each sample was carried out using a KEVEX 7000 Series energy dispersive system (EDS) attached to a JEOL 733 microanalyser.

An accelerating voltage of 15 KV and a beam current of 3 nA were used during the analysis of the samples and each spectrum was collected over a 70 second period. Calibration of the KEVEX EDS system was carried out using a pure rhodonite standard.

Detection limits for the analysed elements are quite variable and depend upon several factors. The best estimate for all elements analysed is approximately 0.1 %.

Mineral chemistries tabulated in the following section are representative of all the minerals analysed.

SAMPLES ANALYSED

777 / 177	Anabama Granodiorite (Richards, 1980)
981 / 23	Anabama Granodiorite
981 / 26	Anabama Granodiorite
981 / 30	Acid Dyke
981 / 35	Lamprophyre
981 / 45	Dacite Porphyry
981 / 153	Anabama Granodiorite
981 / 160	Microgranodiorite

Biotite													
	179core	179rim	179core	179rim	26	153	160	160	45	45	35	35	35
SiO2	36.20	35.68	35.89	35.45	36.20	35.48	34.97	35.89	34.76	34.85	35.33	36.28	37.60
TiO2	3.15	2.20	3.32	2.89	3.22	3.38	2.75	2.94	3.50	3.35	3.18	3.20	3.29
Al2O3	14.71	14.67	14.65	15.65	15.51	15.18	16.30	16.36	16.26	16.17	13.97	14.68	14.35
Fe2O3													
FeO	19.07	17.90	19.10	18.20	17.71	18.46	19.61	19.30	20.76	20.41	16.70	16.59	13.58
MnO	0.47	0.33	0.30	0.23	0.56	0.25	0.01	0.21	0.49	0.43	0.25	0.21	0.36
MgO	12.10	12.19	11.73	12.04	11.46	11.64	9.40	9.88	9.92	9.77	12.45	13.56	16.43
CaO	0.04	0.19	0.16	0.29	0.29	0.22	0.10	0.24	0.08	0.18	0.25	0.05	0.09
Na2O	0.00	0.19	0.00	0.01	0.01	0.00	0.00	0.01	0.00	0.00	0.00	0.00	0.15
K2O	9.48	9.65	9.52	9.70	9.37	9.39	9.55	9.52	9.72	9.64	8.53	9.15	9.01
Total	95.24	92.99	94.66	94.46	94.31	94.00	92.68	94.34	95.47	94.78	90.66	93.72	94.85
	Structural formula based on 22 oxygens per formula unit												
Si	6.05	6.09	6.04	5.96	6.06	5.99	6.02	6.04	5.86	5.90	6.12	6.07	6.11
Ti	0.40	0.28	0.42	0.37	0.40	0.43	0.36	0.37	0.44	0.43	0.41	0.40	0.40
Al	2.90	2.95	2.91	3.10	3.06	3.02	3.31	3.25	3.23	3.23	2.85	2.90	2.75
Fe3+	0.00	0.00	0.00	0.00	0.00	0.00	0.00	0.00	0.00	0.00	0.00	0.00	0.00
Fe2+	2.66	2.56	2.69	2.56	2.48	2.61	2.82	2.72	2.93	2.89	2.42	2.32	1.85
Mn	0.07	0.05	0.04	0.03	0.08	0.04	0.00	0.03	0.07	0.06	0.04	0.03	0.05
Mg	3.01	3.10	2.94	3.02	2.86	2.93	2.41	2.48	2.49	2.47	3.21	3.38	3.98
Ca	0.01	0.03	0.03	0.05	0.05	0.04	0.02	0.04	0.01	0.03	0.05	0.01	0.02
Na	0.00	0.06	0.00	0.00	0.00	0.00	0.00	0.00	0.00	0.00	0.00	0.00	0.05
K	2.02	2.10	2.04	2.08	2.00	2.02	2.09	2.05	2.09	2.08	1.89	1.95	1.87
Total	17.12	17.23	17.11	17.17	17.00	17.08	17.02	16.98	17.13	17.10	16.98	17.06	17.07
Mg #	53.07	54.82	52.25	54.10	53.55	52.91	46.07	47.70	45.99	46.03	57.05	59.30	68.32
Al / Ti	7.32	10.44	6.92	8.49	7.56	7.04	9.30	8.73	7.28	7.58	6.88	7.20	6.85

	Phlogopite					Hornblende					
	35	35	35	35		179	179	23	23	153	153
SiO2	38.08	37.80	40.05	38.10		43.99	45.32	45.36	47.54	43.27	42.90
TiO2	3.36	3.35	3.17	3.62		0.97	1.39	1.15	1.00	1.30	1.08
Al2O3	12.08	13.62	13.80	13.12		7.87	7.57	7.48	4.56	8.01	8.25
Fe2O3											
FeO	5.24	5.56	4.34	9.52		16.71	15.09	16.46	14.35	16.02	17.33
MnO	0.00	0.00	0.07	0.04		0.35	0.46	0.69	0.34	0.28	0.39
MgO	21.10	22.23	23.55	18.90		11.08	12.90	12.60	13.70	11.67	11.39
CaO	0.19	0.00	0.28	0.16		11.83	11.64	12.15	11.78	11.67	11.64
Na2O	0.00	0.00	0.00	0.00		0.14	0.75	1.05	0.45	0.95	1.05
K2O	9.17	9.18	10.05	9.21		0.91	0.82	0.90	0.52	1.06	0.92
Total	89.21	91.74	95.31	92.66		93.86	95.93	97.83	94.24	94.22	94.95
	Structural formula based on 22 oxygens per formula unit					Structural formula based on 23 oxygens per formula unit					
Si	6.33	6.11	6.21	6.22		7.16	7.15	7.10	7.57	7.03	6.96
Ti	0.42	0.41	0.37	0.44		0.12	0.16	0.14	0.12	0.16	0.13
Al	2.37	2.60	2.52	2.52		1.51	1.41	1.38	0.86	1.53	1.58
Fe3+	0.00	0.00	0.00	0.00		0.00	0.00	0.00	0.00	0.00	0.00
Fe2+	0.73	0.75	0.56	1.30		2.27	1.99	2.15	1.91	2.18	2.35
Mn	0.00	0.00	0.01	0.01		0.05	0.06	0.09	0.05	0.04	0.05
Mg	5.22	5.36	5.44	4.60		2.69	3.03	2.94	3.25	2.82	2.76
Ca	0.03	0.00	0.05	0.03		2.06	1.97	2.04	2.01	2.03	2.02
Na	0.00	0.00	0.00	0.00		0.04	0.23	0.32	0.14	0.30	0.33
K	1.94	1.89	1.99	1.92		0.19	0.16	0.18	0.11	0.22	0.19
Total	17.04	17.13	17.15	17.03		16.09	16.17	16.33	16.01	16.31	16.38
Mg #	87.76	87.69	90.62	77.95		54.16	60.37	57.70	62.99	56.48	53.95
Al / Ti	5.64	6.37	6.82	5.68	Ca:Mg:Fe	20:27:23	20:30:20	20:29:22	20:32:19	20:28:22	20:28:24

	Chlorite		Sphene						Potassium Feldspar		
	35	30	179rim	179core	179rim	179core	26	30	160	30	35
SiO2	34.74	27.73	27.89	27.67	28.00	28.34	27.93	21.95	61.90	61.76	61.71
TiO2	0.16	0.00	36.16	35.43	36.61	35.63	35.36	48.63	0.05	0.18	0.16
Al2O3	14.80	20.27	1.31	1.06	1.22	1.35	1.28	4.00	17.67	17.65	17.94
Fe2O3											
FeO	12.62	21.80	0.96	2.01	1.00	1.09	1.61	2.28	0.00	0.00	0.00
MnO	0.20	0.35	0.05	0.22	0.00	0.00	0.00	0.01	0.00	0.13	0.00
MgO	22.77	14.58	0.17	0.20	0.15	0.16	0.00	0.05	0.06	0.00	0.00
CaO	0.04	0.18	26.48	26.20	27.12	25.97	26.66	20.49	0.44	0.29	0.47
Na2O	0.00	0.00	0.17	0.00	0.37	0.00	0.10	0.00	1.28	0.00	0.00
K2O	3.36	1.12	0.00	0.02	0.01	0.00	0.05	0.06	14.69	15.56	16.29
Total	88.69	86.03	93.19	92.80	94.48	92.54	92.99	97.46	96.08	95.57	96.58
	Structural formula based on 28 oxygens per formula unit		Structural formula based on 20 oxygens per formula unit						Structural formula based on 32 oxygens		
Si	6.81	5.86	3.93	3.93	3.90	4.00	3.95	2.96	11.91	11.95	11.88
Ti	0.02	0.00	3.83	3.79	3.83	3.78	3.76	4.94	0.01	0.03	0.02
Al	3.42	5.05	0.22	0.18	0.20	0.22	0.21	0.64	4.01	4.03	4.07
Fe3+	0.00	0.00	0.00	0.00	0.00	0.00	0.00	0.00	0.00	0.00	0.00
Fe2+	2.07	3.85	0.11	0.24	0.12	0.13	0.19	0.26	0.00	0.00	0.00
Mn	0.03	0.06	0.01	0.03	0.00	0.00	0.00	0.00	0.00	0.02	0.00
Mg	6.66	4.59	0.03	0.04	0.03	0.03	0.00	0.01	0.02	0.00	0.00
Ca	0.01	0.04	3.99	3.99	4.04	3.93	4.04	2.96	0.09	0.06	0.10
Na	0.00	0.00	0.05	0.00	0.10	0.00	0.03	0.00	0.48	0.00	0.00
K	0.84	0.30	0.00	0.00	0.00	0.00	0.01	0.01	3.61	3.84	4.00
Total	19.87	19.76	12.16	12.20	12.22	12.10	12.20	11.78	20.12	19.93	20.07
Mg #	76.28	54.37							Ab 84	0	0

Plagioclase									
	179	179	26 rim	26 core	153	45 rim	45 core	160	30
SiO2	54.68	59.73	61.49	55.19	58.34	60.39	55.58	59.68	62.52
TiO2	0.08	0.25	0.00	0.15	0.00	0.02	0.00	0.03	0.00
Al2O3	23.13	24.96	23.34	26.96	24.49	23.18	26.71	22.92	20.67
Fe2O3									
FeO	0.00	0.08	0.17	0.01	0.09	0.05	0.19	0.00	0.03
MnO	0.12	0.03	0.15	0.00	0.06	0.23	0.01	0.17	0.00
MgO	0.00	0.18	0.00	0.00	0.13	0.00	0.00	0.06	0.00
CaO	6.51	6.82	4.98	9.25	6.38	5.26	8.91	4.94	2.43
Na2O	9.47	7.49	8.12	5.88	7.47	7.47	6.04	8.65	9.00
K2O	0.55	0.18	0.15	0.07	0.15	0.59	0.20	0.32	0.00
Total	94.54	99.72	98.40	97.51	97.11	97.19	97.63	96.77	94.64
Structural formula based on 32 oxygens per formula unit									
Si	10.48	10.68	11.07	10.15	10.70	11.02	10.22	10.97	11.57
Ti	0.01	0.03	0.00	0.02	0.00	0.00	0.00	0.00	0.00
Al	5.23	5.26	4.95	5.85	5.30	4.99	5.79	4.97	4.51
Fe3+	0.00	0.00	0.00	0.00	0.00	0.00	0.00	0.00	0.00
Fe2+	0.00	0.01	0.02	0.00	0.01	0.01	0.03	0.00	0.00
Mn	0.02	0.00	0.02	0.00	0.01	0.04	0.00	0.03	0.00
Mg	0.00	0.05	0.00	0.00	0.04	0.00	0.00	0.02	0.00
Ca	1.34	1.31	0.96	1.82	1.25	1.03	1.76	0.97	0.48
Na	3.52	2.60	2.83	2.10	2.65	2.64	2.15	3.08	3.23
K	0.13	0.04	0.03	0.02	0.04	0.14	0.05	0.07	0.00
Total	20.72	19.98	19.89	19.96	20.00	19.87	19.99	20.12	19.79
Mg #	72	67	75	53	68	72	55	76	87

APPENDIX 3

METHOD OF WHOLE ROCK ANALYSIS AND MINERAL SEPERATION TECHNIQUES AND MAJOR ELEMENT, TRACE ELEMENT AND NORMATIVE COMPOSITIONS : SAMPLE LOCATION MAPS

APPENDIX 3

ANALYTICAL TECHNIQUES :

1 Sample Preparation for XRF:

The sample preparation method was as follows :

(a) Weathered surfaces were trimmed from the rock before crushing in the jaw crusher.

(b) The crushed sample was then milled in a tungsten - carbide mill for approximately one and a half minutes.

(c) Approximately 2 grams of milled powder was ignited to 960 degrees for 12 hours to determine percentage loss of volatiles.

(d) Approximately 1 gram of ignited powder was weighed out with approximately 4 grams of flux. This powder mixture was fused into buttons for whole rock analyses, using X.R.F. techniques.

(e) Approximately 5 grams of unignited rock powder was mixed with approximately 0.7 ml of P.V.A solution and made into pressed pellets, using boric acid as a support medium, for trace element determination.

2 Analytical Method

Whole rock analyses were determined by x - ray fluorescence.

Major Elements

The following major elements were analysed for using a programmable Phillips PW 1480 X - ray spectrometer: SiO_2, $Al2O_3$, Fe_2O_3, MnO, MgO, CaO, Na_2O, K_2O, TiO_2, P_2O_5 and SO_3.

Trace Element Analysis

The following trace elements were analysed for using a programmable Phillips PW 1480 X - ray spectrometer: Y, Sr, Rb, Nb, Zr, Th, Pb, U, Ga, Zn, Ba, Sc, Cr, V, Co, Ce, Nd, La, Cu and Ni.

3 Mineral Separation

Biotite mineral separation was required for two samples. The biotite obtained was to be analysed for their Rubidium and Strontium isotope compositions.

3.1 Flotation

a) Two to five centimetres of ground up sample (up to 500 microns) was placed into one of the glass flotation containers and washed several times to remove the fine material.

b) Approximately 20-25 ml of Armac T solution was added and the pH lowered to 3 using dilute H_2SO_4.

c) The agitator was lowered to almost the bottom of the container and turned on and left to coat the particles with Armac T. After ten minutes the air valve is opened and the water froths up.

d) The 'mica froth' was scraped off and washed thoroughly through a nylon sieve and dried on a hot plate.

3.2 Frantz Magnetic Separator

The resultant mica fraction from the flotation still contained some quartz grains and the bulk of this was removed using the Frantz #2 magnetic separator.

Finally a pure biotite sample was obtained by selectively hand picking over the samples to remove any contaminants.

4 Results

In the following tables major elements are expressed as weight %, CIPW normative mineralogy as weight % and trace elements as ppm. Total iron is given as Fe_2O_3, for CIPW norm calculations a ratio $FeO / FeO + Fe_2O_3 = 0.68$ was used on a program written by Webb (1992).

				Anabama	Granite			
Sample No.	153	151	156	154	152	163	23	167
SiO2	60.42	60.57	60.76	61.24	62.25	62.88	63.01	63.05
TiO2	0.87	0.9	0.79	0.78	0.8	0.79	0.81	0.74
Al2O3	18.01	17.66	18.02	17.81	17.55	16.78	16.84	17.11
Fe2O3*	5.3	5.37	5.76	5.4	4.82	5.61	5.06	4.73
MnO	0.07	0.07	0.08	0.08	0.07	0.08	0.09	0.07
MgO	2.6	2.56	2.53	2.46	2.31	2.31	2.16	1.85
CaO	4.96	4.94	3.96	4.3	4.53	3.59	4.18	4.06
Na2O	4.31	4.22	4.15	4.16	4.2	3.72	4.37	3.97
K2O	2.02	2.27	2.69	2.39	2.17	2.67	1.7	3.2
P2O5	0.22	0.25	0.23	0.22	0.21	0.26	0.24	0.21
SO3	0.03	0.03	0.07	0.03	0.03	0.04	0.02	0.03
LOI	0.74	0.67	1.09	0.77	0.75	1.2	1.22	0.56
Total	99.56	99.51	100.13	99.63	99.69	99.94	99.7	99.59
Cr	41	38	39	36	38	28	33	21
Ni	21	21	20	15	19	16	18	10
Sc	12.3	12.5	12.5	11.4	10.6	11.8	12.5	10
V	104.1	103.2	102.5	90.9	93.9	97.9	89.9	81.4
Pb	7.1	6.2	8.7	4.7	7.4	6.8	4.3	9.2
Cu	44	31	91	38	17	62	12	18
Zn	57	54	67	63	57	64	54	55
Co	72.6	57.8	52.8	99.2	60	57.7	44.3	63.7
Rb	109.5	110.2	152.6	131.7	116.9	148.2	89.5	121.1
Sr	526.9	504.4	564.9	522.9	511.6	418.6	464.8	428.7
Ba	602	648	687	739	580	701	381	1250
Ga	22	23.2	23.6	23.4	22.4	22.5	21.9	20.6
Y	24.6	24.6	24.8	21.4	20.4	33.5	28.2	31
Nb	13.7	14.7	14	13.6	12.8	19.4	20.9	18.7
Zr	249.7	255	229.5	239.4	241.9	258	252.8	245.9
Th	10.2	20.4	12.4	15.5	15	25.5	16.1	21.5
U	2.6	4.8	6.5	3	4.7	4.1	2.9	2.6
La	33	59	46	46	39	78	53	59
Ce	59	95	82	75	62	132	96	100
Nd	23	31	33	28	22	44	42	36
qz	12.27	12.2	13.03	14.06	15.63	18.96	18.12	15.51
or	11.91	13.36	15.87	14.08	12.8	15.75	10.02	18.87
ab	36.45	35.66	35.09	35.19	35.51	31.47	36.98	33.57
an	23.2	22.59	18.16	19.92	21.15	16.14	19.24	18.82
hy-en	6.48	6.37	6.29	6.12	5.75	5.75	5.37	4.61
-fs	3.23	3.26	3.79	3.5	2.94	3.67	3.18	2.97
di-di	-	0.18	-	-	-	-	-	-
-dh	-	0.08	-	-	-	-	-	-
mt	2.45	2.48	2.66	2.5	2.22	2.59	2.32	2.18
il	1.64	1.7	1.49	1.47	1.52	1.49	1.41	1.4
c	0.23	-	1.63	1.08	0.55	1.86	1.75	0.23
ap	0.5	0.57	0.54	0.5	0.47	0.61	0.5	0.47
Total	98.36	98.45	98.55	98.42	98.54	98.29	98.89	98.63

			Anabama	Granite		
Sample No.	25	777-179	164	18	140	Ave. MORUYA Griffin et al. (1978)
SiO2	63.77	63.78	63.98	64.06	66.88	64.39
TiO2	0.71	0.65	0.8	0.75	0.66	0.75
Al2O3	16.45	17.56	16.38	16.87	15.49	15.55
Fe2O3*	5.1	4.11	5.12	5	4.09	4.6
MnO	0.07	0.07	0.07	0.05	0.06	0.1
MgO	1.98	1.75	1.99	2.11	1.59	2.25
CaO	4	4.3	3.97	3.55	3.2	4.12
Na2O	4.04	4.41	3.9	3.9	3.82	3.94
K2O	1.97	2.52	2.81	2.55	2.75	2.18
P2O5	0.25	0.16	0.25	0.22	0.2	0.18
SO3	0.03	na	0.03	0.03	0.01	-
LOI	0.91	0.66	0.63	0.87	1.03	-
Total	99.28	99.97	99.94	99.96	99.77	98.06
Cr	28	na	22	29	19	
Ni	8	26	10	13	7	
Sc	10.5	11	11.5	11.5	7.4	
V	84.6	na	86	87.1	68.2	
Pb	5.4	8	7.5	8.9	10.8	
Cu	13	14	11	3	2	
Zn	52	48	51	55	40	
Co	104.3	9	55.7	77.8	77.3	
Rb	113.2	98	130.8	131.7	126.8	
Sr	421.4	228	435.2	411.7	349.1	
Ba	414	741	858	718	875	
Ga	22.2	na	20.8	20.4	18.1	
Y	34	25	37.9	14.3	25.6	
Nb	20.9	20	23	17.8	16.9	
Zr	252.3	199	293.9	236.8	253.9	
Th	19.1	na	27.2	23.1	36.1	
U	3.9	na	3.5	6.1	1.8	
La	59	na	65	50	88	
Ce	108	na	107	96	130	
Nd	40	na	37	35	39	
qz	20.4	15.97	18.23	20.09	24.37	
or	11.64	14.86	16.59	15.03	16.2	
ab	34.14	37.29	32.99	32.99	32.31	
an	18.26	20.29	18.09	16.22	14.56	
hy-en	4.93	4.36	4.95	5.25	3.96	
-fs	3.34	2.57	3.19	3.15	2.52	
di-di	-	-	-	-	-	
-dh	-	-	-	-	-	
mt	2.36	1.9	2.36	2.32	1.9	
il	1.34	1.23	1.52	1.41	1.24	
c	0.99	0.15	0.29	1.75	0.9	
ap	0.57	0.37	0.57	0.5	0.47	
Total	97.97	98.99	98.78	98.71	98.43	

	Acid	Dykes	Int.	Dykes	Dacite	Porphyry
Sample No.	30	40	37	47	44a	45
SiO2	68.92	71.83	61.6	64.55	70.15	68.5
TiO2	0.41	0.21	0.55	0.45	0.43	0.48
Al2O3	15.79	15.79	16.22	16.85	15.2	15.97
Fe2O3*	2.68	1.19	3.41	3.87	2.75	2.96
MnO	0.04	0.02	0.03	0.09	0.04	0.06
MgO	1.4	0.6	2.91	1.47	1.09	1.37
CaO	2.13	1.67	1.73	3.9	2.58	3.47
Na2O	4.81	5.73	3.76	4.43	4.8	4.8
K2O	2.28	1.6	5.52	1.95	1.92	1.72
P2O5	0.15	0.05	0.22	0.16	0.12	0.14
SO3	0.02	0.01	0.07	0.03	0.03	0.02
LOI	1.64	1.19	3.74	1.82	0.32	0.61
Total	100.28	99.89	99.76	99.56	99.43	100.1
Cr	34	16	11	15	28	36
Ni	19	16	8	8	12	16
Sc	4	2.6	7.3	5.7	5.4	5.6
V	40.8	15	80.9	53.2	39.8	50.5
Pb	14.8	1	2.2	4.8	3.9	4.9
Cu	22	12	0	19	23	8
Zn	48	25	18	118	34	72
Co	43.6	54.1	29.4	44	59.1	54
Rb	52	44.2	129.2	98.4	65.3	62.6
Sr	770.3	516.8	305	1116.9	582.6	743.5
Ba	624	500	1470	655	525	436
Ga	18.7	17.3	20	19	19.2	20
Y	7.8	5.6	15.7	12	13.4	11.2
Nb	8.1	4.3	9.1	6.9	12.5	9.9
Zr	146.3	100.2	165.4	134.6	141.7	154.4
Th	6.1	6	11.6	7.3	13.5	12.4
U	0.3	1.4	1.1	0.3	1.8	0.6
La	23	12	52	28	33	36
Ce	44	25	90	51	61	60
Nd	18	9	36	20	24	23
qz	25.2	27.76	10.27	19.99	27.31	23.97
or	13.47	9.41	32.57	11.52	11.3	10.13
ab	40.7	48.46	31.78	37.45	40.59	40.59
an	9.62	7.98	7.18	18.32	12.06	16.36
hy-en	3.48	1.49	7.25	3.65	2.71	3.4
-fs	1.7	0.71	2.08	2.74	1.72	2.1
di-di	-	-	-	-	-	-
-dh	-	-	-	-	-	-
mt	1.23	0.53	1.57	1.78	1.27	0.93
il	0.77	0.39	1.03	0.85	0.8	0.91
c	1.88	1.71	1.44	0.74	0.81	0.22
ap	0.34	0.1	0.5	0.37	0.27	0.3
Total	98.39	98.54	95.67	97.41	98.84	98.91

	Dacite	Porphyry	Aplite	Qtz Porphyry	Diorite
Sample No.	46	86	91	100	138
SiO2	68.67	68.84	76.22	76.15	69.11
TiO2	0.48	0.37	0.12	0.13	0.39
Al2O3	15.95	16.1	13.01	14.03	16.24
Fe2O3*	3.13	2.87	0.5	0.97	2.71
MnO	0.06	0.03	0.01	0.01	0.05
MgO	1.38	1.17	0.14	0.3	1.03
CaO	3.36	3.08	0.73	0.97	3.78
Na2O	4.56	4.62	2.89	4.38	4.68
K2O	1.84	2.18	5.39	2.85	1.47
P2O5	0.14	0.16	0.03	0.06	0.1
SO3	0.02	0.01	0.01	0.01	0.02
LOI	0.54	0.35	0.54	0.54	0.28
Total	100.13	99.78	99.7	100.39	99.84
Cr	34	14	17	16	21
Ni	16	<5	<5	<5	0
Sc	5.6	6.1	4.1	4.1	5.4
V	48.4	35.1	9.6	10	33.8
Pb	4.6	4.4	7.5	15.1	8.3
Cu	8	15	39	14	1
Zn	47	22	6	11	31
Co	60.7	84.5	119.6	93.3	89.7
Rb	75.3	53.2	154.4	63.5	60.3
Sr	715	810.9	151.4	218.7	490.5
Ba	448	593	385	594	310
Ga	19.7	19.9	15.8	18.3	20.3
Y	11.7	11.3	10.8	15.7	8.7
Nb	10.4	8.7	20.6	9.5	4.6
Zr	154.5	176.1	84	75.1	159.6
Th	12	10.5	41.6	8.8	6.8
U	2.8	2	5.6	3.2	1.2
La	31	46	35	19	25
Ce	53	80	63	39	39
Nd	20	31	16	17	14
qz	25.32	24.88	37.02	37.16	26.1
or	10.86	12.86	31.84	16.81	8.68
ab	38.55	39.07	24.44	37.03	39.6
an	15.83	14.25	3.38	4.41	18.1
hy-en	3.43	2.91	0.34	0.74	2.56
-fs	2.02	1.91	0.25	0.63	1.79
di-di	-	-	-	-	-
-dh	-	-	-	-	-
mt	1.44	1.32	0.23	0.44	1.25
il	0.91	0.7	0.23	0.24	0.73
c	0.66	0.92	1.18	2.13	0.31
ap	0.3	0.37	0.07	0.13	0.24
Total	99.32	99.19	98.98	99.72	99.36

Fine Qtz./Plag. Rock		Micro - Granodiorite Dykes					
Sample No.	105	75	160	95	165	128	80
SiO2	75.74	71.29	72.22	72.88	74.13	76.5	76.56
TiO2	0.17	0.07	0.23	0.06	0.09	0.05	0.08
Al2O3	13.18	17.05	14.76	15.74	14.45	12.56	13.24
Fe2O3*	3.07	0.65	2.57	0.6	1.09	0.62	0.35
MnO	0.02	0.01	0.02	0.01	0.02	0.01	0.01
MgO	0.46	0.19	0.57	0.15	0.28	0.07	0.1
CaO	0.03	2.64	1.22	1.93	1.47	0.69	1.09
Na2O	0.15	5.5	3.48	4.81	3.98	2.34	3.29
K2O	4.67	2.41	3.91	3.29	4.17	6.4	4.99
P2O5	0.07	0.03	0.13	0.02	0.03	0.01	0.02
SO3	0.07	0.01	0.02	0.01	0.01	0.01	0.01
LOI	2.61	0.26	0.95	0.28	0.5	0.2	0.2
Total	100.22	100.11	100.07	99.8	100.22	99.45	99.94
Cr	14	18	12	18	17	19	17
Ni	<5	<5	<5	<5	<5	<5	<5
Sc	3.1	1.9	4.5	2.7	2.5	1.1	0.8
V	45.4	8.1	29.5	6.9	11.6	12.5	6.2
Pb	1.1	8.2	15	9.9	12.3	12.1	9.6
Cu	2	25	16	21	35	2	12
Zn	21	10	30	11	18	6	9
Co	60.2	137.4	159.7	75.2	92.4	114.2	148.2
Rb	162.9	60.9	124.8	87.5	116.1	154.8	128.1
Sr	10.7	608.8	166.7	441.6	225.5	215.7	233.8
Ba	307	348	569	710	554	865	676
Ga	32.1	20.8	20.2	17.9	16.3	12.2	15.9
Y	1.9	11.8	22.9	8.5	10.4	3.9	8
Nb	36.5	9.9	19.6	5.6	8.8	2.4	14.6
Zr	65.9	72.2	194.7	57.5	68.4	33.9	80.9
Th	2.8	9.5	32.7	5.7	20.4	21.6	41.5
U	0.6	1.6	11.7	1.5	6.4	1.3	3.4
La	3	9	39	11	15	6	4
Ce	6	18	75	17	27	16	7
Nd	2	10	29	8	12	3	4
qz	55.35	24.05	33.09	27.8	31.18	36.63	35.83
or	27.56	14.2	23.1	19.43	24.61	37.8	29.45
ab	1.26	46.52	29.42	40.7	33.67	19.77	27.8
an	-	12.89	5.2	9.48	7.1	3.42	5.3
hy-en	1.14	0.47	1.42	0.37	0.69	0.17	0.24
-fs	2.39	0.46	1.86	0.45	0.83	0.46	0.24
di-di	-	-	-	-	-	-	-
-dh	-	-	-	-	-	-	-
mt	1.41	0.3	1.18	0.25	0.49	0.28	0.14
il	0.32	0.12	0.42	0.11	0.17	0.09	0.15
c	7.97	0.68	2.9	0.8	0.79	0.53	0.49
ap	0.13	0.07	0.3	0.03	0.07	-	0.03
Total	97.53	99.76	98.89	99.42	99.6	99.15	99.67

		Lamprophyres			
Sample No.	131	35	147	Ave. Truro Morris (1991)	Ave. CAL Rock (1987)
SiO2	77.23	55.24	55.34	55.5	51.5
TiO2	0.08	1.28	1.34	2.15	1.3
Al2O3	12.8	13.05	13.18	12.96	14
Fe2O3*	0.55	5.83	6.71	9.1	6.67
MnO	0.01	0.07	0.05	0.11	0.15
MgO	0.08	6.36	6.87	6.08	6.9
CaO	0.67	4.25	3	1.56	6.6
Na2O	2.95	2.41	1.97	1.21	2.7
K2O	5.58	6.81	7.41	5.77	3.8
P2O5	0.01	1.03	1.05	0.85	0.71
SO3	0.01	0.07	0.09	-	-
LOI	0.29	3.33	2.24	4.74	4.9
Total	100.26	99.74	99.25	100.03	99.23
Cr	18	356	366	78	462
Ni	<5	135	144	148	186
Sc	1.1	21.7	21.7	24	20
V	7.1	180.8	175.2	504	167
Pb	17.1	5.1	5.7	na	20
Cu	4	141	305	155	52
Zn	7	66	79	116	82
Co	133.1	43.8	46.5	38	35
Rb	207.6	274.1	323.1	na	124
Sr	57.7	218.9	298	422	896
Ba	201	2825	3212	1434	1900
Ga	15	16.8	18	na	21
Y	8.3	30.3	27.1	na	25
Nb	6.9	30.2	31.2	16	18
Zr	52.3	752.7	758.1	366	276
Th	30.6	103.5	103.5	na	20
U	2.6	13.1	11.2	na	5
La	23	235	181	na	113
Ce	40	436	359	na	216
Nd	12	183	152	na	122
qz	37.05	0.12	2.42		
or	32.96	40.24	43.79		
ab	24.91	20.39	16.68		
an	3.31	4.68	5.24		
hy-en	0.19	15.84	17.11		
-fs	0.36	3.03	3.65		
di-di	-	6.57	1.86		
-dh	-	1.09	0.34		
mt	0.25	2.7	3.11		
il	0.15	2.43	2.54		
c	0.7	-	-		
ap	-	2.44	2.49		
Total	99.88	99.53	99.23		

	Granophyres	
Sample No.	54	134
SiO2	74.94	76.37
TiO2	0.07	0.1
Al2O3	13.54	13.95
Fe2O3*	0.45	0.95
MnO	0.01	0.02
MgO	0.13	0.28
CaO	0.4	0.11
Na2O	2.8	4.4
K2O	6.55	3.09
P2O5	0.03	0.02
SO3	0.01	0.01
LOI	0.42	0.84
Total	99.34	100.13
Cr	15	14
Ni	<5	<5
Sc	1.4	2
V	5.7	4.3
Pb	13.9	11.6
Cu	31	3
Zn	6	19
Co	108.7	96.8
Rb	147.3	101
Sr	185.5	73.1
Ba	2196	393
Ga	14.1	18.3
Y	5.6	14.7
Nb	5.4	9.2
Zr	25.4	56.7
Th	10.3	8.3
U	0.9	1.4
La	13	21
Ce	24	41
Nd	7	15
qz	32.52	38.07
or	38.69	18.26
ab	23.65	37.19
an	1.79	0.44
hy-en	0.32	0.69
-fs	0.3	0.69
di-di	-	-
-dh	-	-
mt	0.19	0.42
il	0.12	0.18
c	1.19	3.22
ap	0.07	0.03
Total	98.77	99.16

Additional Ratios and Information

Sample No. (A 981 -)	Total Iron as FeO	Mg #	Rb / Sr	K/Rb	mol Al2O3 / (CaO+Na2O+K2O)
153	4.77	32.9	0.21	184	0.98
151	4.83	32.3	0.22	206	0.96
156	5.18	30.5	0.27	176	1.06
154	4.86	31.3	0.25	181	1.03
152	4.34	32.4	0.23	186	1
163	5.05	29.2	0.35	180	1.08
23	4.55	29.9	0.19	190	1.01
167	4.26	28.1	0.28	264	0.99
25	4.59	28	0.27	174	1.03
777 - 179	3.7	28.3	0.43	257	1
164	4.61	28	0.3	215	0.98
18	4.5	29.7	0.32	194	1.08
140	3.68	28	0.36	217	1.03
30	4.33	34.3	0.07	438	1.11
40	5.16	33.5	0.09	362	1.11
37	3.38	46	0.42	427	1.06
47	3.99	27.5	0.09	198	1.02
44a	2.57	28.4	0.11	294	1.04
45	2.66	31.6	0.08	275	0.99
46	2.82	30.6	0.11	244	1.02
86	2.58	29	0.07	410	1.04
91	2.6	21.9	1.02	349	1.09
100	3.94	23.6	0.29	449	1.16
138	2.44	27.5	0.12	244	1
105	0.13	13	15.22	287	2.46
75	4.95	22.6	0.1	396	1.04
160	3.13	18.2	0.75	313	1.21
95	4.33	20	0.2	376	1.05
165	3.58	20.4	0.51	359	1.05
128	2.11	10.1	0.72	413	1.04
80	2.96	22.2	0.55	390	1.03
131	2.65	12.7	3.6	269	1.06
35	2.17	52.2	1.25	248	0.68
147	1.77	50.6	1.08	229	0.79
54	2.52	22.4	0.79	445	1.09
134	3.96	22.8	1.38	306	1.29

Sample Location Map for the Anabama Granite Region

26 Sample number with prefix A981

Unsealed Road

0 5 km

Figure 22

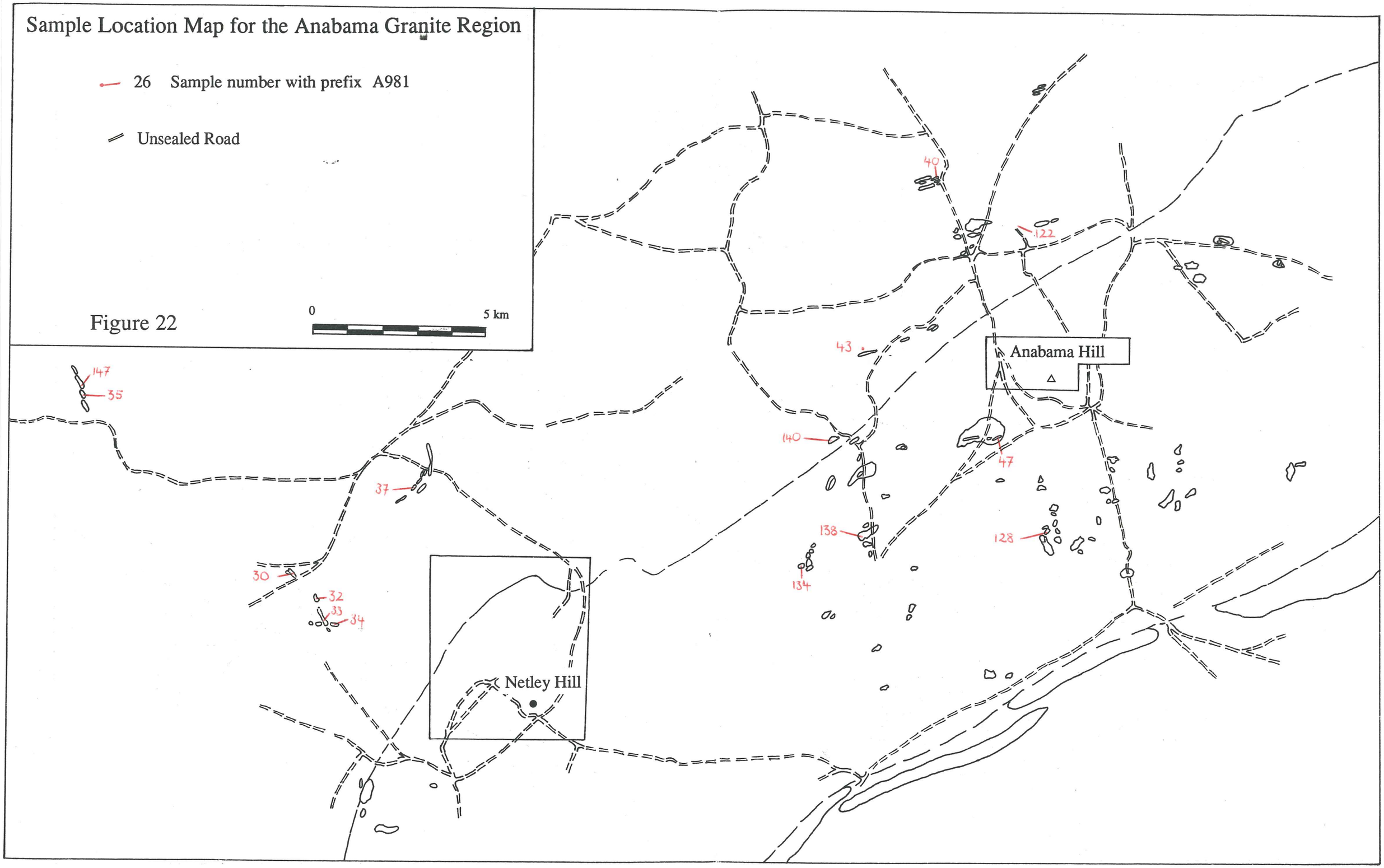

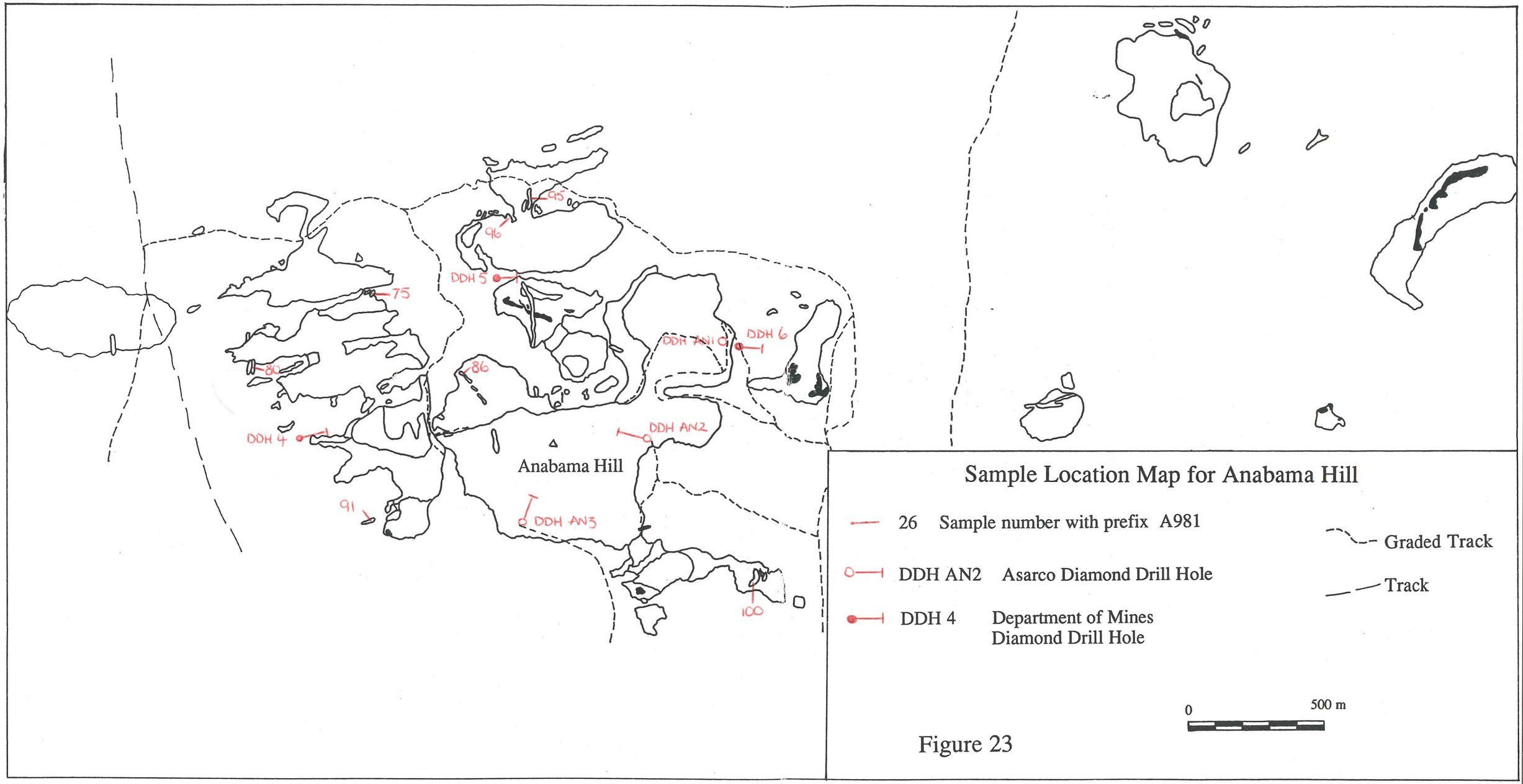

Sample Location Map for Anabama Hill

26 Sample number with prefix A981

DDH AN2 Asarco Diamond Drill Hole

DDH 4 Department of Mines Diamond Drill Hole

Graded Track

Track

0 500 m

Figure 23

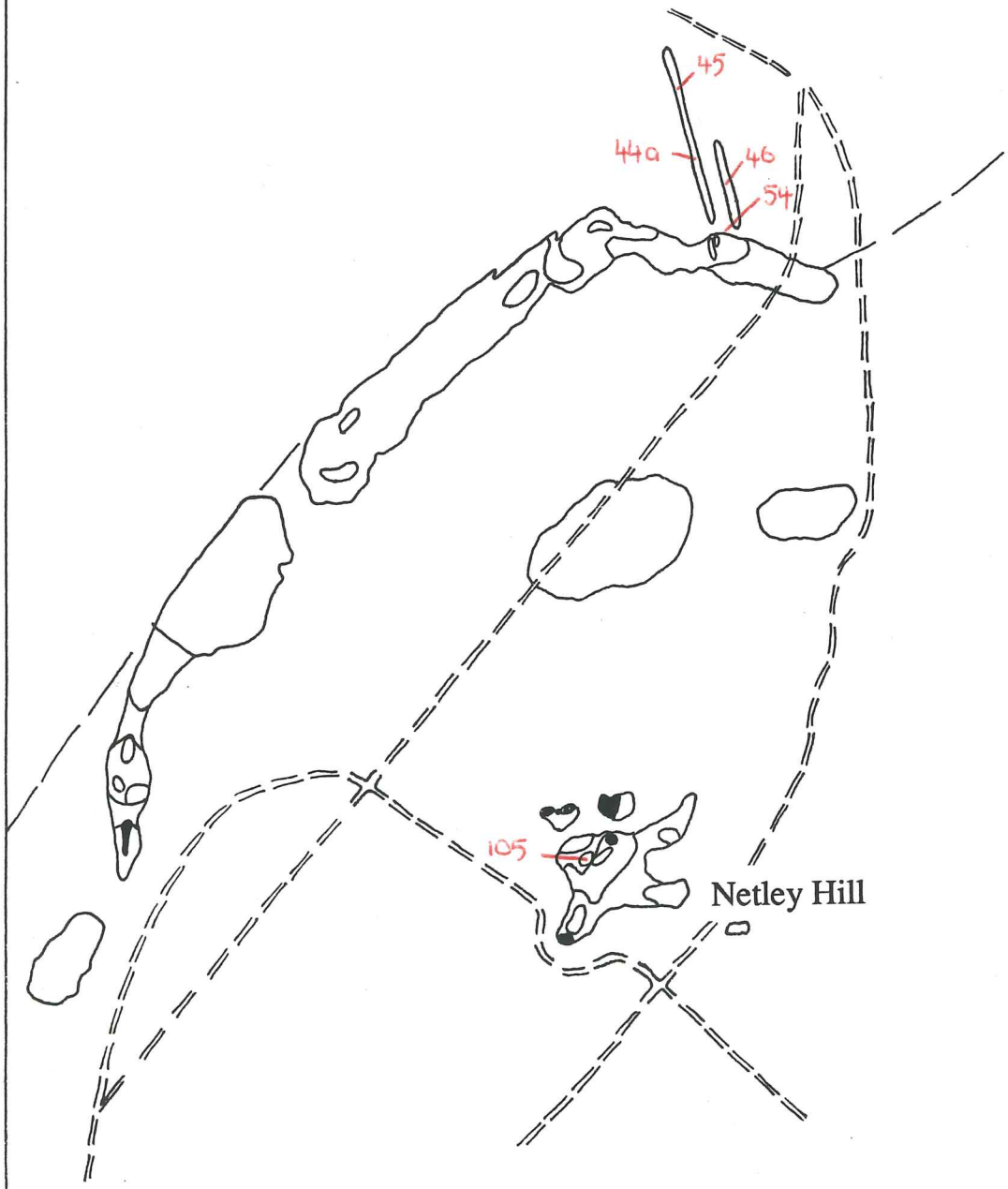

Sample Location Map for Netley Hill

26 Sample number with prefix A981

Track

Figure 24

0 1 2 km

APPENDIX 4

MAJOR AND TRACE ELEMENT MODELLING OF FRACTIONAL AND EQUILIBRIUM CRYSTALLIZATION

Modelling of Major Elements

Modelling of major elements was undertaken using LSMIX, a basic computer program. This program involves the approximation in composition of a more evolved daughter from a less evolved, comagmatic parent. The program uses a least - squares mixing approximation method with the goodness of fit being indicated by the sum of squares of the residuals. If the sum of squares of the residuals is less than 1, it is thought that a good fit has occurred.

Input data is listed with the parent magma on the left, the daughter composition which is to be modelled on the right and appropriate missing mineral compositions in the middle (see text).

Results are listed with the actual composition listed to the modelled composition, and the errors for each respective element. The proportions of the crystallizing phases and the amount of original liquid remaining are also given.

Trace Element Modelling

From the fractions of the components derived from the major element modelling, Rb, Ba, Ce and K modelling was attempted using the Rayleigh fractionation law :

$$C1 / C0 = F^{(D-1)} \qquad (1)$$

and the equilibrium crystallization model :

$$C1 / C0 = 1 / (F+D-FD) \qquad (2)$$

where C1 = concentration of the trace element in the derived melt
C2 = concentration of the trace element in the parent
F = fraction of the melt with respect to the original parent
D = bulk distribution coefficient of a given trace element

PART A - Fractional Crystallization of the Anabama granite

Mineral compositions used were as follows.

	Biotite	Hornblende	Plagioclase
SiO_2	35.48	42.9	55.9
TiO_2	3.38	1.08	0.08
Al_2O_3	15.18	8.25	25.29
FeO	20.5	19.26	0.12
MnO	0.25	0.39	0
MgO	11.64	11.39	0.04
CaO	0.22	11.64	7.8
NaO	0	1.05	6.72
K_2O	9.39	0.92	0.23
P_2O_5	0	0	0

Distribution coefficients used were as follows.

	Biotite	Hornblende	Plagioclase
Rb	2.24 (3)	0.014 (1)	0.041 (1)
Ba	9.7 (3)	0.044 (1)	0.30 (1)
Ce	0.318 (3)	1.5 (2)	0.30 (2)
K	2.5 (3)	0.081 (2)	0.10 (2)

from (1) Nagasawa and Schnetzler (1971)
(2) Cox et al. (1979)
(3) Higuchi and Nagasawa (1969)

RESULTS

MAJOR ELEMENT MODELLING

Sample 140 from Sample 153

	Estimated	Observed	Residuals	Weight Component	Fraction	Standard Deviation
SiO_2	60.42	60.42	-0.0027	gran 140	0.568	0.0119
TiO_2	0.7	0.87	-0.1691	biotite	0.063	0.0098
Al_2O_3	17.98	18.01	-0.03	hornblende	0.082	0.0107
FeO	5.23	5.3	-0.0663	plagioclase	0.299	0.0113
MnO	0.08	0.07	0.0119			
MgO	2.58	2.6	-0.0152			
CaO	5.11	4.96	0.1534			
NaO	4.26	4.31	-0.0492			
K_2O	2.3	2.02	0.2793			
P_2O_5	0.11	0.22	-0.1065			

Sum of squares of Residuals = 0.14955

Sample 25 from Sample 153

	Estimated	Observed	Residuals	Weight Component	Fraction	Standard Deviation
SiO_2	60.41	60.42	-0.0066	gran 25	0.712	0.01
TiO_2	0.73	0.87	-0.1355	biotite	0.051	0.0066
Al_2O_3	18.04	18.01	0.0276	hornblende	0.038	0.0074
FeO	5.43	5.3	0.1299	plagioclase	0.207	0.0088
MnO	0.08	0.07	0.0074			
MgO	2.44	2.6	-0.1570			
CaO	4.92	4.96	-0.0394			
NaO	4.31	4.31	-0.0009			
K_2O	1.96	2.02	-0.0590			
P_2O_5	0.18	0.22	-0.0421			

Sum of squares of Residuals = 0.06754

Sample 167 from Sample 153

	Estimated	Observed	Residuals	Weight Component	Fraction	Standard Deviation
SiO_2	60.40	60.42	-0.0235	gran 167	0.741	0.0294
TiO_2	0.68	0.87	-0.1891	biotite	0.01	0.0186
Al_2O_3	17.97	18.01	-0.0398	hornblende	0.08	0.0203
FeO	5.26	5.3	-0.0420	plagioclase	0.178	0.0258
MnO	0.09	0.07	0.0154			
MgO	2.40	2.6	-0.2023			
CaO	5.32	4.96	0.3637			
NaO	4.22	4.31	-0.0918			
K_2O	2.57	2.02	0.5547			
P_2O_5	0.16	0.22	-0.0644			

Sum of squares of Residuals = 0.53328

Sample 23 from Sample 153

	Estimated	Observed	Residuals	Weight Component	Fraction	Standard Deviation
SiO_2	60.41	60.42	-0.0124	gran 23	0.766	0.0139
TiO_2	0.83	0.87	-0.0419	biotite	0.049	0.0085
Al_2O_3	18.03	18.01	0.0244	hornblende	0.028	0.0097
FeO	5.43	5.3	0.1327	plagioclase	0.165	0.0120
MnO	0.09	0.07	0.0220			
MgO	2.55	2.6	-0.0535			
CaO	4.82	4.96	-0.1355			
NaO	4.48	4.31	0.1740			
K_2O	1.82	2.02	-0.1981			
P_2O_5	0.18	0.22	-0.0361			

Sum of squares of Residuals = 0.11266

Sample 30 from Sample 153

	Estimated	Observed	Residuals	Weight Component	Fraction	Standard Deviation
SiO_2	60.40	60.42	-0.0166	acid 30	0.518	0.0165
TiO_2	0.61	0.87	-0.2594	biotite	0.073	0.0148
Al_2O_3	17.98	18.01	-0.0324	hornblende	0.118	0.0159
FeO	5.20	5.3	-0.1033	plagioclase	0.305	0.0170
MnO	0.09	0.07	0.0151			
MgO	2.93	2.6	0.3329			
CaO	4.88	4.96	-0.0811			
NaO	4.67	4.31	0.3560			
K_2O	2.04	2.02	0.0227			
P_2O_5	0.08	0.22	-0.1424			

Sum of squares of Residuals = 0.34445

Sample 40 from Sample 153

	Estimated	Observed	Residuals	Weight Component	Fraction	Standard Deviation
SiO_2	60.38	60.42	-0.0395	acid 40	0.465	0.0209
TiO_2	0.62	0.87	-0.2539	biotite	0.104	0.0210
Al_2O_3	17.99	18.01	-0.0219	hornblende	0.131	0.0223
FeO	5.25	5.3	-0.0488	plagioclase	0.316	0.0236
MnO	0.09	0.07	0.0165			
MgO	3.00	2.6	0.3971			
CaO	4.79	4.96	-0.1707			
NaO	4.92	4.31	0.6144			
K_2O	1.91	2.02	-0.1060			
P_2O_5	0.02	0.22	-0.1967			

Sum of squares of Residuals = 0.68344

Sample 47 from Sample 153

	Estimated	Observed	Residuals	Weight Component	Fraction	Standard Deviation
SiO_2	60.41	60.42	-0.0052	int 47	0.691	0.0112
TiO_2	0.63	0.87	-0.2445	biotite	0.068	0.0076
Al_2O_3	18.00	18.01	-0.0106	hornblende	0.066	0.0084
FeO	5.35	5.3	0.0497	plagioclase	0.189	0.0104
MnO	0.10	0.07	0.0348			
MgO	2.56	2.6	-0.0407			
CaO	4.95	4.96	-0.0077			
NaO	4.40	4.31	0.0925			
K_2O	2.09	2.02	0.0660			
P_2O_5	0.11	0.22	-0.1094			

Sum of squares of Residuals = 0.09021

TRACE ELEMENT MODELLING

Sample 140 from Sample 153

	Parent	Observed Daughter	Predicted Daughter (1)	Predicted Daughter (2)
Rb	109.5	126.8	158.7	152.8
Ba	602	875	436.7	483.5
Ce	59	130	76.9	74.0
K	20200	27500	27847.5	26762.3

Sample 25 from Sample 153

	Parent	Observed Daughter	Predicted Daughter (1)	Predicted Daughter (2)
Rb	109.5	113.2	133.7	131.9
Ba	602	414	448.8	482.0
Ce	59	108	70.9	69.9
K	20200	19700	23894.4	23554.3

Sample 167 from Sample 153

	Parent	Observed Daughter	Predicted Daughter (1)	Predicted Daughter (2)
Rb	109.5	121.1	142.5	141.8
Ba	602	1250	678.8	471.7
Ce	59	100	65.3	64.7
K	20200	32000	25749.0	25560.3

Sample 23 from Sample 153

	Parent	Observed Daughter	Predicted Daughter (1)	Predicted Daughter (2)
Rb	109.5	89.5	125.9	124.8
Ba	602	381	443.1	474.4
Ce	59	96	68.4	67.8
K	20200	17000	22606.8	22414.9

Sample 30 from Sample 153

	Parent	Observed Daughter	Predicted Daughter (1)	Predicted Daughter (2)
Rb	109.5	52	166.3	157.9
Ba	602	624	392.9	458.6
Ce	59	44	77.2	73.5
K	20200	22800	28901.2	27389.0

Sample 40 from Sample 153

	Parent	Observed Daughter	Predicted Daughter (1)	Predicted Daughter (2)
Rb	109.5	44.2	166.5	154.9
Ba	602	500	274.7	388.9
Ce	59	25	80.7	75.5
K	20200	16000	28478.6	26578.2

Sample 47 from Sample 153

	Parent	Observed Daughter	Predicted Daughter (1)	Predicted Daughter (2)
Rb	109.5	98.4	131.9	129.6
Ba	602	655	383.1	436.9
Ce	59	51	69.8	68.7
K	20200	19500	23416.8	23047.2

PART B - Fractional Crystallization of an Average Basalt composition

Mineral and rock compositions used were as follows.

	Augite	OPX	Pigeonite	Basalt	Archean
SiO_2	52.7	50.0	51.47	49.05	63.55
TiO_2	0.34	0.49	0.29	1.56	0.81
Al_2O_3	1.84	0.47	1.56	15.94	14.42
FeO	6.5	34.0	23.0	11.05	7.37
MnO	0.16	0.84	0.52	0.19	0.11
MgO	15.15	11.51	21.68	6.59	3.3
CaO	21.58	1.74	1.45	11.0	3.78
NaO	0.49	0.2	0.07	2.77	2.85
K_2O	0.01	0.05	0.03	0.64	3.01
P_2O_5	0	0	0	0.16	0.2

Sample 153 from Sample an Average basalt

	Estimated	Observed	Residuals	Weight Component	Fraction	Standard Deviation
SiO_2	60.40	60.42	-0.0197	basalt	0.400	0.0552
TiO_2	1.20	0.87	0.3261	Archean	0.827	0.0370
Al_2O_3	18.06	18.01	0.0518	augite	-0.099	0.0252
FeO	5.40	5.3	0.1021	opx	-0.132	0.0174
MnO	0.04	0.07	-0.0293			
MgO	2.35	2.6	-0.2474			
CaO	5.16	4.96	0.2023			
NaO	3.39	4.31	-0.9190			
K_2O	2.74	2.02	0.7184			
P_2O_5	0.23	0.22	0.0095			

Sum of squares of Residuals = 1.58368

Sample 153 from Sample an Average basalt

	Estimated	Observed	Residuals	Weight Component	Fraction	Standard Deviation
SiO_2	60.38	60.42	-0.0350	basalt	0.409	0.0601
TiO_2	1.20	0.87	0.3296	Archean	0.822	0.0401
Al_2O_3	18.14	18.01	0.1285	augite	-0.109	0.0317
FeO	5.34	5.3	0.0375	opx	-0.153	0.0403
MnO	0.04	0.07	-0.0327	pigeonite	0.030	0.0491
MgO	2.63	2.6	0.0286			
CaO	5.02	4.96	0.0588			
NaO	3.39	4.31	-0.9177			
K_2O	2.73	2.02	0.7078			
P_2O_5	0.23	0.22	0.0098			

Sum of squares of Residuals = 1.47644

APPENDIX 5

SIMPLIFIED LITHOLOGICAL LOGS AND CORE SAMPLE LOCATIONS AND NUMBERS

LEGEND


Granite / Granodiorite


Partly Greisened Granite / Granodiorite


Porphyritic Granodiorite

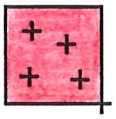
Microgranodiorite


Granite Breccia


Acid Dyke


Andesite


Greisened Granite / Granodiorite


Dacite Porphyry

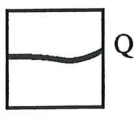

Quartz vein

Fault

ASARCO DDH AN 1 - SIMPLIFIED GEOLOGICAL LOG

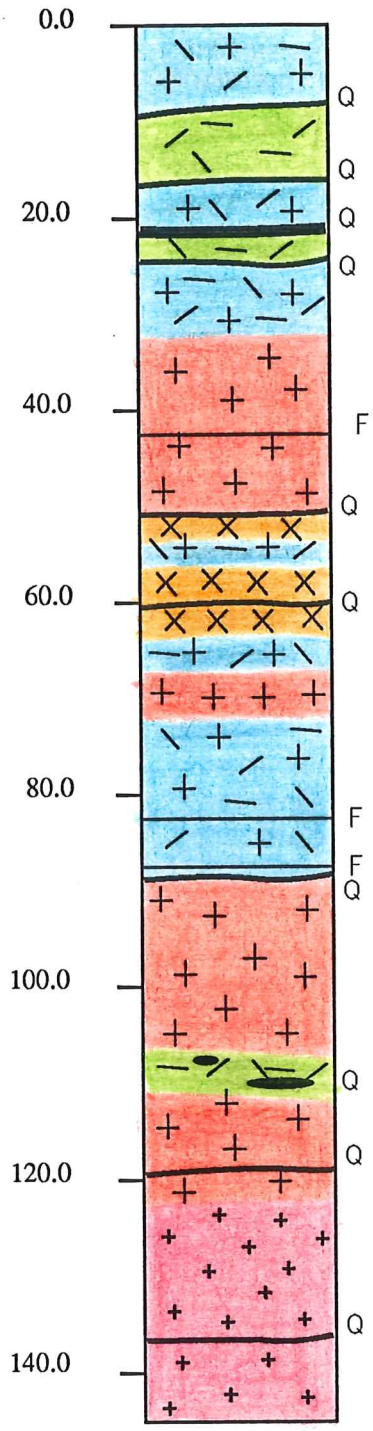

Sample Locations and Numbers
(prefix A981/)

16
17
18
19
20
21
22
23
24
25
26
27
28
29

ASARCO DDH AN 2 - SIMPLIFIED GEOLOGICAL LOG

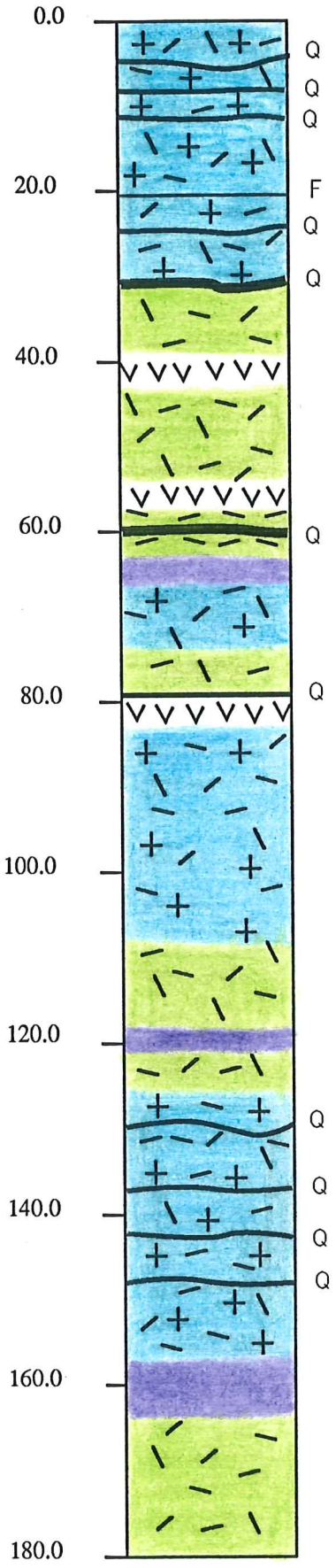

Sample Location and Numbers
(prefix A981/)

1
2
3
4
5
6
7
8
9
10

ASARCO DDH AN 3 - SIMPLIFIED GEOLOGICAL LOG

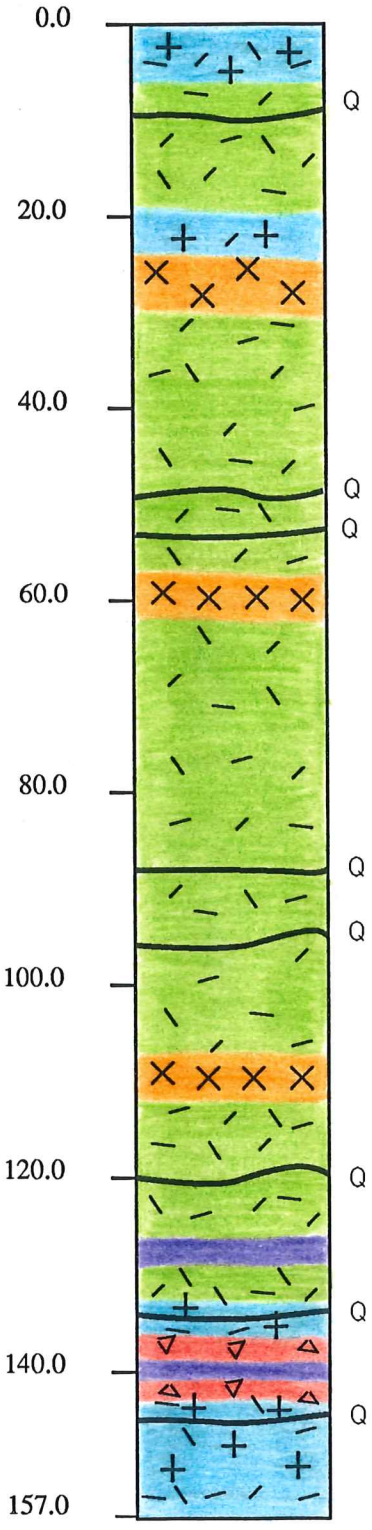

Sample Locations and Numbers
(prefix A981/)

11

12

13

14

15

DDH 4 - SIMPLIFIED GEOLOGICAL LOG

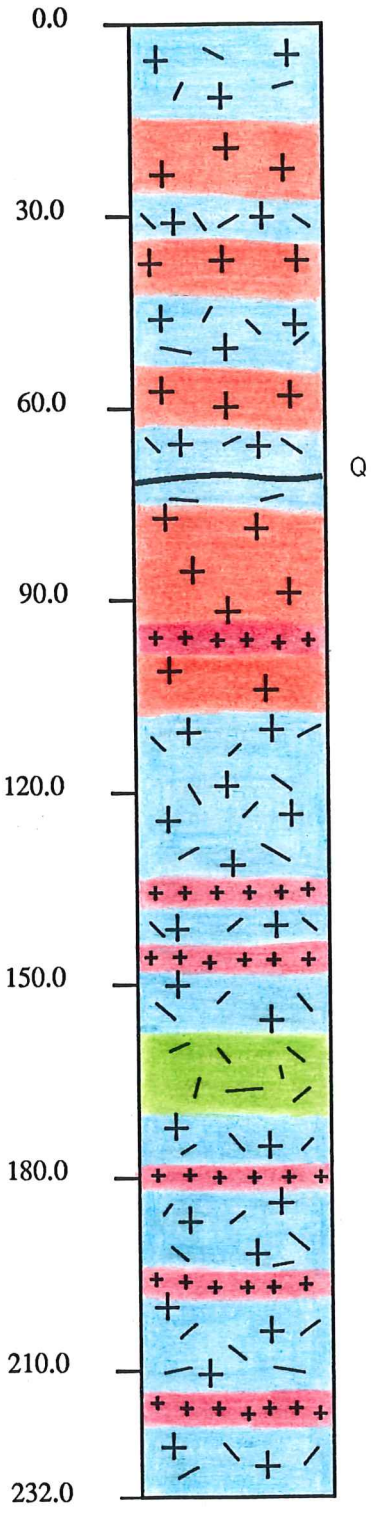

Sample Locations and Numbers
(prefix A981/)

164
165
166
167

DDH 5 - SIMPLIFIED GEOLOGICAL LOG

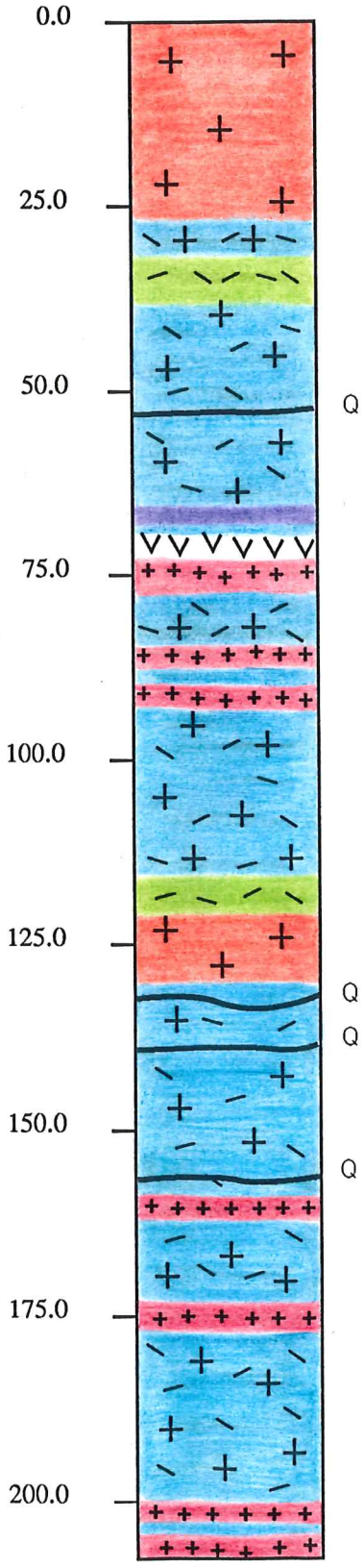

Sample Locations and Numbers
(prefix A981/)

148
149
150
151
152
153
154
155
156
157

DDH 6 - SIMPLIFIED GEOLOGICAL LOG

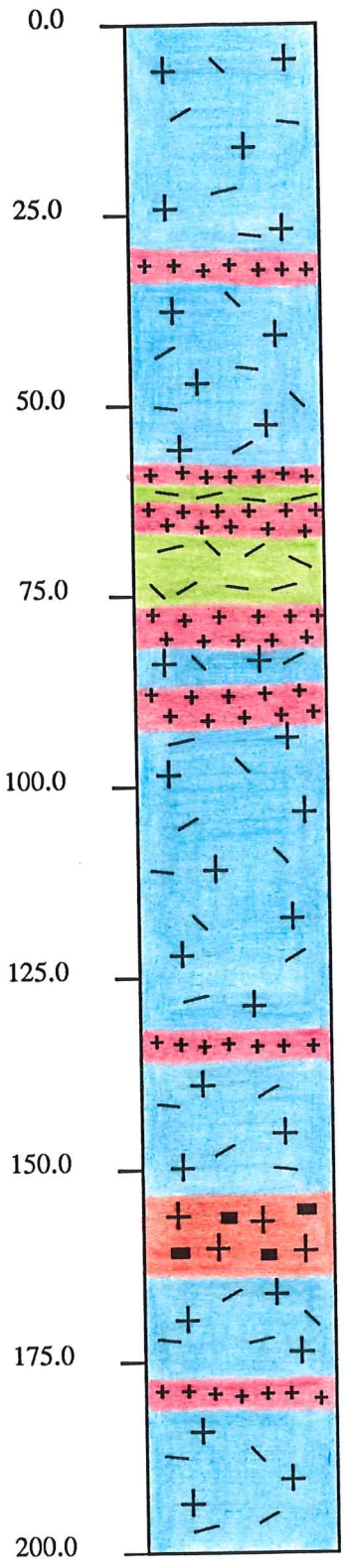

Sample Locations and Numbers
(prefix A981/)

158
159
160
161
162
163

GEOLOGY OF THE ANABAMA GRANITE AND SURROUNDS, OLARY PROVINCE, S.A.

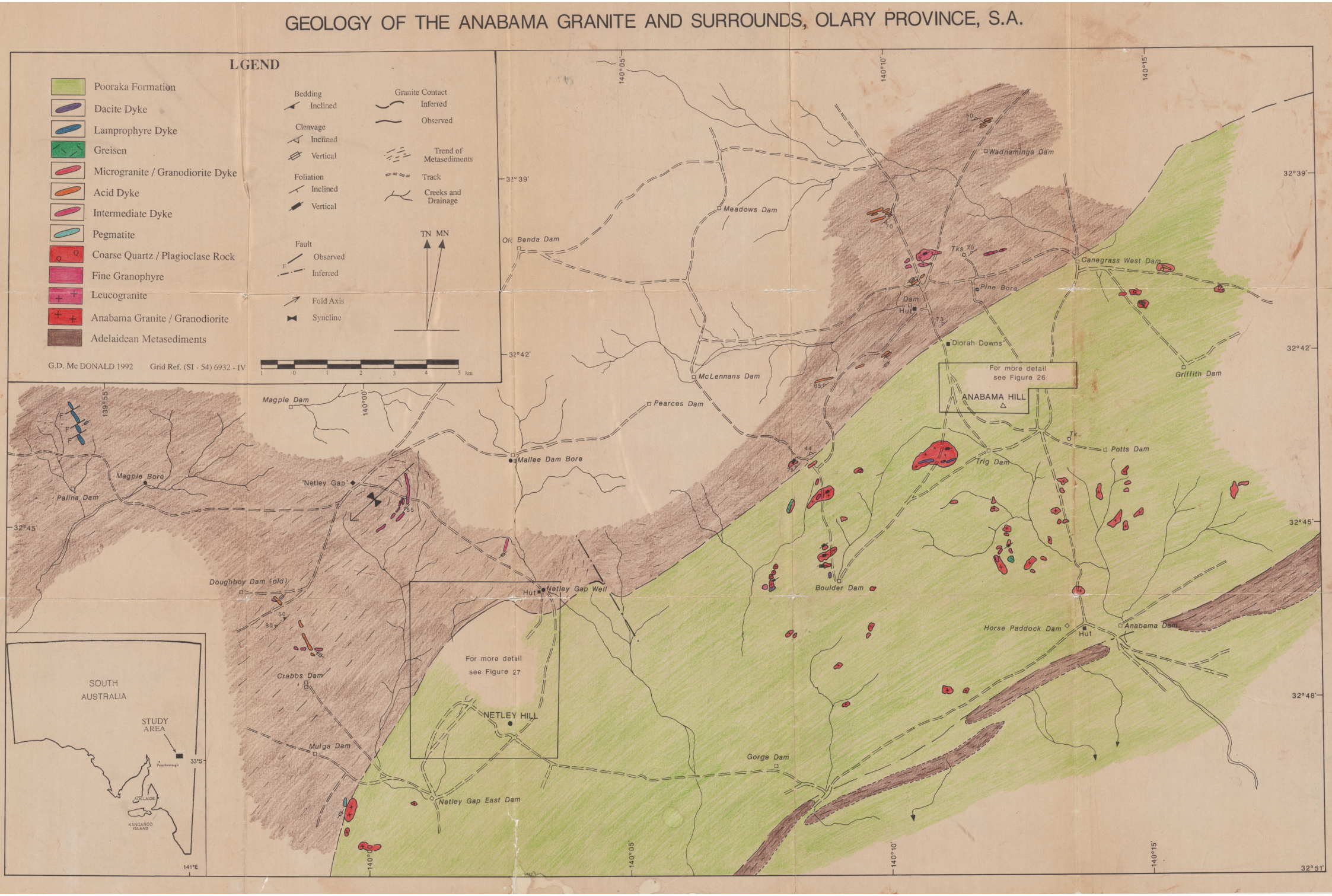

GEOLOGY OF ANABAMA HILL, OLARY PROVINCE, S.A.

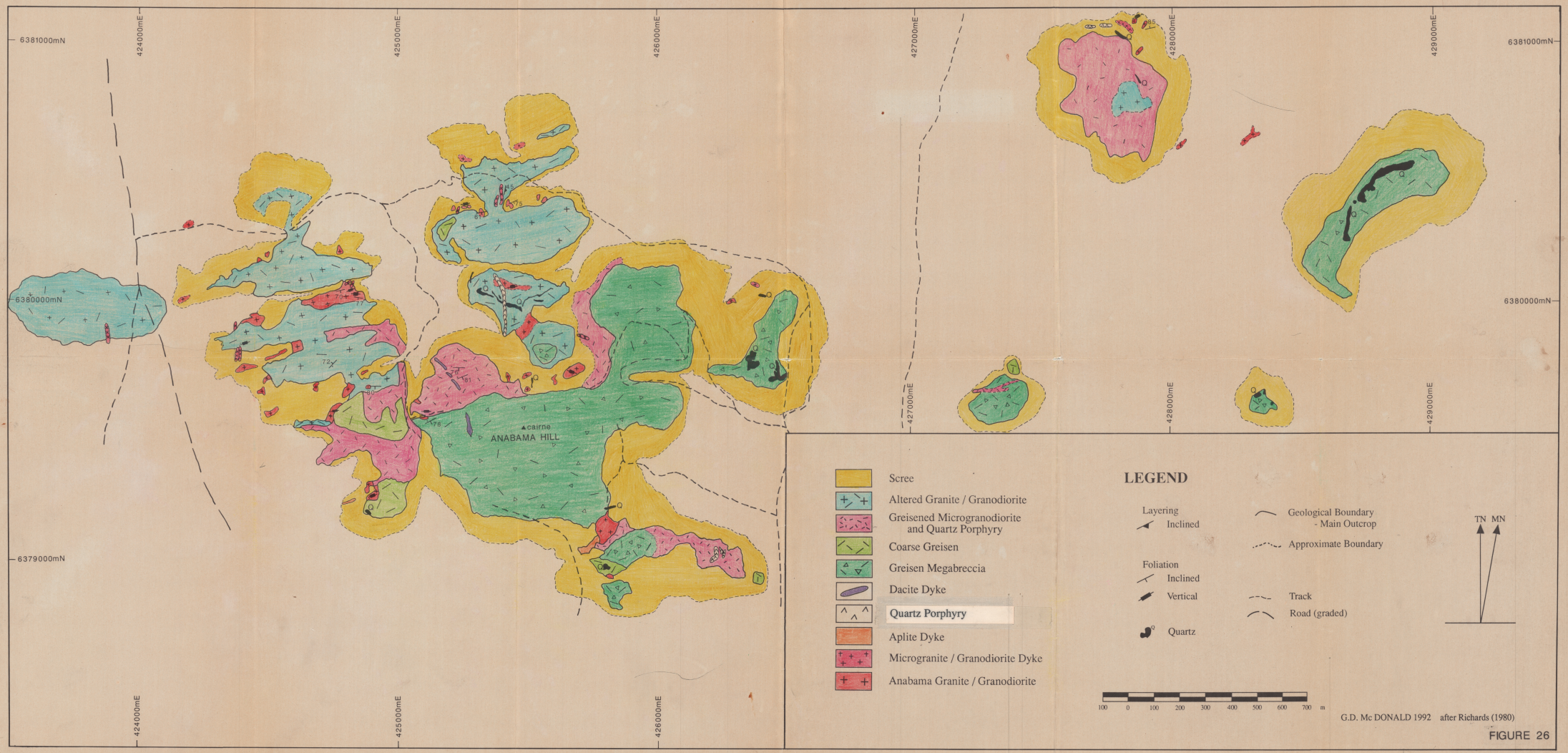

G.D. Mc DONALD 1992 after Richards (1980)

FIGURE 26

GEOLOGY OF THE NETLEY HILL REGION, OLARY PROVINCE, S.A.

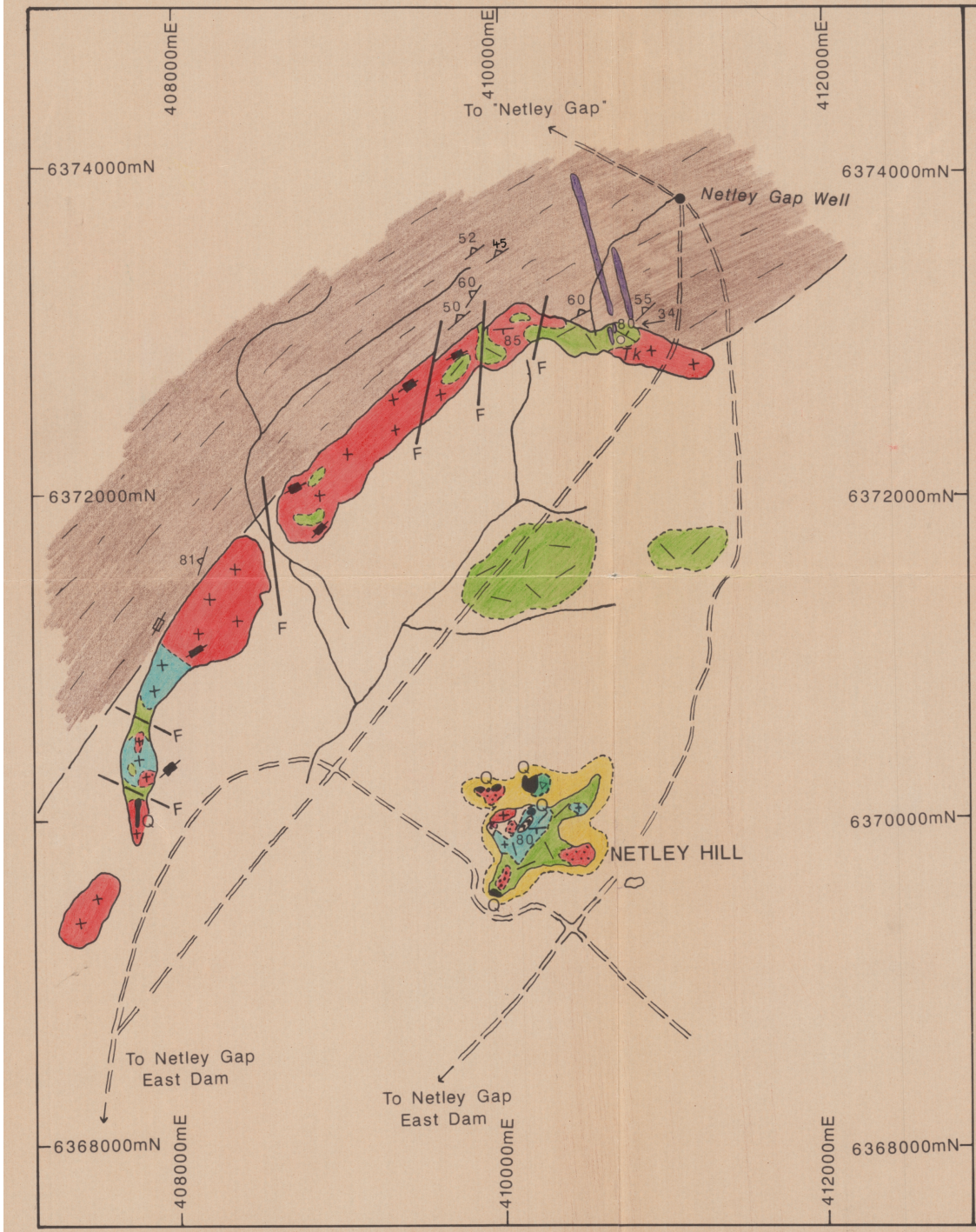

LEGEND

- Scree
- Fine Quartz / Plagioclase rock
- Altered Granite / Granodiorite
- Greisened Microgranodiorite and Quartz Porphyry
- Coarse Greisen
- Greisened Megabreccia
- Dacite Porphyry
- Quartz Porphyry
- Biotite Granite / Granodiorite
- Adelaidean Metasediments

TN MN

Cleavage
- Inclined
- Vertical

Foliation
- Inclined
- Vertical

Fault
- Observed
- Inferred

Granite Contact
- Inferred
- Observed

Quartz

Trend of Metasediments

Track

Creeks and Drainage

Geological Boundary - Main outcrop

Approximate Boundary

Lineation

500 0 1000 2000 m

G.D. Mc DONALD 1992

FIGURE 27